ENGINEERING RESEARCHES

Research, Methodology and Innovation

Editors
Halil Ibrahim KURT
Engin ERGUL

Engineering Sciences

ENGINEERING RESEARCHES

Research, Methodology and Innovation

Editors
Halil Ibrahim KURT
Engin ERGUL

LIVRE DE LYON
Lyon 2024

ENGINEERING RESEARCHES

Research, Methodology and Innovation

Editors
Halil Ibrahim KURT
Engin ERGUL

LIVRE DE LYON
Lyon 2024

ENGINEERING RESEARCHES: Research, Methodology and Innovation

Editors • Prof. Dr. Halil Ibrahim KURT • ORCID: 000-0002-5992-8853
Dr. Engin ERGUL • ORCID: 0000-0003-3347-5400

Cover Design • Motion Graphics
Book Layout • Motion Graphics

First Published • March 2024, Lyon

e-ISBN: 978-2-38236-663-9

DOI Number: 10.5281/zenodo.10869302

Publisher • Livre de Lyon
Address • 37 rue marietton, 69009, Lyon France
website • http://www.livredelyon.com
e-mail • livredelyon@gmail.com

PREFACE

Today, it is very important for engineers and researchers to present their theoretical and applied studies in journals and books that offer publication opportunities in relevant fields. The book "ENGINEERING RESEARCHES: Research, Methodology and Innovation" brings together scientists and engineers who evaluate various engineering fields, giving importance to studies and applications from different disciplines, and some examples of experimental, theoretical and compilation studies that have been done recently in different fields are included.

The editor and the editorial board expect that this book will attract the attention of academics and researchers in the fields of engineering sciences and be useful to the scientific world. We would like to thank the chapter authors for their contributions, the referees who reviewed the studies, and the Livre de Lyon publishing house for preparing the book for printing.

Prof. Dr. Halil Ibrahim KURT and Dr. Engin ERGUL

CONTENTS

CHAPTER I

INVESTIGATION OF THE USABILITY OF POLYMER BINDERS IN THE PRODUCTION OF PERVIOUS CONCRETE

Abdurrahim Emre ÖZDEMİR[1] & Serdal ÜNAL[2] & Mehmet CANBAZ[3]

[1](MSc), Eskişehir Osmangazi University, Institute of Science,
E-mail: emreozdemir1989@hotmail.com
ORCID: 0000-0002-8395-0401

[2](MSc), Eskişehir Osmangazi University, Institute of Science,
E-mail: serdalunall@gmail.com
ORCID: 0000-0002-5200-9969

[3](PhD), Eskişehir Osmangazi University,
Department of Civil Engineering,
E-mail: mcanbaz@ogu.edu.tr
ORCID: 0000-0002-0175-6155

1. Introduction

Composite materials are obtained by combining two or more components in order to obtain a superior material by correcting each other's weaknesses. In the production of composite materials, it is aimed to have high strength and durability features according to the usage area of the material obtained. Composite materials produced using different methods and components consist of a matrix phase, which is a continuous phase, and a reinforcement phase dispersed in this phase. (Ersoy, 2001)

Polymer concrete composites are composite materials in which polymer resin is used instead of cement, which reacts with water in normal concrete to bind aggregates together. They were first developed in the 1950s and became known in the 1970s. Today, it is used in precast structures, bridge panels, hazardous waste containers and machine parts. The use of polymers instead of

Portland cement in concrete increases the mechanical properties of concrete. It also makes concrete impervious to water and chemicals and resistant to abrasion. Due to these properties, polymer concretes are widely used as repair materials in sidewalks, roads and buildings. (Fattah ve Hawary, 1999)

Polymer is a macromolecular structure formed by a large number of small molecules called monomers, which are connected to each other by chemical bonds as a result of polymerization reaction under appropriate conditions and formed in a long, chain-like structure.Polymer chains can be linear, branched and cross-linked.Chain structure and size are the main factors determining the properties of polymers. (Saçak, 1998)

Polymer concrete composites are obtained by using polymer instead of all or part of the cement paste used in traditional concrete production.They are generally divided into three different classes according to their production methods.These are polymer concrete (PC), polymer modified concrete (PMC) and polymer impregnated concrete (PIC) (Ohama, 1997).

Polymer concretes are polymer and aggregate mixtures in which polymer is used as binder.In polymer concretes, polyester, polystyrene, acrylic and epoxy are mostly preferred as resins, but vinyl ester, furan and urethane are also used.Polymer concretes are used in drainage, underground pipe and chimney production and tunnel lining due to their advantages such as high strength and durability, low permeability and fast setting.

Polymer-modified concrete is a type of polymer concrete obtained by adding polymers such as acrylic, styrene butadiene rubber (SBR), polyvinyl acetate and ethylene vinyl acetate between 10% and 20% of Portland cement. PMC production, which is more cost-effective than polymer concrete, can be supported by fiber reinforcement for higher bending strength and crack control.

Polymer impregnated concretes are produced by impregnating low viscosity monomers such as methyl methacrylate into concrete and then polymerized by radiation or thermal effects. In this way, the compressive strength of concrete is increased three to four times. Due to the low permeability of the polymer, resistance to freeze-thaw and acid effect is obtained. Due to these properties, it is preferred in many applications such as bridge supports, concrete pipe production and hazardous waste material containment. (Fowler, 1999)

Gorninski et al. (2004) studied the determination of the modulus of elasticity of polymer concrete specimens obtained by using fly ash and river sand as fillers and orthophthalic and isophthalic polyester resin as binders. They used the mixing ratios determined as cost-effective in their previous studies. The amounts of fly ash constituted 8%, 12%, 16% and 20% of the aggregate in

different batches. As a result of this study, polymer concretes with compressive strength values ranging from approximately 100 MPa to 120 MPa were obtained. It was reported that fly ash increased the modulus of elasticity and compressive strength of polymer concrete.

Jafari et al. (2018) investigated the effect of the amount of resin used on mechanical properties in order to obtain the appropriate polymer/aggregate ratio in the production of polymer concrete. Damaged and undamaged experiments were carried out on specimens produced using 10%, 12% and 14% epoxy resin and aggregates of two different grain sizes (4.75-9.5 mm and 9.5-19 mm) and conditioned at temperatures of -15 °C, 25 °C and 65 °C. As a result of their studies, it was stated that the increase in the amount of epoxy resin and aggregate grain size increased the mechanical properties, but the increase in temperature decreased the strength. The best compressive and bending strength values were obtained for specimens with epoxy resin content of 14%, aggregate grain size of 9.5-19 mm and conditioned at -15 °C.

Another research on polymer concretes produced with polyester resin is the effect of plastic waste addition on the mechanical properties of polymer concrete by Bulut and Şahin in 2017. Unsaturated polyester resin, quartz sand and gravel as filler material and plastic waste were used in the production phase. The mechanical properties of the specimens prepared with three different resin/filler ratios (10-90%, 15-85% and 20-80%) were compared by adding plastic waste at 0%, 5%, 15% and 25% of the filler material. The experimental results showed that the increase in the resin content increased the compressive strength of the specimens as the resin wrapped the filler material better and formed a strong adherence. It was reported that the highest compressive strength of 76.3 MPa was obtained in specimens with 15% resin content. It was observed that the addition of plastic waste decreased the compressive strength, but this decrease was less at 5% usage. 17.1 MPa bending strength was obtained in specimens produced with a resin/filler ratio of 15-85% and 5% of the filler material with the addition of plastic waste. As a result of their study, they stated that the use of 5% plastic waste in the repair of concrete and asphalt roads in order to save energy, protect the environment and reduce costs will not cause any negativity (Bulut and Şahin, 2017).

Krzyzak et al. (2018) studied the behavior of the specimens obtained by using epoxy and expanded perlite between 0 and 32% by volume at high temperatures. The temperature values measured on the surfaces of the specimens and the mass losses occurring were revealed with experimental data. It was stated that the mass loss decreased with the increase in the proportion of expanded perlite, while the specimens without perlite deteriorated faster under

the influence of high temperatures. In the specimens where expanded perlite was used to form a layer on top, temperature values above 1000 °C were observed on the melting surfaces and it was observed that these layers were protective layers against heat transfer.

Pervious concrete differs from traditional concrete in that it contains interconnected voids. Only coarse aggregate, especially crushed stone, is used more in concrete and fine aggregate is not used. Thus, it is more air and water pervious than conventional concrete. Pervious concrete is also called "pervious sandless concrete" or "porous concrete". (Bilgiç,2019)

The first and most important environmental benefit of pervious concrete is that it allows rain-flood water and surface runoff water to infiltrate underground. The infiltration of rainwater into the ground provides a great benefit to the renewal of groundwater. With increasing urbanization and decreasing rainfall rates, the underground water system is being damaged more and more every year, especially in cities. Pervious concrete helps water to permeate into the ground at the same rate as open soil areas, and sometimes even faster. This is because the water passing through the concrete evaporates less and more water can pass into the soil without being exposed to the open air. (Bilgiç,2019)

Due to population growth, rapid urbanization and construction, the consumption of natural resources and the problems arising from this consumption are increasing day by day. For this reason, scientists and technical staff are seeking to develop different methods to find solutions to these problems. Decreasing impervious surface area due to urbanization is one of these problems. Pervious concrete, a special type of concrete that helps rapid drainage of rainwater that cannot be transferred to the soil and transfer it to subsoil layers, is an innovative alternative to solve this problem. Pervious concrete has become increasingly popular due to its various ecological benefits, such as reducing rainwater noise between the pavement and the tire, reducing urban heat island effects, and partially retaining pollutants that may enter groundwater. Due to these environmental benefits, pervious concretes are increasingly being used in parking lots, driveways, secondary roads, sidewalks and walkways. Pervious concretes are considered a sustainable material, especially due to its open pore structure, and many of its positive properties are attributed to its open pore structure. This structure is associated with the macro-sized and interconnected nature of the voids within the concrete. This structure can usually be achieved with coarse aggregates with batch gradation. (Canbaz ve Çelikten, 1999)

In recent years, excessive rainfall due to climate change has jeopardized the safety of life and property in cities. This situation is more prevalent in

cities where the soil-air relationship is largely cut off due to concretization and rainwater is prevented from being absorbed by the soil.

In particular, pavements and roads to prevent urban deformations caused by increased flooding and excessive rainfall, to direct rainwater to the ground, to reduce the amount of water discharged by urban infrastructure, to regulate the atmospheric balance between soil and air and to allow groundwater renewal, It would be beneficial to use pervious concrete in construction works such as car parks, low water crossings, tennis courts, traditional concrete paving, slope stabilisation, greenhouses, aquatic centres and zoos, hydraulic structures, pavement drainage, spur and bank walls, noise barriers, walls.

The unit weight of pervious concrete is between 1500 and 1800 kg/m3 and the optimum Dmax is 12.5 mm. The Dmax value is usually limited to 22 mm. The reason for this limitation is to provide sufficient surface area for aggregate bonding, which can affect the mechanical and physical performance of pervious concrete. To obtain pervious concrete, the water/cement ratio is usually chosen in the range of 0.30-0.40. The compressive strength of pervious concrete generally ranges from 2.8 to 28 MPa and the bending strength from 1 MPa to 4 MPa.

The void content in pervious concrete affects infiltration rates and compressive strength. Optimisation of the mix design is necessary to determine the appropriate void content. Many studies have concluded that the properties and performance of pervious concrete depend on the water/cement ratio, aggregate/cemented material ratio, aggregate sizes and grades, type of binder material and compaction techniques.

A small amount of fine aggregate, typically 5-7%, is used to increase freeze-thaw resistance and improve mechanical properties. It has also been found that the use of mineral admixtures and superplasticisers increases the compressive strength, while the use of silica fume reduces the permeability of pervious concrete due to its fineness.

Pervious concrete helps to replenish groundwater, reduce slime pollution, prevent erosion, control local storm sewer systems and control the life cycle of a living entity in the aquatic ecosystem and terrestrial ecosystem. The use of pervious concrete allows rainwater to filter into the soil as a source of groundwater, so that surface runoff can be managed and aquifer levels in the soil can be maintained. It provides a great solution for stormwater management by integrating paving and drainage, therefore reducing the amount of land required to manage stormwater runoff and reducing the budget required for collection and detection systems for untreated stormwater runoff and the sewerage system. (Bilgiç,2019)

In this study, pervious concrete, the importance of which has been emphasized more in recent years, was obtained with polymer binders. With the polymer resin to be used instead of cement paste, it is aimed to improve the strength properties of traditional cementitious pervious concrete due to its hollow structure and to produce a material that is more resistant to environmental effects encountered in the application area and has a longer service life. In addition, the aggregate gradation to be preferred in order to provide high hydraulic conductivity at appropriate strength values in pervious concrete works has been studied.

2. Material and Method

Crushed stone and river sand as filling material, polyester resin as binder, hardener and accelerator were used in the production of pervious concrete with polymer binder.

In the experimental study, orthophthalic based unsaturated polyester resin was used as binder as seen in Table 1.

Table 1. Properties of Resin

Appearance	Colour	Odour	Flash Point	Resolution	Viscosity cps (25°C)	Specific Gravity
Liquid	Colourless	Strien odour	>23°C <60°C	Water insoluble	350-500	1.17

In the experimental study, the filling material shown in Figure 1.

1) Crushed stone (7-8) mm
2) River sand (3-4) mm
3) River sand (2-3) mm was used.

Figure 1. Pervious polymer concrete aggregates

Hardeners are accelerators or heat-activated chemicals that regulate the curing of polyester resin. They initiate cross-linking reactions between the resin and reactive monomers. In this way, solidification of the resin is provided. Methyl ethyl ketone peroxide (Mek Peroxide) was used as hardener in the experimental study.

Accelerators are used in the curing of unsaturated polyester resins with organic peroxides at room temperature. Accelerator activates the hardener and enables the reaction to start. Cobalt octoate was used as accelerator in the experimental study.

Firstly, cylindrical specimens with a diameter of 10 cm were prepared to determine whether permeability was achieved. In these productions, an specimens was made to determine the appropriate resin/aggragate ratio (R/A). Specimens were produced with (R/A) varying between 10% and 14% by mass for different aggregate granulometries. The specimens obtained are shown in Figure 2.

Figure 2. Pervious polymer concrete specimens

After it was determined that permeability was achieved, production was carried out in three-cavity moulds with 40x40x160 mm dimensions shown in Figure 3. to determine some physical and mechanical properties. During the production, two different aggregate types (crushed stone and river sand), three different granulometries (7-8 mm) (3-4 mm), (2-3 mm) and different ratios of polyester resin were used and their effects on physical and mechanical properties were investigated.

Figure 3. Pervious polymer concrete tests

3. Discussion

The unit weight of hardened polymer-bonded pervious concrete specimens was determined in accordance with TS EN 1015-10: 2001 standard. Unit weight values were calculated by measuring and averaging over three specimens for pervious concrete series with polymer binder. The unit weights of the specimens obtained by using different sizes of aggregates are shown in Figure 4.

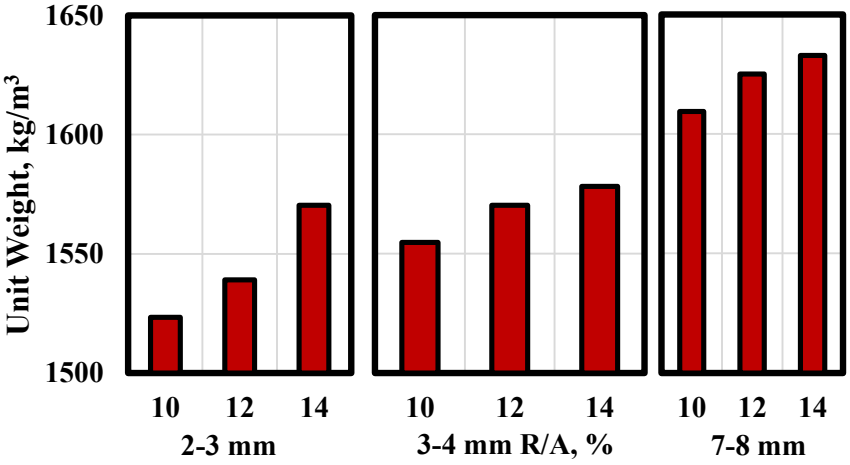

Figure 4. Unit weights of pervious polymer concrete

The ratio of the void volume of a material to its total volume is defined as porosity and is expressed as %. Materials with voids have high porosity. The porosities of the specimens obtained by using aggregates of different sizes are shown in Figure 5.

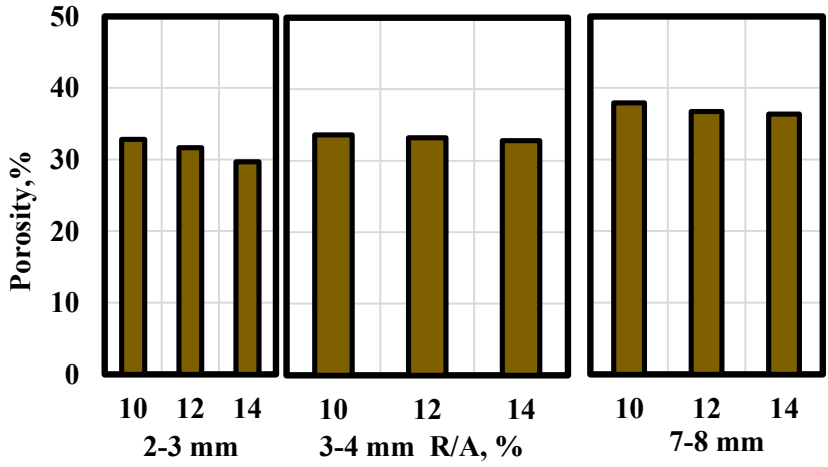

Figure 5. Porosity of pervious polymer concrete

Ultrasonic pulse test is one of the non-destructive test methods used for easy and harmless determination of concrete quality. It is based on the determination of the propagation speed of ultrasonic pulse waves generated between the transmitter and receiver sensors of the ultrasonic tester in concrete (Zebari et al., 2017). Ultrasonic pulse velocity values were obtained by dividing the length of the specimen by the passage time of the wave. The results are shown in Figure 6.

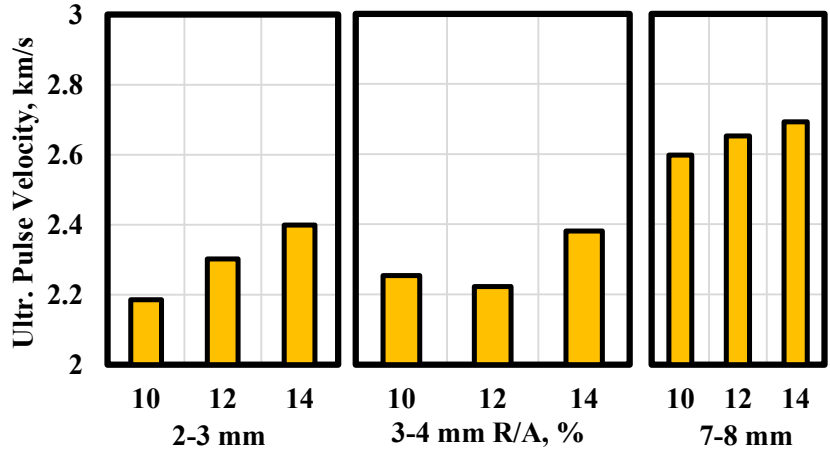

Figure 6. Ultrasonic pulse velocities of pervious polymer concrete

Pervious concretes are mostly preferred for concrete roads. Bending strength is more effective as strength in concrete roads and bending strength is more experimentally investigated. In this study, bending test with loading from the centre point, also known as three-point, was performed. Determined bending strengths are shown in Figure 7.

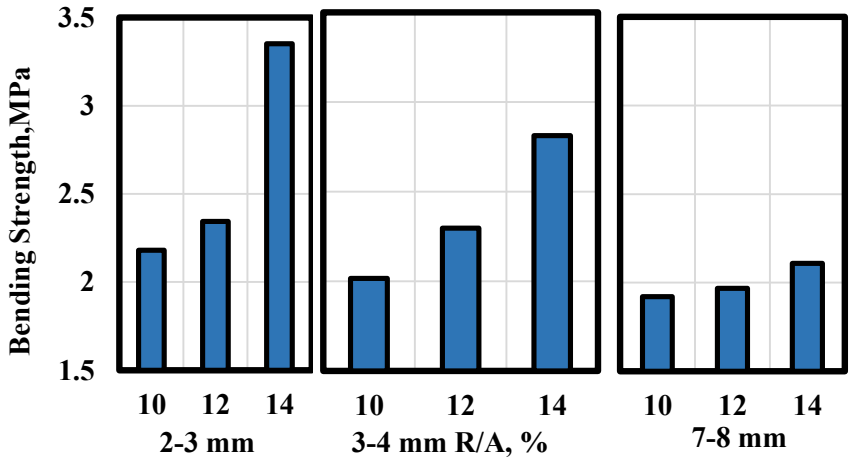

Figure 7. Bending strength of pervious polymer concrete

4. Conclusion

It was observed that the porosity values of the pervious concretes varied between 28% and 38%, the specimens obtained by using crushed stone with 7-8 mm grain size contained more voids, while the specimens obtained by using river sand with 2-3 mm grain size contained less voids, and the increase in the amount of resin slightly reduced the void ratio.

It was observed that the ultrasonic pulse velocity values of pervious polymer concrete specimens varied between 2.1 and 2.7 km/h, the ultrasonic pulse velocity values of the specimens obtained by using crushed stone with a grain size of 7-8 mm were larger and the increase in the amount of resin increased the ultrasonic pulse velocity value slightly.

It was observed that the bending strength of the obtained specimens varied between 1.9 and 3.40 MPa, and the strength increased as the resin amount increased. Higher values were obtained in specimens produced with smaller grain size aggregates. The highest bending strength value was obtained in specimens with 2-3 mm grain size and resin/aggragate ratio of 14%.

At the end of the experimental study, it was determined that polymer binders can be used as binders in the production of pervious concrete. It is recommended to investigate the change of properties of pervious polymer concrete in aggressive environments.

Acknowledgements

This work has been supported by Eskisehir Osmangazi University Scientific Research Projects Coordination Unit under grant number #2022-2391.

References

Abdel-Fettah, H.A., El-Hawary, M., 1999, Flexural behaviour of polymer concrete, Construction and Building Materials, 13, p.253-262.

Bulut, H.A., Şahin R., 2017, A study on mechanical properties of polymer concrete containing electronic plastic waste, Composite Structures, 178, p. 50-62.

Bilgiç, E., 2019, Use of excess paste theory and ımage analysıs to ınvestıgate propertıes of pervıous concrete, Master of Science, İzmir Institute of Technology, p.3-7

Canbaz, M., Çelikten S., "Demiryolu altyapısı için geçirimli beton boruların tasarımı," Demiryolu Mühendisliği, no. 13, pp. 43-52, Jan. 2021.

Ersoy, H.Y., 2001, Kompozit Malzeme, Literatür Yayıncılık , s.11-13.

Fowler, D.W., 1999, Polymers in concrete: a vision for the 21st century, Cement & Concrete Composites, 34, p.449-452.

Geçirimli beton kılavuzu. 2018, Türkiye Hazır Beton Dergisi: T.C. Çevre ve Şehircilik Bakanlığı. p. 55-72.

Gorninski, J.P., Molin D.C.D., Kazmierczak C.S., 2004, Study of the modulus of elasticity of polymer concrete compounds and comparative assessment of polymer concrete and portland cement concrete, Cement and Concrete Research, 34, p.2091-2095.

Jafari, K., Tabatabaeian M., Joshaghani, A., Ozbakkaloglu, T., 2018, Optimizing the mixture design of polymer concrete: An experimental investigation, Construction and Building Materials, 167, p.185-196.

Krzyzak, A., Kucharczyk, W., Gaska, J., Szczepaniak R., 2018, Ablative test of composites with epoxy resin and expanded perlite, Composite Structures, 202, p.978-987.

Ohama, Y., 1997, Recent Progress in Concrete- Polymer Composites, Review Article, 5, p.31-40.

Saçak, M., 1998, Polimer kimyasına giriş, A.Ü.F.F. Döner sermaye işletmesi yayınları, s.1

TS EN 1015-10, 2001, Kâgir harcı-Deney metotları- Bölüm 10: Sertleşmiş harcın boşluklu kuru birim hacim kütlesinin tayini,Türk Standardları Enstitüsü, Ankara, s.1-3.

Zebari, Z., Bedirhanoğlu, İ., Aydın, E., 2017, Beton basınç dayanımının ultrasonik ses dalgası yayılma hızı ile tahmin edilmesi, Mühendislik Dergisi, 1, s.43-52.

CHAPTER II

THE USABILITY OF MECHANICAL ALLOYING TO IMPROVE THE SELF-CLEANING PERFORMANCE OF BUILDING MATERIALS

Serdal ÜNAL[1] & Abdurrahim Emre ÖZDEMİR[2] & Mehmet CANBAZ[3]

[1](MSc), Eskişehir Osmangazi University, Institute of Science,
E-mail: serdalunall@gmail.com
ORCID: 0000-0002-5200-9969

[2](MSc), Eskişehir Osmangazi University, Institute of Science,
E-mail: emreozdemir1989@hotmail.com
ORCID: 0000-0002-8395-0401

[3](PhD), Eskişehir Osmangazi University, Department of Civil Engineering E-mail: mcanbaz@ogu.edu.tr
ORCID: 0000-0002-0175-6155

1. Introduction

Ball mill grinding is a simple and efficient method for producing submicron or nanostructured powders. Ball milling is widely used for the production of nanocrystalline materials. In the literature, the difference between the terms mechanical alloying and mechanical grinding is that mechanical alloying is defined as the process of grinding mixtures in powder form (different elements or compounds), while mechanical grinding is defined as the grinding of powders of uniform composition (pure metals or alloys). While only grain size reduction is desired in mechanical grinding, compound formation is also desired in mechanical alloying. Mechanical alloying process is used as a general term covering both mechanical grinding and mechanical alloying (Erkuş, 2019).

Mechanical alloying is one of the interesting and rapidly developing methods for the preparation of nanostructured powder materials on an industrial scale (Avar et al; 2019). Compared to solidification, it is easier to obtain the nanocrystalline phase by mechanical alloying. Since the mechanical alloying process takes place in the solid state, the conditions determined by the equilibrium diagrams can be exceeded. Therefore, it is possible to produce nanocrystalline alloys in a wider composition range at room temperature by mechanical alloying. Although many theoretical models describing the alloying process have been studied in order to predict the product obtained after alloying, the basic mechanisms of alloying are still unclear. The ball alloying energy induces significant mechanochemical phase changes during the ceramic powder production process. In addition, the products obtained from alloying can consist of many different phases, including contamination from the mill (Çelik, 2017).

There are many different types of mills used in the mechanical alloying of different elements and compounds. Spex mixer mill, vibrating mill, planetary ball mill, atritor mill are some of them. Among these mill types, the planetary ball mill is the most frequently used mill type. During the ball alloying process, it has been observed that the powders undergo elastic and plastic deformation due to the high energy generated between the balls and the grinding vials. During alloying, three different processes take place: cold-boiling, crushing and annealing of the powder particles. Mechanical alloying with a ball mill is a very complex process as the process depends on many process variables such as mill type, grinding conditions, temperature, chemical structure of the powder and properties of the grinding conditions (Timuçin et al., 2012).

The planetary mill is named after the planet-like movements of the grinding elements. The grinding vial on a rotating disk is also rotated around its own axis by a special mechanism. The centrifugal forces generated by the rotation around its axis and the rotation on the supporting support act on the contents inside the grinding vial. The forces generated by the reciprocal rotations also act in opposite directions and cause a frictional effect that causes the material to grind. As the balls inside the grinding vial become airborne and move through the vial, they collide with the walls of the vial and create the impact effect. The balls and powders in planetary ball mill vials are shown schematically in Figure 1 (Soni, 2000).

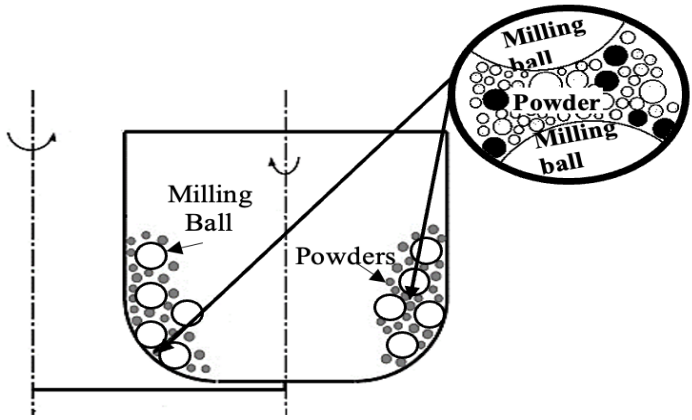

Figure 1. Representation Of The Movements Of Milling Balls And Powders İn Planetary Ball Mill.

2. Mechanical Alloying Mechanism

Planetary ball mills move in a similar way to the movement of the planets around the sun. In mechanical alloying, mixed powders or pre-alloyed powders are loaded into the abrasion vial together with the abrasive and subjected to severe deformation. In this process, the powder particles are flattened in cycles, broken by cold welding and welded again. The fracture and boiling processes, as well as their velocities and dominant states, depend mostly on the deformation properties of the initial powder. The initial impact of abrasive balls causes flattening and cold deformation of ductile metal powders. Severe plastic deformation increases the surface volume fraction of the particles and cracks on the surfaces of the absorbed contaminants. Brittle intermediate metal powders disintegrate and decrease in size. Oxide dispersed particles disintegrate much more severely (Suryanarayana, 2001). Figure 2 shows the collision motions between vials and powder particles in a planetary ball mill. With continued mechanical deformation, there can be a reduction in the particle size of the fragments formed by this mechanism, and with an increase in the surface energy of the material, there can be other significant changes affecting the surface as well as chemical, physicochemical and structural properties. This is manifested by the presence of various crystal differentiations such as increased grain boundaries, voids, stacking defects and deformed and broken chemical bonds. Consequently, the alloying of mixtures of two or more solids causes micro-homogenization of the starting components and induces the formation and synthesis of new fine particles (Lü and Lai, 2013).

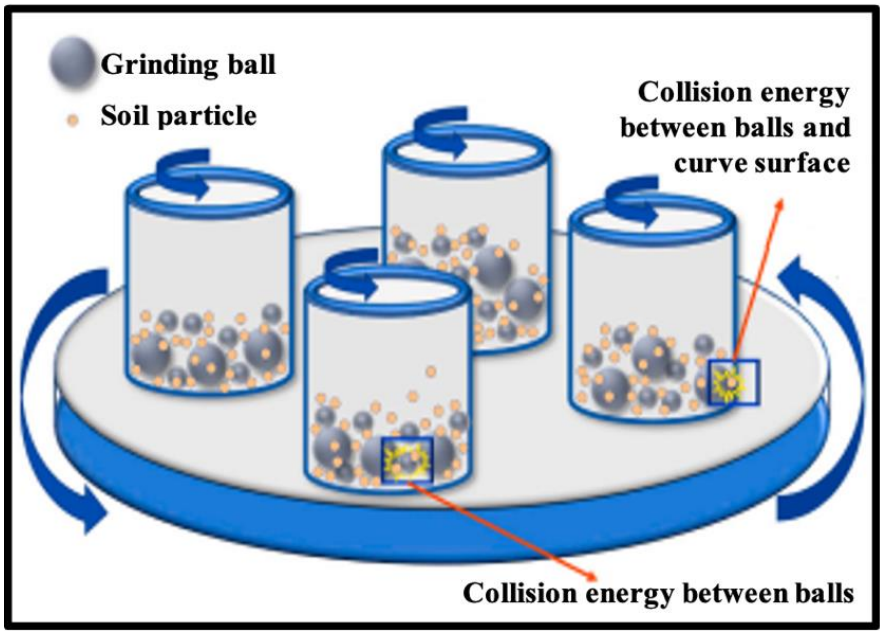

Figure 2. Collisional Movements Between Vial and Powder Particles in Alloying with Planetary Ball Mill.

Mechanical alloying has been applied to many different powder mixtures. Different alloying systems have been found according to the type of grinding material used and the mechanical, mutual reactivity and solubility properties of the components. Benjamin and Volin described the five progressive stages of alloying as follows.

a) Flattening of particles: The particles are crushed into a thin layer.

b) Particles begin to coalesce: The flattened particles coalesce to form thin layered structures or stratified compound particles.

c) Formation of equal-sized particles: The layered structures are no longer flat, but thinner and rounder. This shape change occurs after extreme deformation of the powders.

d) Random coalescence orientation: Particles of similar size begin to coalesce in different directions and the layered structures become smaller.

e) Stabilization: The structure of matter begins to form gradually as particles formed in different directions coalesce [Benjamin and Volin, 1974].

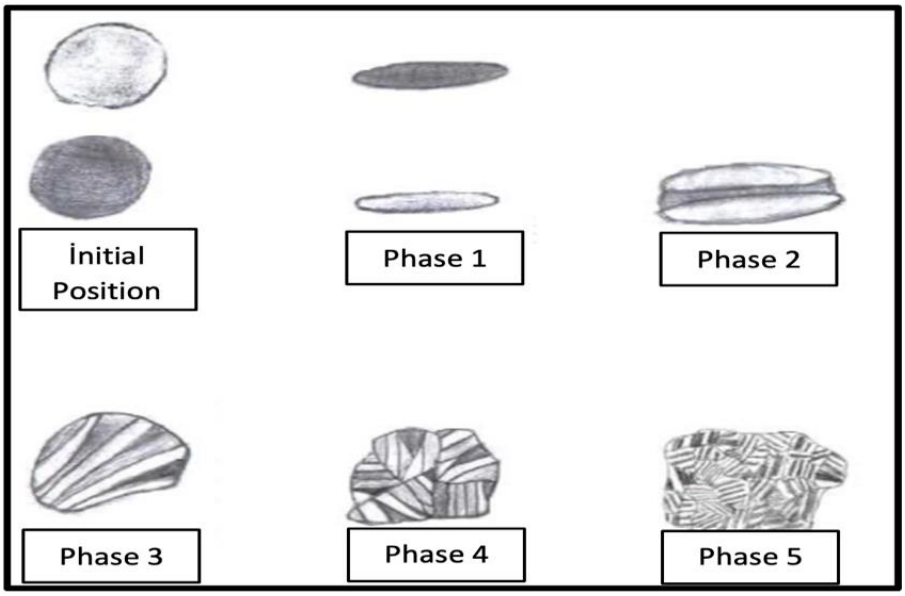

Figure 3. Five Phases of Mechanical Alloying.

The starting powders to be mechanically alloyed can be two or more metallic, intermetallic or dispersoid powders. The mechanical alloying process starts with the disintegration and mixing of two or more original powders, which are combined after a certain period of grinding (dry or wet) to obtain the final product. The morphology of the powder exposed to the impact of the balls is modified. The effect of ball impact on the milled powders depends on the type of powder components. When powders are cold welded and excessively mechanically deformed as a result of initial ball-powder-ball collisions, it leads to flattening and hardening of the ductile metal. Therefore, the powders flatten and coalesce and atomically clean metal interfaces are formed. This results in very close contact between the powders and a layered composite structure consisting of various combinations of powder components (Erkuş, 2019)

3. Grinding Systems in Mechanical Alloying

There are three different grinding systems in the mechanical alloying method. These are: Ductile - Ductile, Ductile - Brittle, Brittle - Brittle. In the early stages of grinding, the powder particles are ductile (if ductile-ductile or ductile-brittle powder combinations are used) and have a high tendency to weld together to form large powder particles. At this stage, the particle size can grow,

reaching up to three times the initial particle size. To control this, process control additives are added to the composition. At this stage of grinding, the composite particles have a stratified structure containing various combinations of the initial powder mixtures. With continued deformations, hardening continues, either by a fatigue mechanism or by re-fracture of the brittle laminated powder particles. In the absence of strong agglomeration forces, the size of the powder particles formed by this mechanism continues to decrease. Due to the continued impact of the grinding balls, the structure of the particles becomes stable and homogeneous in terms of initial composition. However, the particle size remains the same. Figure 4 shows a scanning electron micrograph showing the curved lamellar structure obtained during the grinding of a ductile-ductile component system (Ag-Cu) (Suryanarayana and Al-Aqeeli, 2013).

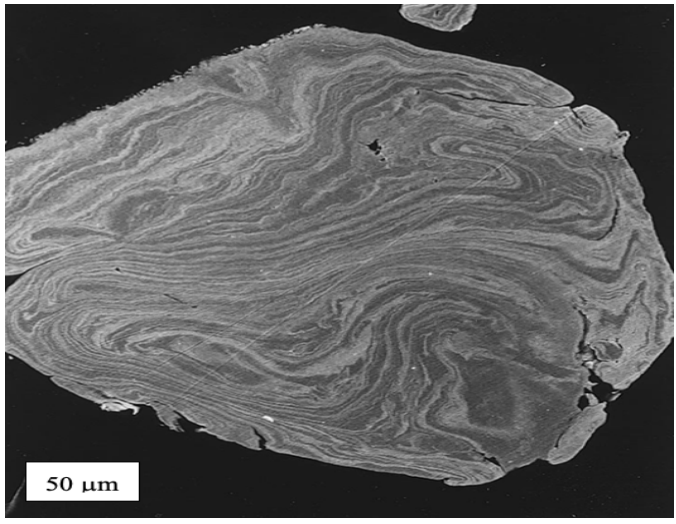

Figure 4. Electron Micrograph Showing The Curved Structure Obtained During Grinding Of A Ductile-Ductile Component System (Ag-Cu).

In the ductile-brittle system, ductile metal powders are first flattened by ball-powder-ball collisions, while brittle powders are broken. The broken brittle powders are embedded in the ductile component. Brittle components settle along the gaps between the layers. As a result of progressive grinding times, the powders undergo deformation hardening, the layers multiply and become smaller in size. With continued grinding, the layers become even smaller, the interlayer space increases and if the brittle powders do not dissolve, they are regularly dispersed into the ductile matrix. Figure 5 shows a schematic of the microstructural evolution during grinding of a ductile - brittle powder combination (Suryanarayana, 2001).

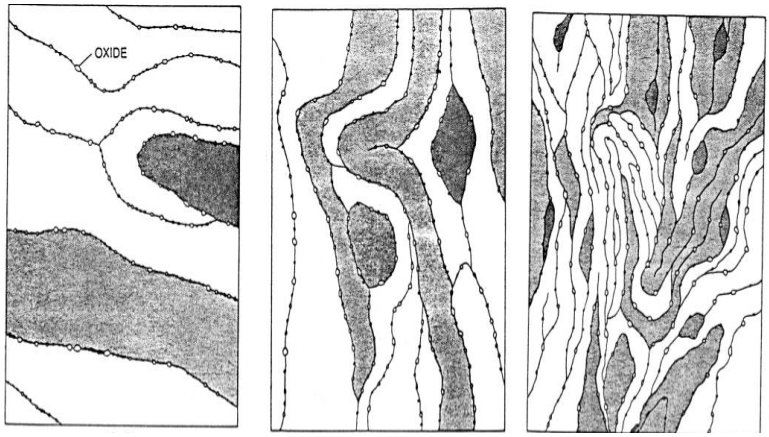

Figure 5. Schematic Of Microstructural Evolution During Milling Of A Ductile - Brittle Powder Combination.

In systems comprising two or more brittle materials, alloying might not be anticipated. This is due to the lack of a ductile component, which prevents welding or joining, and alloying is not expected to take place in the absence of welding. Nonetheless, alloying has been observed in certain brittle-brittle systems, such as Si-Ge and Mn-Bi. Brittle powders disintegrate during grinding and the particle size decreases continuously. However, powder particles of very small size show a ductile behavior and no further size reduction is possible. This is also called the grindability limit. Figure 6 shows a transmission electron micrograph showing the homogeneous distribution of Er_2O_3 particles (Suryanarayana, 2001).

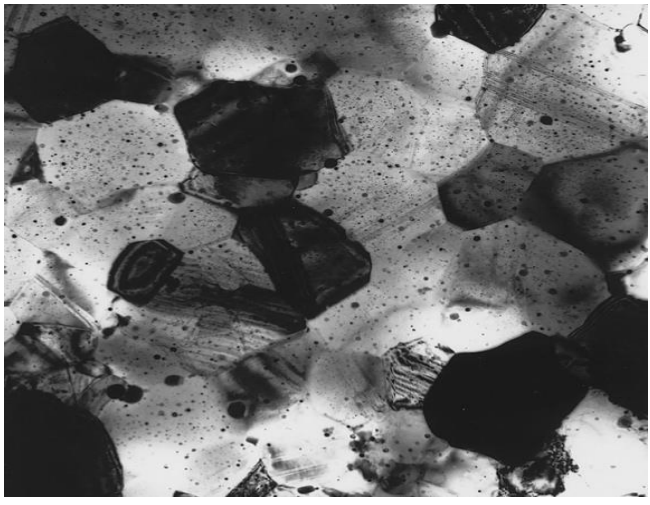

Figure 6. Electron Micrograph Showing Distribution Of Er_2O_3 Particles İn A Mechanically Milled Titanium Aluminide Alloy Matrix.

4. Mechanical Alloying Parameters

The variables affecting the alloying process in mechanical activation are as follows:

- Initial powder size
- Mill type
- Alloying material
- Ball diameter
- Sample rate
- Occupancy rate in the environment
- Mill atmosphere
- Alloying speed
- Alloying time
- Alloying vials

Initial powder size: In the mechanical alloying process, pure powders or pre-alloyed powders with an initial powder size distribution range from 1 μm to 200 μm are used. Powder size is one of the most important parameters in mechanical alloying. When the initial powder size is coarse, sufficient mechanical alloying does not take place in the specified time and the time needs to be increased. However, in this case, excessive contamination occurs and this facilitates the emergence of unwanted different phases in the structure.

Mill Type: There are different types of high energy grinding devices used in mechanical alloying. Commonly used mills are SPEX shakers, planetary ball mills and atritor type mills. SPEX shakers are laboratory type grinders that can grind about 10-20 g of powder at a time. This type of grinder has a container that holds the grinding balls and the powder to be ground, and after the powders and balls are placed in this container, the device is shaken back and forth several thousand times per minute. The movement of the container during grinding can be described by an infinity sign. With each rocking of the vial, the balls strike the powder particles and/or the vial lids, thus performing the grinding process. Another type of grinder used for mechanical alloying is the planetary ball mill. The vials of these grinders move in a planet-like motion, hence their name. These vials are placed on a rotating carrier disk and rotate on this disk, which is rotated by a special mechanism, and on their own centers. Due to the centrifugal force created by both the carrier disk and the grinding vials rotating in its own center, the main material and grinding balls inside the grinding vials move (Kaçakgil, 2021).

Ball Diameter: Alloying time increases with increasing ball diameter. Because; small diameter balls cause rapid particle shrinkage as they provide more impact effect for a given volume. If extremely fine powder size is desired to be obtained at the end of grinding, the ball diameter should be increased. In addition, another point to be considered in the use of balls is that the balls should be selected from a wear-resistant material. Thus, contamination that may occur as a result of alloying can be prevented.

Alloying speed: The higher the speed of the mill, the higher the energy input to the solid. However, there are certain limitations to the maximum speed that can be used depending on the mill design. For example, by increasing the rotational speed in a conventional ball mill, the speed of movement of the balls will be increased. Above a critical speed, the balls will become attached to the inner walls of the vial, thus failing to fall and exert any impact force. Therefore, it is imperative to maintain the velocity just below this critical threshold, ensuring that the balls fall from their maximum height to generate the utmost impact energy. Another constraint at maximum speed is the potential for elevated vial temperatures due to the high speeds (or grinding intensity). In some cases, this may be a necessary parameter to promote homogenization and/or alloying of the solid. However, in some cases, this increase in temperature can be a disadvantage because the increased temperature accelerates the transformation process and causes the separation of saturated solid solutions or other semi-stable phases formed during alloying. In addition, the high temperatures generated can also contaminate the solids. During nanocrystal formation, the average crystal size is reported to increase due to increased dynamic recrystallization at higher milling intensities.

Alloying time: Alloying time is one of the most important parameters. The times required vary depending on the type of mill used, density, ball-to-material ratio and temperature. Each combination of these parameters should be decided according to the solid to be used. However, it should be noted that if the solid is milled for longer than required, the level of contamination increases and some undesirable phases are formed.

Ball/Material ratio: The ratio of ball to solid material by mass is an important variable in the alloying process. This has been studied by different researchers from 1:1 to a very low value of 220:1. This ratio has specific effects required to achieve a certain phase in the solids being alloyed. At a high ball-to-material ratio, due to the increase in the mass ratio of the balls, the number of collisions per unit time increases and, as a result, more energy is transferred to the solid particles and thus product formation occurs faster.

Mill atmosphere: The mill atmosphere is also an important variable for the mechanical alloying process. The biggest impact of the mill atmosphere is dust pollution.

Alloying vial: In mechanical alloying, the material of the grinding vial is as important as the material of the balls. Because due to the impacts of the grinding balls on the inner wall of the vial, some of the material of the vial breaks away from the surface and mixes with the powder. This changes the chemical structure of the powder. For this reason, hardened steel, tool steel, hardened chromium steel, WC-Co are generally used as grinding vial materials (Güler, 2006).

5. Advantages of Mechanical Alloying

Mechanical alloying and mechanically alloyed materials have many advantages. We can list these advantages as follows:

- Although the alloying process is a solid state process, one of the phases that make up the composition may sometimes be present in the liquid phase. Some nitrides can also be produced by means of the atmosphere used in the alloying process.
- Mechanical alloying is one of several new processing techniques that enable the design of advanced materials.
- Alloys that are overly stable or have limited solubility within each other can be produced with higher dissolution rates.
- The most important role for the strength of ODS materials is played by the oxide particles homogeneously distributed in the matrix. These particles constitute an important barrier for dislocation movements. With mechanical alloying, it is possible to produce oxide particles very small (5-50 nm) and very close to each other (100-150 nm) in the structure.
- The structure of the powders obtained by mechanical alloying can be obtained completely homogeneous. Thus, the segregation problem is completely eliminated.
- Mechanical alloying is basically a powder metallurgy technique in which solid materials are processed in an inert environment in a ball mill. Liquids can be present in the process as a control agent or reactant.
- Unlike other production methods, thermodynamically alloying has no compositional limitations. Thus, it is possible to produce materials with very wide and unusual compositions.

- It reduces the production cost of materials and alloys and enables them to be produced directly.
- It is possible to produce materials resistant to external influences.
- Suitable for fabrication.
- It is possible to produce and alloy a large amount of powder at a time.
- Considering the performance / unit price, it makes it possible to produce cheap materials (Milli; 2017).

6. Self-Cleaning By Mechanical Alloying

Self-cleaning performance of semiconductors can be improved by mechanical alloying. Self-cleaning of cementitious substrates is a topic that has recently been highly investigated. The self-cleaning effect occurs by photocatalysis reaction. Semiconductor materials are required for photocatalysis reactions to take place. Semiconductors are materials with a filled valence band and an empty conduction band in their atomic structure. Bands are the possible energy levels that an electron can occupy in a material. A band filled with electrons and an empty band are separated by a band gap. In semiconductors, the width of the band gap is smaller than in electrical insulators, but they have a larger band gap compared to metals (Vasilache et al., 2012). Electrons in the outer orbital are called 'valence electrons'. The main task of valence electrons is to ensure the bonding of atoms with each other. The band at the highest energy level where valence electrons are located is called the valence band. The band located outside the valence band and at the lowest level is called the conduction band. If a photon is absorbed from a UV source or from the visible region of the electromagnetic spectrum, an electron in the valence band is excited and jumps to the conduction band, creating a vacancy for that electron in the valence band. The reaction thus results in an excited electron(e^-) - positive hole(h^+) pair. This e^- - h^+ pair undergoes reduction and oxidation reactions of chemicals on the surface of the photocatalyst. The chemical structure of the semiconductor material remains unchanged if equal numbers of e^- and h^+ are consumed during the reactions (Ünal and Canbaz, 2022; Ângelo et al., 2013).

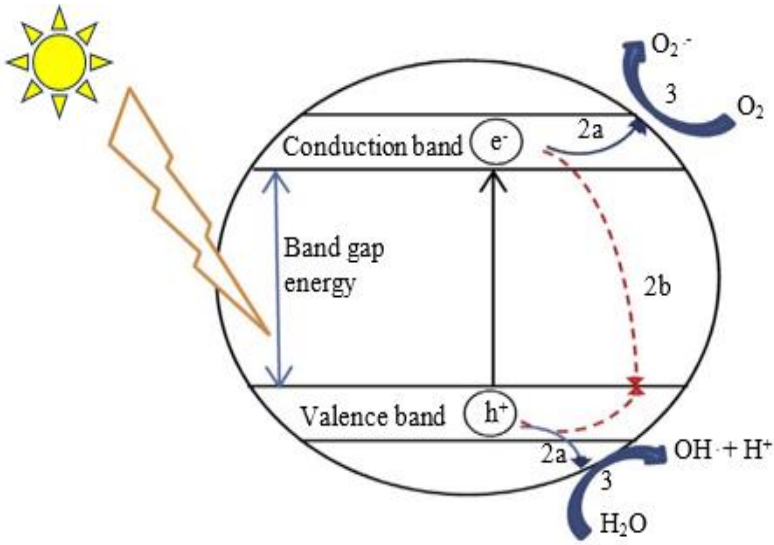

Figure 7. The Main Reactions Of The Photocatalysis Mechanism Are: Electron-Hole Pair Formation (1), Separation And Migration Of Charges To Surface Reactions (2a) And Recombination (2b), And Active Surface Chemical Reactions (3) (Ângelo Et Al., 2013).

For the photocatalysis mechanism to be activated, the photon energy from the light source must be equal to or higher than the band gap energy of the semiconductor. Otherwise, the electron-vacancy pair will not be formed. The formed electron-hole pair comes to the surface by diffusion and performs oxidation and reduction reactions (Nakata and Fujishima, 2012).

$$E_{photon} > E_{bg} \quad (1)$$

The photomineralization (degradation of organic compounds) of organic compounds on materials by photocatalysis reactions can be easily understood by the following master equation (Carp et al., 2004):

$$\text{Organic Compound} \xrightarrow{Semiconductor} CO_2 + H_2O + \text{Mineral Asid} \quad (2)$$

7. Self-Cleaning Application with Mechanical Alloying

7.1. Method

Concretes that decompose organic compounds that come on it due to natural or human-induced pollutant sources with the photocatalyst in its structure are called self-cleaning concretes. Titanium dioxide (TiO_2) is generally used as a photocatalyst in self-cleaning concretes. However, it has been observed that the photocatalytic activity capabilities of these concretes are limited due to the high band gap energy of TiO_2 used as photocatalyst and the need to improve these

capabilities has emerged. In the researches, the idea of modifying TiO_2 with various metals has come to the forefront. With this in mind, this study aims to investigate the photocatalytic properties and activity times of TiO_2-containing concretes mechanically alloyed with zinc (Zn). As a photocatalyst material in concretes, mechanical alloying of TiO_2 in anatase structure with zinc metal was carried out due to its high photocatalysis ability. The experimental studies aimed to determine the composition ratios showing the best photocatalytic performance. Fritsch brand planetary ball mill with a double container was used in mechanical alloying. The planetary ball mill, powders and balls of different diameters used in the study are shown in Figure 8.

Figure 8. Powders, balls and planetary ball mill used in alloying

In the process of modification of TiO_2 powder, the ratios of Zn powder to be loaded into TiO_2 were first determined. As a result of preliminary studies, 5% and 15% Zn was loaded into TiO_2 as optimum ratios, especially for the mechanical alloying method. While determining the weights, attention was paid to the realization of effective collision in the vials. Balls weighing 1082.78 g were placed in the first vial and 1082.29 g in the other vial. Three different diameter balls (8mm, 14mm, 20mm) were selected for effective collision. These balls were added to both containers in the same number. As a result of the preliminary studies; ball weight/powder weight ratio was determined as 10:1, rotation speed as 200 rpm and rotation time as 4 hours. The weights of the powders and balls in the vials of the planetary ball mill are shown in Table 1.

Table 1. Amount of ingredients in the planetary ball mill.

	Ball (gr)	**TiO_2 powder (gr)**	**Zn powder (gr)**	**Total powder (gr)**
1.Vial	1082.78	103.12	5.156	108.278
2.Vial	1082.29	94.112	14.116	108.229

7.2. Results

Cube concrete specimens with dimensions of 7 × 7 × 7 cm were produced with Zn-TiO_2 powder compounds obtained by mechanical alloying. The concrete specimens produced consist of four different groups. These groups are: Control specimens, specimens containing unmodified TiO_2 at 5% of the cement content, specimens containing TiO_2 modified with Zn at 5% of the TiO_2 content and specimens containing TiO_2 modified with Zn at 15% of the TiO_2 content. These four groups are coded as 0T0Zn- 5T0Zn- 5T5Zn- 5T15Zn respectively. These concrete samples were stained with the Rhodamine-B contaminant specified in the Italian UNI 11259 standard and self-cleaning experiments were carried out in a closed environment and the color change rates on the concrete sample surfaces at the end of 26 hours and 7 days were calculated. Table 2 shows the discoloration values of the specimens at the end of 26 hours and 7 days.

Table 2. Degradation rates after 26 hours and 7 days

	0T0Zn (%)	**5T0Zn (%)**	**5T5Zn (%)**	**5T15Zn (%)**
26 Hours	4.75	45.81	51.28	52.89
7 Days	20.71	57.54	71.21	73.96

7.3. Discussion and Conclusions

When the 26-hour and 7-day decolorization values of the concrete samples were examined, it was observed that the maximum decolorization percentages were reached by concrete samples containing TiO_2 mechanically alloyed with Zn. This result proves that the mechanical alloying method is a valid method to improve the self-cleaning performance of the material in cementitious systems. 15% of TiO_2 alloyed with Zn is more effective than the samples containing 5% of TiO_2 alloyed with Zn. In the literature, there are studies on the alloying of TiO_2 with metals with high photocatalysis ability such as silver. In this study, TiO_2 mechanically alloyed with zinc using a planetary ball mill was found to positively improve the self-cleaning performance of TiO_2 on concrete surfaces. It is recommended that this study should be further investigated by mechanically alloying different photocatalysts with different metals to obtain self-cleaning performance on cementitious systems.

Acknowledgements

This work has been supported by Eskisehir Osmangazi University Scientific Research Projects Coordination Unit under grant number #2022-2334.

References

Ângelo, J., Andrade, L., Madeira, L. M., & Mendes, A. (2013). An overview of photocatalysis phenomena applied to NOx abatement. Journal of environmental management, 129, 522-539.

Avar, B., Şimşek, T., Göğebakan, M. (2019). Mekanik Alaşımlama ile Üretilen Nanokristal $Fe_{60}Al_{30}Cu_{10}$ (at. %) Tozların Yapısal ve Mekanik Özellikleri. Gazi University Journal of Science Part C: Design and Technology, 7(1), 184-191.

Benjamin, J. S., Volin, T. E. (1974). The mechanism of mechanical alloying. Metallurgical transactions, 5, 1929-1934.

Carp, O., Huisman, C. L., Reller, A. (2004). Photoinduced reactivity of titanium dioxide. Progress in solid state chemistry, 32(1-2), 33-177.

Cerrahoğlu K, E. (2021). Biyoatıklar ile Cu (II), Pb (II) VE Zn (II) gideriminde mekanokimyasal ön işlemin etkisi: Kinetik, termodinamik ve optimizasyon. Doktora Tezi. Kocaeli Üniversitesi.

Çelik, E. (2017). Mekanik alaşımlama yöntemi ile üretilen Co alternatifi FeCuNiSnPMoMn alaşımının sıcak presleme karakteristiklerinin incelenmesi. Fırat Üniversitesi Mühendislik Bilimleri Dergisi, 29(1), 145-150.

Erkuş, S. (2019). Mekanik alaşımlama yöntemiyle süperiletken magnezyum diborür (MgB_2) üretimi. Doktora Tezi. Eskişehir Osmangazi Üniversitesi.

Güler, Ö. (2006). Oksit takviyeli bakır kompozitin mekanik alaşımlama yöntemi ile üretilmesi ve elektriksel özelliklerinin incelenmesi. Yüksek Lisans Tezi.Elazığ: Fırat Üniversitesi.

Lü, L., Lai, M. O. (2013). Mechanical alloying. Springer Science & Business Media.

Milli, A. (2017). Mekanik alaşımlama yöntemi ile (B_4C+ FeTi) takviyeli Fe esaslı kompozit üretimi. Master's thesis. Tekirdağ: Namık Kemal Üniversitesi.

Nakata, K., Fujishima, A. (2012). TiO_2 photocatalysis: Design and applications. Journal of photochemistry and photobiology C: Photochemistry Reviews, 13(3), 169-189.

Soni, P. R. (2000). Mechanical alloying: fundamentals and applications. Cambridge Int Science Publishing.

Suryanarayana, C. (2001). Mechanical alloying and milling. Progress in materials science, 46(1-2), 1-184.

Suryanarayana, C., Al-Aqeeli, N. (2013). Mechanically alloyed nanocomposites. Progress in Materials Science, 58(4), 383-502.

Timuçin, M., Öztürk, A., Park, J., Karakaş, G. (2012). Mekanik bilyalı öğütmeyle yüksek etkinlikte fotokatalitik TiO_2 tozu ve nano boyutlu titanya sol üretimi.

Ünal, S., Canbaz, M. (2022). Effect of industrial wastes on self-cleaning properties of concrete containing anatase-TiO_2. Revista de la construcción, 21(3), 493-505.

Vasilache, V., Aghiniţei, E., Leluţiu, L., Benţa, M. D. (2012). Photocatalysis processes used for disinfection. A mathematical approach. reactions, 4, 5.

CHAPTER III

THE EVOLUTION OF MICROFLUIDIC TECHNOLOGY: A DECADE OF RAPID ADVANCEMENTS

Emre GÖRGÜN

Sivas Cumhuriyet University, Sivas Technical Sciences Vocational School, Railway Systems Department, Sivas, Turkey
E-mail: emregorgun@cumhuriyet.edu.tr
ORCID: https://orcid.org/0000-0002-1971-456X

1. Introduction

Over the last ten years, there has been a rapid and significant advancement in microfluidic technology, and this trend is expected to continue throughout the next decade. Microfluidics is a technology that involves manipulating small amounts of fluids at very small scales, even down to the nanoscale. It has had a significant impact on various fields, including biomaterial fabrication, drug discovery, diagnostics, single-cell analysis, and electronics. Microfluidics offers precise flow control and high integration, which has led to advancements in materials science and the development of new applications (Nge, Rogers, & Woolley, 2013). Microfluidic platforms have opened up interesting possibilities for creating nanomaterials with unique architectures in the field of biomaterial manufacturing (Cheng & Wu, 2012). Microfluidic technology provides a dependable approach for producing nanoparticles, microfibers, and 3D structures by carefully controlling the multiphasic flows and using highly regulated methods (Lee, Chang, Wang, & Fu, 2011). These structures have intricate shapes and can be adjusted according to their composition. Microfluidics revolutionizes cell manipulation by introducing advanced procedures that enable the accurate manipulation of cellular function development and provide novel insights into the field of cell biology. Moreover, the sophisticated functionalities of microfluidics, such as its ability to handle

large amounts of samples efficiently, minimal use of reagents, and capacity for parallel processing, make it an excellent medical diagnostic platform for the isolation of CTCs (circulating tumor cells) and analysis of individual cells. These applications have demonstrated significant potential, transitioning from basic research to industrial applications.

Currently, there is significant interest in the field of wearable electronics based on microfluidics, which combines flexible electronics with microfluidic devices for medical diagnosis and treatment. An inherent benefit of microfluidic chips is their ability to precisely control the movement of conductive fluids, thereby establishing a connection between electronic and biological processes. Microfluidic technology has the potential to fundamentally transform the current state of affairs and enable the development of novel applications. In this study, we investigated the influence of microfluidics on the production of biomaterials, manipulation of cells, and development of flexible electronics over the last ten years. Recent successful instances of microfluidic technology with a specific emphasis on human healthcare have been explored.

Technological breakthroughs in microfluidics sometimes stem from the development of novel compounds for equipment that provides trustworthy and long-lasting abilities. A variety of materials have recently been developed for manufacturing microfluidic instruments. Glass and silicon were utilized first, then paper, hydrogels, and polymers. In the early phases of microfluidic device development, silicon and glass were favored as substrates owing to their superior surface stability and accessibility. Unfortunately, the widespread use of microfluidics has been hindered by the high cost and strict requirements for silicon and glass. A novel type of liquid glass that does not require cleanroom space for the fabrication of microfluidic devices was developed. Amorphous silica nanopowder and a photocurable monomer mixture, which is readily reconstituted at room temperature, were combined to create this inexpensive liquid glass. Due to their affordability and longevity, polymeric materials including polystyrene (PS), polymethyl methacrylate (PMMA), polycarbonate (PC), and polydimethylsiloxane (PDMS) are now widely used in microfluidic devices.

PDMS is widely used in microfluidics-based systems owing to its low cost, easy surface modification, and excellent gas permeability. Researchers have recently created a 3D-printable version of PDMS, which is a material used to fabricate microfluidic devices. They achieved this using stereolithography printing. To ensure that the 3D-printable PDMS had properties similar to those of regular PDMS, they used commercially available silicone methacrylate

macromers for a process called radical photopolymerization. Ethyl phenyl phosphinate was used as the photoinitiator. The incorporation of high-resolution stereolithography printing with 3D-printable PDMS holds significant promise in advancing the production of microfluidic devices in the next phase of 3D printing. PDMS is particularly well suited for combining microfluidics with flexible electronics owing to its excellent biocompatibility and low modulus, making it an ideal substrate. However, some constraints persist for microfluidic devices based on PDMS. An important obstacle is the integration of rigid reinforcing components with flexible PDMS materials. Another obstacle pertains to the enduring stability of surface alteration using PDMS. Scientists have outlined a straightforward method for chemically attaching commonly used thermoplastic materials to silicone rubber. This involves treating the surfaces of oxidized thermoplastics with (3-aminopropyl) triethoxysilane to introduce amino groups, which are then further oxidized using ultraviolet ozone. Using laser printing, microfluidic devices can be manufactured immediately and inexpensively. This method presents a novel way to create microfluidic devices, offering benefits, such as scalability and a wide range of materials.

Recently, there has been significant interest in paper-based microfluidics because of its easy disposal, wetting by capillary action, and large surface area. Paper, which is a porous matrix made by compressing cellulose fibers, is an excellent material for microfluidic devices. Paper-based microfluidic technology has significant promise for customized healthcare owing to its adaptable nature and capillary-driven wettability (Fig. 1). A barcode-like paper chip was created for immunoassays with multiplexing using a fast mass-manufacturing technique. This study successfully demonstrated the creation of a paper-based printed circuit board using the technique of printing electrofluids onto paper. This method enabled the installation of standard circuit components. By employing this printing approach on paper, the integration of microfluidics and electronics offers promising prospects for enhancing the functionalities of paper devices. Electrospun nanofibrous membranes are a very promising material for microfluidic chips owing to their extensive surface area.

Microfluidic immunoassays may be performed on electrospun nanofibrous membranes, which provide a stable platform. When choosing the best materials for microfluidic devices, a number of elements must be considered, such as integration, cost, production, and modification. Silicon -polydimethylsiloxane (PDMS) is typically utilized in investigation facilities, whereas paper and plastics are more often encountered in microfluidic devices available for sale.

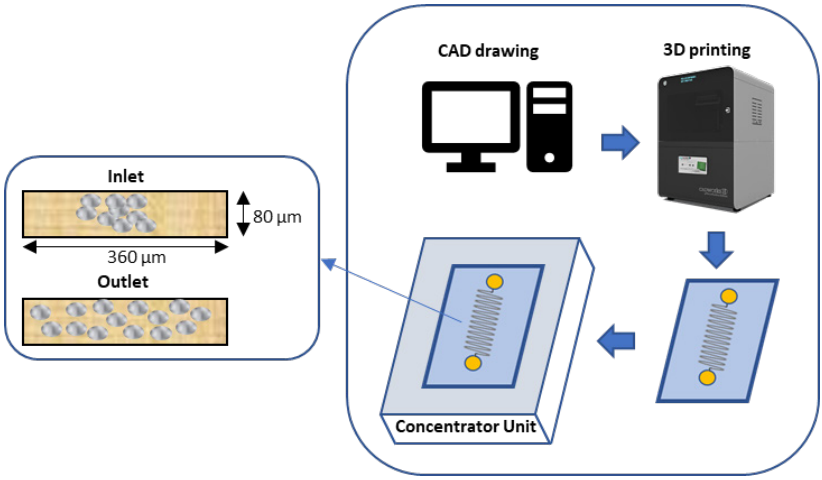

Fig. 1. Microfluidic production stages

The development of materials for bioapplications requires the precise placement of their architectural designs, such as stacked nano/microstructures, and the ability to screen their bioeffects in a multiplexed manner, such as in drug delivery. However, these processes are significantly hindered by batch approaches, which have inherent weaknesses including restricted throughput, poor repeatability, and mediocre selectivity. Microfluidics offers potential solutions to these requirements through the adaptable configuration of microreactors, meticulous regulation of reaction variables, simultaneous execution of several reactions, and incorporation of feedback mechanisms. In addition, microfluidics enables collaboration with emerging manufacturing ideas such as 3D printing to create novel materials or capabilities that are difficult to obtain using large-scale approaches. This section focuses on current advancements in microfluidics as superior substitutes for producing nanomaterials with prospective applications in biological systems.

2. Production

2.1. Nanoparticle Synthesis

Nanoscale particles have a wide range of applications, including sensing, drug delivery, bioimaging, catalysis, and diagnostic systems owing to their large specific surface area and impressive encapsulation ability. However, the current method of producing nanoparticles in batches presents a significant obstacle for their clinical implementation (Niculescu, Mihaiescu, & Grumezescu, 2022). Conventional techniques used for synthesizing batches of materials have a negative impact on the ability to reproduce an efficient and uniform size distribution in clinical research. In addition, it is challenging to perform rapid monitoring and

precise control of the mixing process during batch synthesis (Knauer & Koehler, 2014). A microfluidic arrangement offers a uniform environment in which flow characteristics can be precisely adjusted in small-scale capillary systems. Microfluidic technology offers precise control over the material characteristics owing to its small channel dimensions and significant surface-to-volume ratio. In recent years, significant efforts have been made to develop advanced biomaterials using microfluidics-based systems such as liposomes, polymeric nanoparticles, and organic and inorganic hybrid nanoparticles. In addition to the need for homogeneity, the ability to control structures is an important consideration (Niculescu, Chircov, Birca, & Grumezescu, 2021). PLGA-lipid nanoparticles were synthesized using a two-stage microfluidic process. The flexibility of nanoparticles can be readily adjusted while maintaining consistent chemical composition, size, and surface chemistry. Microfluidics can be used to precisely manipulate the introduction of varying amounts of water between the PLGA and lipid layers. This resulted in the formation of nanoparticles that were either hard (without a water layer) or soft (with a water layer).

In addition to the production of nanoparticles, microfluidic techniques have become more common in creating materials that are inspired by biology. This technique involves manipulating biological fluids in small channels, allowing for step-by-step assembly of artificial cells. These nanovesicles consist of a lipid bilayer that incorporates membrane proteins obtained from the leukocytes. Leukosomes, which are based on microfluidic technology, have a longer shelf life and maintain the basic capabilities of donor cells. The herringbone patterns in microfluidic channels may create chaotic fluid motion and enhance mass transfer, offering precise characteristics for lipid nanoparticles. This precise technology has greatly increased the complexity of artificial biology. Combining synthetic biology and microfluidic platforms that can be easily manipulated will stimulate innovative methods for building intricate and sophisticated synthetic cells.

2.2. Microfiber Production

In recent years, significant progress has been made in the field of micro- and nanofibrous development. These fibers possess exceptional qualities and properties, making them highly suitable for a range of applications, including smart textiles, drug delivery, tissue engineering, environmental protection, and energy generation/storage (Agnello et al., 2016). Various methods have been proposed for manufacturing these fibers. However, these methods are mostly restricted owing to inadequate control over the structure or lack of consistent and costly equipment. Progress in microfluidic platforms has led to significant advancements in fiber generation. Typically, manufacturing processes can be

categorized into two primary groups, distinguished by their respective solvent extraction and in situ crosslinking curative mechanisms. Innovative microfluidic methodologies employing capillary design have been devised to generate fibrous substances that exhibit a wide array of structural attributes (Ding et al., 2023). To achieve the large-scale production of helical microfibers, a scalable fabrication system based on coaxial capillary microfluidics was developed. This system involves pumping a Na-alginate solution as the inner fluid and $CaCl_2$ solution as the outer fluid in opposite directions (Razzaq, Serra, Jacomine, & Chan-Seng, 2022). Once the ratio of the inner flow rate to the outside flow rate reached a certain threshold, the liquid jet initiated the production of helical microfibers inside the channel, exhibiting a random orientation. By manipulating the flow rate, helical microfibers with a certain diameter and pitch could be produced. Helical microfibers, once combined with magnetic nanoparticles or N-isopropylacrylamide, exhibit exceptional adaptability for the creation of intelligent microsprings. Researchers have developed coaxial microfluidic devices that can produce necklace-like knotted microfibers that are capable of carrying fluids and are highly compatible with living cells. The device uses sodium alginate as the outer layer and a solution of $CaCl_2$ as the inner layer. The dispersion of Ca_2+ ions leads to the formation of a solidified calcium alginate layer, resulting in the creation of empty channels. Sodium alginate, which is not cross-linked, consistently drips into a solution of $CaCl_2$ and forms spindle-shaped knots. Specifically, owing to the absence of oil in the process, it is feasible to encapsulate and cultivate live cells inside tangled microfibers. This presents a significant opportunity for future research in the field of bioengineering. In addition to producing microfibers with various structures and compositions, microfluidic systems can also be used to create larger cables and microfiber-containing cells. This approach of using microfluidics is highly significant for manufacturing biomaterials and scaffolds with specific structures for tissue engineering. Compared with traditional methods of producing microfibers, microfluidic techniques offer precise regulation of blending and transportation processes, allowing for the creation of functional microfibers with desired structures and compartments. The limitation of using microfluidics-based microfiber manufacturing lies in its restricted throughput, which can possibly be solved by employing numerous devices in tandem.

2.3. Production of 3D Structures

Three-dimensional (3D) printing is a popular and efficient technique to create structures with specific geometries. It has been used in various fields such

as electrochemical devices, tissue engineering, adaptive robotics, and flexible electronics (He et al., 2015). Nevertheless, the advancement of 3D bioprinting has been hindered primarily by the challenge of accurately manipulating the positioning of various biomaterials or live cells to create complex 3D structures. Microfluidic technology enables accurate control over minuscule amounts of fluid inside the microchannels, making it well suited for additive manufacturing. Given the growing interest in 3D printing and microfluidics, novel advancements have been made to integrate these two methods for constructing 3D tissues. A novel 3D printing method is demonstrated using a custom microfluidic printhead, which enables the precise printing of two different materials. This programmable approach for assembling functional biomaterials significantly advances biofabrication technologies. Nevertheless, the development of intricately structured and efficient 3D tissues continues to encounter insurmountable obstacles. A CaCl2crosslinking solution was specifically formulated to serve as a structural template between several layers to ensure stability and prevent collapse (He et al., 2015, p. 3). Under the influence of UV light, GelMA undergoes covalent crosslinking to form three-dimensional structures. This method can generate high-resolution 3D structures and aid the development of in vitro heterogeneous biomimetic tissues. A recent study showcased a bioprinting platform that utilizes stereolithography and can fabricate several materials. This platform incorporates a microfluidic device that enables rapid switching among various bioinks. A typical digital micromirror device was used to pattern multiple materials. Compared to the current stereolithography platform, this bioprinting platform is capable of completing the washing process within a few seconds, resulting in a considerable improvement in printing speed. The future potential of this resilient platform is vast, particularly for the manufacture of intricate structures and tissues, including cells.

2.4. Utilizing microfluidics technology to develop biomaterials for drug delivery.

Progress in downsizing and integrating contemporary scientific and technical breakthroughs has led to the emergence of microfluidics-based platforms, which provide significant prospects and potential for engineers, biologists, and materials scientists. Microfluidics has enabled precise manipulation of fluids in microchannels, leading to the development of functional biomaterials. Microfluidic-based biomaterials have shown significant potential for effective and regulated medication administration. Microfluidics-based nanoparticles possess unique characteristics that enable the accurate encapsulation and

controlled discharge of active substances. Recent advancements in microfluidics have significantly expedited the clinical application of nanoparticles. In addition to their size and composition, microfluidic systems allow for the precise design of nanoparticle biocompatibility, surface properties, and rigidity, all of which have a profound impact on cellular uptake. Nanoparticles based on microfluidics have emerged as a very effective category of medicinal nanocarriers. Researchers have created hollow, rigid nanovesicles using a multistage microfluidic chip to distribute hydrophilic reagents. The accurate control of fluids and consistent blending in microfluidic devices are crucial for creating drug-loaded nanocarriers.

Microfluidic methods offer a unique foundation for simultaneously integrating different physical input and output modes, such as optics and electricity, to precisely direct the administration of pharmaceutically active agents to designated target sites. A microprobe made of silicon, which included microfluidic channels, was created to enable simultaneous neural recording and drug delivery. Despite the remarkable creativity and superiority of microfluidic technology compared to traditional approaches, there are still numerous challenges to overcome for its clinical implementation. A significant obstacle in microfluidic synthesis is the inability of PDMS microchannels to be compatible with some medications owing to solvent incompatibility. The current approach, which involves the use of solvents and lyophilization techniques, may have negative effects on some medications. Furthermore, there is a need to enhance the manufacturing rate of nanoparticles using microfluidic technology to meet the demands of clinical trials, guaranteeing adequate supply and superior quality. The use of parallel microfluidic devices allows for the parallelization and repeatability of microfluidics, enabling future industrial-scale manufacture of nanoparticles.

Ex vivo models, which involve the manipulation of cells, offer crucial insights into fundamental phenomena, such as disease progression, tissue architecture, and the evolution of life. Microfluidic technology is an efficient and powerful method for high-throughput, cost-effective analysis.

3. The Manıpulation of Cells

3.1. Cellular Configuration

Historically, microfluidics has been used for the creation of small-scale arrangements of biomaterials, often using microfluidic printing or microcontact printing techniques, which may also be adapted to pattern cells using cell suspensions as ink. The precise arrangement of cells and creation of ideal patterns have greatly aided cellular research. Micropatterned cell cultures

provide unparalleled opportunities to investigate intricate and emerging biological phenomena involving interactions between cells (L. Y. Yeo, Chang, Chan, & Friend, 2011). Cell adhesion, which is crucial for cell regulation, is the basis for the formation of multicellular organisms. Through targeted removal of self-assembled monolayers (SAMs) using electrochemical methods, researchers have developed several techniques to control cell adhesion patterns and switching (Nge et al., 2013). Microfluidic channels are used to convey diverse cell types to designated positions and to generate areas with diverse surface characteristics. Cell-cell interactions can be classified into three forms: type-a involves the segregation of many cells, type-b involves the partial liberation of one cell while maintaining the containment of other cells, and type-c involves the complete liberation of cells. The enhanced capacity to create patterns of cells and the simplified process of implementation are anticipated by scientists to greatly facilitate the coculturing of various cell types. The combination of microfluidic channels with holey PDMS membranes allowed for the precise arrangement of various cell types on diverse surfaces. Additionally, this patterning technique can be used on substrates with topographical variations (Fig. 2). This technology offers novel strategies for studying cell interactions and significantly advances the cultivation of synthetic tissues in a controlled laboratory environment.. In summary, microfluidic patterning offers a very effective approach for manipulating cells, establishing a strong basis for studying cell-to-cell interactions, and fabricating tissues and organs.

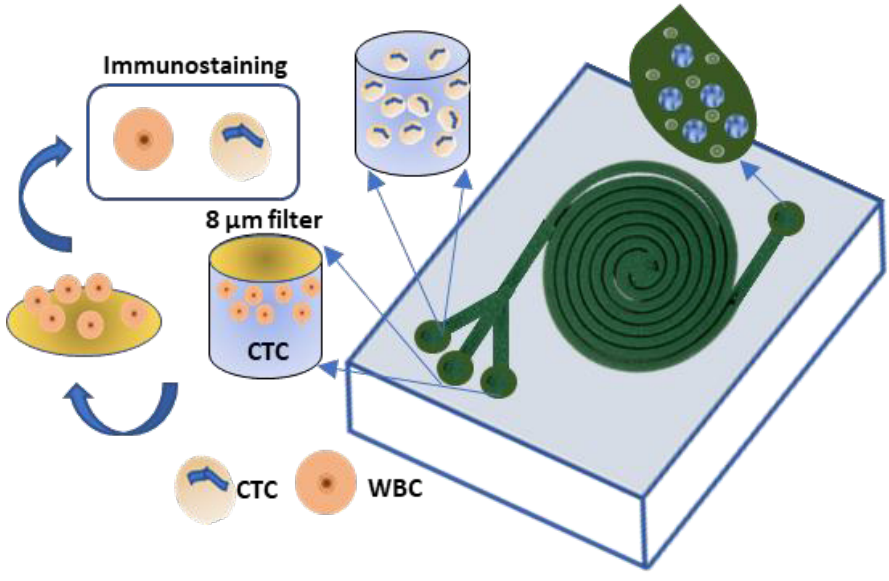

Fig. 2. Device for sorting cells using microfluidics.

3.2. CTC Isolation

Circulating tumor cells (CTCs) are a rare occurrence in which malignant neoplastic cells are released from primary tumors or tumors that have spread to other parts of the body and enter the bloodstream. These cells have the potential to provide valuable insights into tumor and cancer treatments . Efforts to efficiently isolate CTCs have led to significant technological advancements; however, the identification of CTCs among billions of normal blood cells remains a technical challenge. Microfluidics-based systems, which are known for their high-throughput capabilities, have significant potential for cell sorting and detection of rare cells. Scientists have created microfluidic cell sorters that use inertial forces to separate circulating tumor cells (CTCs) from blood cells. This is achieved by combining a sorter with a membrane filter incorporated into the system. This system uses double spiral microchannels to hydrodynamically focus and separate large CTCs captured via a filter at the access point (Erickson & Li, 2004). A novel 3D microfluidic system, known as a cluster chip, was developed to efficiently capture CTC clusters directly from raw blood samples. The cluster chip consists of three triangular pillars: two of these pillars create a narrowing funnel that directs the cells towards the opening, while the third pillar divides the laminar flow. CTC clusters were trapped using a dynamic force equilibrium. The velocity of the chip flow is deliberately controlled to be slower than that of the human capillaries to maintain the structural integrity of CTC clusters. An alternative and efficient method for capturing circulating tumor cells (CTCs) involves the interaction between antibodies and antigens. A microfluidic system was created using graphene oxide (GO) to effectively collect circulating tumor cells (CTCs) owing to its extensive surface area. CTCs are released from the chip when the temperature falls below 13-16 °C, which is the lower critical solution temperature for thermoresponsive polymers (Atencia & Beebe, 2005). Despite the many comprehensive studies on CTC screening, the use of these findings in clinical practice is challenging. Unlabeled microfluidic techniques sometimes exhibit limited specificity, leading to reduced purity. Label-dependent microfluidic methods exhibit a high degree of purity; however, their effectiveness is hindered by the heterogeneity of circulating tumor cells. The future focus of advanced microfluidics-based devices will be on enriching exosomes, circulating tumor DNA, and CTCs.

3.3. Analysis at the level of individual cells

Due to technical difficulties in analyzing individual cells, conventional studies in cell biology often focus on cell populations, disregarding crucial biological data included in the variances seen among individual cells. A

solitary cell is the minuscule unit of analysis that allows a comprehensive understanding of the formation of functional organs (Mu, Zheng, Sun, Zhang, & Jiang, 2013). The diversity of cells does not expose the composition of populations and the relationships between genes and their control, but also offers a significant understanding of the enigmas of life (Andersson & Van den Berg, 2003). Recent advancements in single-cell technologies have made substantial efforts to uncover variations among individual cells. Microfluidics has become a prominent technology for capturing, preserving, and analyzing single cells owing to its ability to control fluids on a small scale (Haeberle & Zengerle, 2007). In this platform, individual cells are enclosed within hydrogel microspheres, which can physically capture genomic DNA while allowing small molecules, such as enzymes, detergents, and small molecules, to pass through. The integration of microgel and droplet microfluidic technologies offers a very efficient approach for producing barcodes, characterized by exceptional quality and precise control (Lee et al., 2011). This droplet-based microfluidic system enables efficient immunological surveillance and antibody screening on a large scale. This technique involves the segregation of individual cells and assay reagents into droplets, which are then studied using two-dimensional droplet arrays to study their kinetics.

Microfluidics-based technology demonstrates superior levels of integration and sensitivity compared to traditional approaches. Recently, scientists have directed their attention to the development of microfluidic technologies for internal shipment, a vital component of biological research. These systems can be used to manipulate cells with high precision. Compared to traditional methods of intracellular delivery, microfluidic systems are recognized as promising avenues to enhance this process. One such technique involves localizing the electric field in the cell, resulting in a significant reduction in the required voltage. Another technique involves the use of a microfluidic platform to mechanically deform cells as they pass through a constriction, thereby enabling membrane disruption-based delivery. The future of microfluidic-based cell manipulation lies in the development of resilient systems that provide a high degree of adaptability and automation. Therefore, considerable resources should be allocated to this captivating field.

4. Organ-On-A-Chip Technology

4.1. Microfluidic Device Mimicking Blood Vessels

A multitude of medications are administered in the bloodstream, and the blood drug test provides essential information about medication and drug

exploration (Sebastian & Dittrich, 2018). The vascular system is crucial for the transportation of medicines across vascular walls and endothelial cells (Bhatia & Ingber, 2014). Recapitulating blood vessels in a laboratory setting offers distinct advantages in enhancing our understanding of intricate vascular processes (Kim, Wu, Young, & Haynes, 2014). Researchers have developed a novel approach for generating tubular structures in which different types of cells are deposited in distinct layers. This is accomplished using microfluidic channels to pattern cells in specific positions. A self-rolled 3D tubular construction may be created by covering a semi-cured PDMS membrane with a stretched PDMS membrane to create mismatched tension and then releasing the two PDMS layers. The adaptable technique not only offers an efficient method for 3D microfabrication but also creates opportunities for the development of tubular tissues filled with cells (Sebastian & Dittrich, 2018). The integration of microfluidic technology with electrospun nanofibers enables the creation of a complex scaffold that mimics blood vessels. The FDA-approved materials, poly(caprolactone) (PCL) and PLGA (Fig. 3), possess the ability to autonomously adapt and preserve the dimensions and form of the vessel after the degradation of the polymer (Angelopoulos, Evangelaras, & Koukouvinos, 2009). This approach is a novel method for fabricating synthetic blood vessels with predetermined geometries.

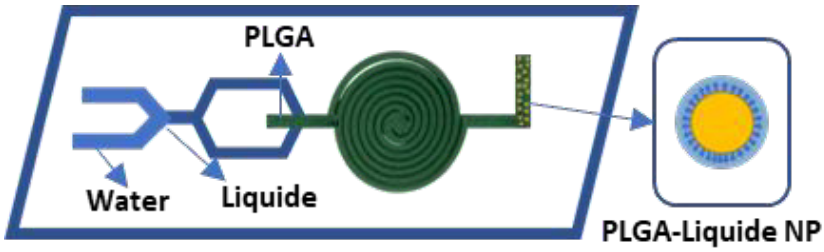

Fig. 3. Microfluidic device for the assembly of polymer-lipid hybrid nanoparticles.

4.2. Application of Drug Screening

Utilization of the microfluidic chip model may also explore the impact of nerves on the advancement of cancer, thus offering current perspectives in the field of anticancer treatment. However, traditional animal models are often costly and time-consuming (Sun, Warden, & Ding, 2019). A model that combines neurons and cancer cells enables efficient screening of drug development (Eduati et al., 2018). This system, which relies on microfluidics, can faithfully replicate the tumor microenvironment and facilitate the investigation of the interactions between nerve cells and cancer cells. In addition, scientists have

used this microfluidic technique to evaluate medications for their ability to block the migration of cancer cells linked with neuritis (Tsui, Lee, Pun, Kim, & Kim, 2013). We used a high-throughput technique to assess the effectiveness of gold nanoclusters in delivering siRNA targeting nerve growth factors. These findings indicate that gold nanoclusters exhibit favorable biocompatibility and efficient loading of medications. This microfluidic model, which is both high-throughput and effective, offers an excellent platform for drug screening and toxicity assessment in clinical applications.

A heart-on-a-chip system was recently created by combining biohybrid structurally colored hydrogels with microfluidic chips. Flexible inverse opal-structured hydrogel films were constructed using bioactive GelMA as a pregel. A heart-on-a-chip has the potential to serve as a functional platform for drug screening and biological research by providing inherent color-sensing feedback. Despite significant advancements in the field of organs-on-chips, the incorporation of microfluidic platforms continues to pose significant hurdles. The efficacy of drug and toxicity screening is substantially limited by the construction of most in vitro models on a single platform, as they fail to replicate the interaction of tissues in the body (Menon, Lim, & Lim, 2019). A wide range of functional models can be combined to automate the monitoring of biophysical parameters. This integration allows for the highly sensitive real-time monitoring of organoids. Organs-on-chips show significant potential for monitoring drugs, although there are various obstacles to overcome before the process of drug discovery can be expedited. Current organ-on-chip systems are limited in their ability to perform basic drug tests on certain features. The intercellular connections within the multiorgan-on-a-chip system are an additional factor to be considered in therapeutic settings. Ultimately, the accuracy of disease models necessitates the enhancement of both flexibility and dependability of these systems.

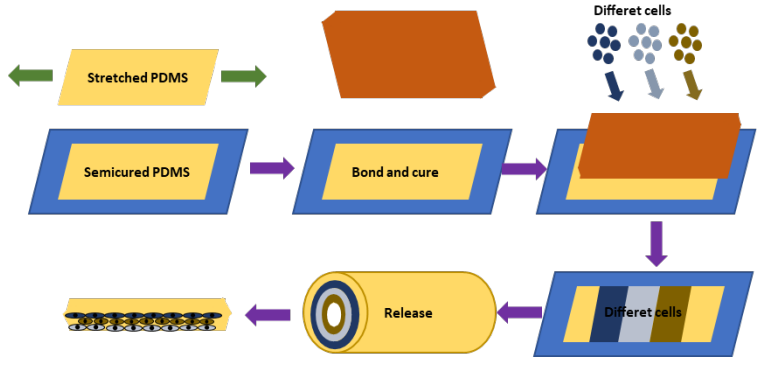

Fig. 4. Tubular structures formed by the process of stress-induced rolling of a membrane.

In the realm of cellular manipulation within the biological domain, microfluidics introduces enhanced methodologies for regulating cell development in terms of their spatial and temporal dimensions. The improved capabilities of microfluidics, such as its ability to efficiently handle large amounts of samples, minimal use of reagents, and capacity for the simultaneous analysis of many cells, make it an ideal platform for isolating circulating tumor cells and conducting single-cell analysis (Fig. 4). Obstacles persist. Conventional microfluidic devices are often limited to processing relatively simple materials for cell separation. In addition, it is important to consider the cost and productivity of microfluidic platforms.

5. Versatıle Biodevıce

Flexible electronics, capable of maintaining functionality while being mechanically deformed, provide clear benefits over current rigid electronics and have garnered significant attention in recent times. Contrary to contemporary electronic gadgets that include rigidity and non-biodegradability, organisms often exhibit softness, elasticity, and the ability to self-repair, akin to the human skin.

5.1. Wearable Sensors

The distinctive characteristics of wearable electronics, including low modulus, great flexibility, and excellent stretchability, have garnered considerable interest (Chen, Zheng, Liu, & Xu, 2019). These devices can be used to monitor human activities and health status. Microfluidic technology, known for its precise manipulation of fluids, is well suited for wearable electronic systems and represents a new era in this field (Fallahi, Zhang, Phan, & Nguyen, 2019). Microfluidics are mostly used in wearable sensors for extracting, manipulating, and dispensing liquids. Microfluidics combined with wearable devices may effectively regulate medication release, thereby enabling precise medical treatment. Currently, there is growing interest in microfluidic technology and wearable electronics (Li, Ma, Cao, Pan, & Shi, 2020). The fundamental idea behind this wearable system is the use of microfluidics to assemble high-strength components, thereby providing mechanical separation between the rigid elements and flexible enclosures. This intelligent approach not only focuses on the creation of wearable electronics for health monitoring, but also introduces hard-soft composite systems. This wearable electronic device has access ports that allow it to collect sweat directly from the skin when attached. In the integration of near-field communication electronics, quantitative information is

automatically retrieved and evaluated in addition to color changes. This feature has the potential to detect the early signs of human health issues (J. C. Yeo & Lim, 2016).

The increasing popularity of wearable consumer electronics has led to a strong need for pressure sensors that are durable, affordable, and extremely sensitive, particularly for health-monitoring purposes. Microfluidic sensors often rely on fluctuations in capacitance or resistance in conductive fluids, such as ionic liquids and liquid metals (Koh et al., 2016). An innovative microfluoronic film, both pressure-sensitive and transparent, was presented. A microfluidic diaphragm pressure sensor was presented to attain a high resolution and low limit of detection. This sensor employs an equivalent Wheatstone bridge circuit and consists of four sets of sensing grids made of Galinstan microchannels.

5.2. Adaptive Robotics

Adaptive robots have demonstrated superior adaptability to humans and the environment compared with traditional robots made of rigid materials (Nguewou-Hyousse, Franchi, & Paley, 2018). This advanced technology has great potential in fields such as medicine and manufacturing. Microfluidics offers several advantages including high precision, easy integration, and compatibility with various materials. This integration has resulted in the development of delicate devices that exhibit humanlike behaviors, such as movement, deformation, growth, and response to external stimuli (Fang et al., 2022). Hydrogels, polymers, and elastomers are commonly used materials for constructing frameworks for adaptive robots in microfluidics, such as in the production of microchips (Filippi, Yasa, Kamm, Raman, & Katzschmann, 2022). The integration of electronics into flexible structures is essential to enable adaptive robots to sense, move, and control. This can be easily accomplished via microfluidics, which involves the application of conductive inks onto soft materials using printing, patterning, and packaging techniques (Shao et al., 2022). Progress in bio-microdevices, such as organ-on-a-chip, holds the potential for the development of adaptive robots based on biohybrids. This combination of fields is referred to as “soft microfluidics,” which involves the use of soft fluidics and soft biohybrids to enable adaptive robots.

Various research teams have thoroughly documented adaptive robots that use pneumatic or hydraulic actuators and control. A composite material consisting of an elastomer and paper was created using soft lithography (Chiolerio & Quadrelli, 2017). When subjected to pressures ranging from 100 to 200 millibars, the pneumatic channel expanded in areas that were most flexible.

The presence of embedded paper stripes restricts the deformation of the channel, resulting in the asymmetrical elongation of the device. This technique enables the gadget to flex, rotate, and elongate in order to imitate the functionalities of a mussel. Nevertheless, the use of paper prevents the gadget from achieving full softness. The robot's control system incorporates microfluidic logic and utilizes a multimaterial, an embedded 3D printing technique, to create air-filled pathways inside a molded, elastic robot structure.

The use of live organisms, such as cells and microbes, in microfluidics has emerged as a novel approach to enhance the functionality of microdevices. Cardiomyocytes are often used to power microfluidic systems such as pumps and soft devices. Recently, biohybrids have been combined with structural color materials to achieve the ability to regulate themselves, similar to chameleons. The device was created by cultivating cardiomyocytes on a synthetic inverse opal hydrogel film, which resulted in the display of various colors as the cells underwent contraction and relaxation cycles. This paper provides a pathway towards the development of flexible and autonomous "living robots."

6. Conclusion

Over the past few decades, significant advancements have been achieved in the field of microfluidics-based biomaterials and biodevices. Microfluidic-based biomaterials, such as those used for pharmaceutical transport, chemical examination, and organ regeneration, are expected to provide a wide array of novel products. Microfluidics-based biodevices have the potential to transform developing industries, such as flexible electronics and wearable devices, enabling applications that now only exist in science fiction. The next decades hold great promise in the field of microfluidics, with the potential for significant advancements and thrilling developments.

However, other obstacles must also be overcome. Microfluidic-based biomaterials continue to advance, leading to the production of more intelligent multifunctional biomaterials. However, it is necessary to design dependable and adaptable microfluidic systems that can be seamlessly integrated with cutting-edge technologies. Microfluidics, as a technological platform, enables the precise manipulation of fluids, exhibiting features of miniaturization and integration. Hence, it will assume a progressively significant function in the amalgamation of biomaterials, particularly for the meticulous management of material composition, enhancement of uniformity, and augmentation of controllability, all of which are arduous to accomplish via traditional approaches. In the next few years, it will be imperative to optimize the use

of microfluidics, which leverage the properties of laminar flow and droplets in microchannels, to devise novel techniques for the production of biomaterials that are otherwise challenging to obtain using traditional approaches. Furthermore, the advancement of microfluidics has focused on automating, integrating, and intelligently synthesizing biomaterials.

Microfluidic systems have shown significant promise in the field of biomedical research, particularly in the areas of cell biology and organs-on-chip. Organs-on-chips, although more closely resembling live beings compared to traditional cell studies, nevertheless have challenges in accurately replicating the complexity of biological tissues. However, the use of microfluidics to study living creatures and enhance our understanding of people, as well as to investigate natural principles, will continue until organs-on-chips may replace animal experiments as well as trials in humans. The combination of flexible electronics and microfluidic technology offers promising opportunities for healthcare monitoring and diagnostics. In the foreseeable future, it is likely that microfluidics will be incorporated seamlessly into every element of human physiology. Microfluidics will have growing significance in several fields, ranging from pharmaceuticals to biological tissues, organs, and even smart wearable devices.

References

Agnello, S., Gasperini, L., Reis, R. L., Mano, J. F., Pitarresi, G., Palumbo, F. S., & Giammona, G. (2016). Microfluidic production of hyaluronic acid derivative microfibers to control drug release. *Materıals Letters*, *182*, 309–313. https://doi.org/10.1016/j.matlet.2016.07.014

Andersson, H., & Van den Berg, A. (2003). Microfluidic devices for cellomics: A review. *Sensors and Actuators B: Chemical*, *92*(3), 315–325.

Angelopoulos, P., Evangelaras, H., & Koukouvinos, C. (2009). Small, balanced, efficient and near rotatable central composite designs. *Journal Of Statıstıcal Plannıng And Inference*, *139*(6), 2010–2013. https://doi.org/10.1016/j.jspi.2008.09.001

Atencia, J., & Beebe, D. J. (2005). Controlled microfluidic interfaces. *Nature*, *437*(7059), 648–655.

Bhatia, S. N., & Ingber, D. E. (2014). Microfluidic organs-on-chips. *Nature Biotechnology*, *32*(8), 760–772.

Chen, G., Zheng, J., Liu, L., & Xu, L. (2019). Application of Microfluidics in Wearable Devices. *Small Methods*, *3*(12), 1900688. https://doi.org/10.1002/smtd.201900688

Cheng, S., & Wu, Z. (2012). Microfluidic electronics. *Lab on a Chip*, *12*(16), 2782–2791.

Chiolerio, A., & Quadrelli, M. B. (2017). Smart Fluid Systems: The Advent of Autonomous Liquid Robotics. *Advanced Science*, *4*(7), 1700036. https://doi.org/10.1002/advs.201700036

Ding, X., Zhuge, W., Zhang, Y., Ding, S., Wang, J., & Zhou, G. (2023). Microfluidic generation of bioinspired core-shell structured microfibers for cultured meat. *Chemıcal Engıneerıng Journal*, *478*, 147467. https://doi.org/10.1016/j.cej.2023.147467

Eduati, F., Utharala, R., Madhavan, D., Neumann, U. P., Longerich, T., Cramer, T., … Merten, C. A. (2018). A microfluidics platform for combinatorial drug screening on cancer biopsies. *Nature Communications*, *9*(1), 2434.

Erickson, D., & Li, D. (2004). Integrated microfluidic devices. *Analytica Chimica Acta*, *507*(1), 11–26.

Fallahi, H., Zhang, J., Phan, H.-P., & Nguyen, N.-T. (2019). Flexible microfluidics: Fundamentals, recent developments, and applications. *Micromachines*, *10*(12), 830.

Fang, J., Zhuang, Y., Liu, K., Chen, Z., Liu, Z., Kong, T., … Qi, C. (2022). A Shift from Efficiency to Adaptability: Recent Progress in Biomimetic Interactive Soft Robotics in Wet Environments. *Advanced Science*, *9*(8), 2104347. https://doi.org/10.1002/advs.202104347

Filippi, M., Yasa, O., Kamm, R. D., Raman, R., & Katzschmann, R. K. (2022). Will microfluidics enable functionally integrated biohybrid robots? *Proceedings of the National Academy of Sciences*, *119*(35), e2200741119. https://doi.org/10.1073/pnas.2200741119

Haeberle, S., & Zengerle, R. (2007). Microfluidic platforms for lab-on-a-chip applications. *Lab on a Chip*, *7*(9), 1094–1110.

He, Y., Qiu, J., Fu, J., Zhang, J., Ren, Y., & Liu, A. (2015). Printing 3D microfluidic chips with a 3D sugar printer. *Mıcrofluıdıcs And Nanofluıdıcs*, *19*(2), 447–456. https://doi.org/10.1007/s10404-015-1571-7

Kim, D., Wu, X., Young, A. T., & Haynes, C. L. (2014). Microfluidics-Based in Vivo Mimetic Systems for the Study of Cellular Biology. *Accounts of Chemical Research*, *47*(4), 1165–1173. https://doi.org/10.1021/ar4002608

Knauer, A., & Koehler, J. M. (2014). Screening of nanoparticle properties in microfluidic syntheses. *Nanotechnology Revıews*, *3*(1), 5–26. https://doi.org/10.1515/ntrev-2013-0018

Koh, A., Kang, D., Xue, Y., Lee, S., Pielak, R. M., Kim, J., … Rogers, J. A. (2016). A soft, wearable microfluidic device for the capture, storage, and

colorimetric sensing of sweat. *Science Translational Medicine*, *8*(366). https://doi.org/10.1126/scitranslmed.aaf2593

Lee, C.-Y., Chang, C.-L., Wang, Y.-N., & Fu, L.-M. (2011). Microfluidic mixing: A review. *International Journal of Molecular Sciences*, *12*(5), 3263–3287.

Li, S., Ma, Z., Cao, Z., Pan, L., & Shi, Y. (2020). Advanced Wearable Microfluidic Sensors for Healthcare Monitoring. *Small*, *16*(9), 1903822. https://doi.org/10.1002/smll.201903822

Menon, N. V., Lim, S. B., & Lim, C. T. (2019). Microfluidics for personalized drug screening of cancer. *Current Opinion in Pharmacology*, *48*, 155–161.

Mu, X., Zheng, W., Sun, J., Zhang, W., & Jiang, X. (2013). Microfluidics for Manipulating Cells. *Small*, *9*(1), 9–21. https://doi.org/10.1002/smll.201200996

Nge, P. N., Rogers, C. I., & Woolley, A. T. (2013). Advances in Microfluidic Materials, Functions, Integration, and Applications. *Chemical Reviews*, *113*(4), 2550–2583. https://doi.org/10.1021/cr300337x

Nguewou-Hyousse, H., Franchi, G., & Paley, D. A. (2018). Microfluidic circuit dynamics and control for caterpillar-inspired locomotion in a soft robot. *2018 IEEE Conference on Control Technology and Applications (CCTA)*, 286–293. IEEE. Retrieved from https://ieeexplore.ieee.org/abstract/document/8511335/

Niculescu, A.-G., Chircov, C., Birca, A. C., & Grumezescu, A. M. (2021). Nanomaterials Synthesis through Microfluidic Methods: An Updated Overview. *Nanomaterıals*, *11*(4), 864. https://doi.org/10.3390/nano11040864

Niculescu, A.-G., Mihaiescu, D. E., & Grumezescu, A. M. (2022). A Review of Microfluidic Experimental Designs for Nanoparticle Synthesis. *Internatıonal Journal Of Molecular Scıences*, *23*(15), 8293. https://doi.org/10.3390/ijms23158293

Razzaq, W., Serra, C. A., Jacomine, L., & Chan-Seng, D. (2022). Microfluidic elaboration of polymer microfibers from miscible phases: Effect of operating and material parameters on fiber diameter. *Journal Of The Taıwan Instıtute Of Chemıcal Engıneers*, *132*, 104215. https://doi.org/10.1016/j.jtice.2022.104215

Sebastian, B., & Dittrich, P. S. (2018). Microfluidics to Mimic Blood Flow in Health and Disease. *Annual Review of Fluid Mechanics*, *50*(1), 483–504. https://doi.org/10.1146/annurev-fluid-010816-060246

Shao, Q., Dong, X., Lin, Z., Tang, C., Sun, H., Liu, X.-J., & Zhao, H. (2022). Untethered Robotic Millipede Driven by Low-Pressure Microfluidic

Actuators for Multi-Terrain Exploration. *IEEE Robotics and Automation Letters*, *7*(4), 12142–12149.

Sun, J., Warden, A. R., & Ding, X. (2019). Recent advances in microfluidics for drug screening. *Biomicrofluidics*, *13*(6). Retrieved from https://pubs.aip.org/aip/bmf/article/13/6/061503/238888

Tsui, J. H., Lee, W., Pun, S. H., Kim, J., & Kim, D.-H. (2013). Microfluidics-assisted in vitro drug screening and carrier production. *Advanced Drug Delivery Reviews*, *65*(11–12), 1575–1588.

Yeo, J. C., & Lim, C. T. (2016). Emergence of microfluidic wearable technologies. *Lab on a Chip*, *16*(21), 4082–4090.

Yeo, L. Y., Chang, H., Chan, P. P. Y., & Friend, J. R. (2011). Microfluidic Devices for Bioapplications. *Small*, *7*(1), 12–48. https://doi.org/10.1002/smll.201000946

CHAPTER IV

ELECTRIC VEHICLE FIRE ON RO-RO PASSENGER SHIPS: RISKS, RULES AND REGULATIONS

Burak GÖKSU

(Dr.), Zonguldak Bulent Ecevit University, Zonguldak, Turkey
E-mail: burakgoksu@beun.edu.tr
ORCID: 0000-0002-6152-0208

1. Introduction

Maritime transportation encompasses the utilization of various waterborne vessels, such as ships, boats, and other watercraft, to convey individuals and commodities across different bodies of water. Shipping is responsible for around 80-90% of global trade, facilitating the transportation of more than 10 billion tons of solid and liquid bulk goods over the world's oceans on an annual basis (Walker et al., 2018). Within this particular framework, maritime transportation is crucial in establishing connections among states worldwide, fostering trade, and making significant contributions to the overall global economy. The transportation of substantial quantities of goods and individuals across extensive distances is a crucial aspect of international trade (Rodrigue et al., 2020). For decades, it has been utilized as an essential means of transportation for commodities and individuals. There are ongoing advancements that are influencing the industry in accordance with technological advancements and environmental considerations (Wan et al., 2018).

Ro-Ro (Roll-on/Roll-off) transportation serves a significant role in the global logistics and transportation sector, facilitating the smooth transfer of commodities and vehicles across domestic and international locations. Approximately 73% of the ferry and Ro-Ro lines under consideration are deemed obligatory, as they lack alternative land routes; and approximately 63% serve as the sole connections between island regions and the mainland, while the absence of suitable infrastructure characterizes the remaining 10%, rendering road

transport unfeasible (Kotowska, 2015). This mode of transportation provides a pragmatic and economically efficient resolution for the conveyance of goods, hence assuming a pivotal function in the facilitation of commercial activities and exchange (Spaniol and Rowland, 2022). Ro-Ro vessels are a specific kind of maritime vessel that has been purposefully engineered to facilitate the streamlined conveyance of wheeled cargo, encompassing cars, trucks, trailers, and various other types of wheeled machinery. The nomenclature "roll-on/roll-off" is derived from the loading and unloading technique, wherein vehicles have the capability to autonomously enter and depart the vehicle using their own wheels (Göksu and Bayramoglu, 2023). Ro-Ro vessels possess specific characteristics and functionalities that render them very suitable for this particular use.

Car transportation services provide a convenient and efficient means of transporting vehicles, catering to both personal and corporate needs. Vehicle logistics has shown a notable increase over the past decade, with an average annual growth rate of 4% (Iannone et al., 2016). They offer a significant service to people and corporations seeking to transport their vehicles while minimizing the accumulation of traffic and any damage to the vehicle (Taiebat et al., 2018). Car transportation, sometimes referred to as vehicle transportation, is a specialized service dedicated to the movement of vehicles between different locations. This service is frequently utilized by people, businesses, automotive dealerships, and other entities for a multitude of objectives (Kaptan, 2022). Numerous ports across the globe, such as Vigo, Santander, Pasajes, Barcelona, Sagunto, Setúbal, Le Havre, Livorno, Sheerness (Medway ports), Bristol, Copenhagen, Malmö, Goteborg, Emden, Zeebrugge/Ghent, Antwerp, and Rotterdam, have undergone the installation of Ro-Ro terminals (Chen et al., 2021). The utilization of this method facilitates the worldwide transportation of individuals and commodities, as it enables automobile manufacturers, dealers, and customers to transfer vehicles efficiently and economically across international borders. An emerging paradigm in the automotive supply chain views the Ro-Ro port terminal as a new decoupling point between the supply chain forecast-driven and demand-driven sides if it can allow buffering, warehousing with pre-delivery inspections, and postponement customization (Dias et al., 2010).

Accidents, fires, or explosions occurring at these supply points can result in substantial consequences, encompassing the loss of human lives, environmental deterioration, and financial implications. There are multiple reasons that can contribute to ship accidents and fires, encompassing human mistakes, technical failures, adverse weather conditions, and navigational challenges (Weng and Yang, 2015). The occurrence of ship accidents and fires underscores the significance of safety regulations, crew training, and regular equipment maintenance in order to

proactively minimize such incidents and mitigate their effects in the event that they happen (Brcko et al., 2023). Furthermore, there is ongoing collaboration between international organizations and maritime authorities to design and implement safety standards and response procedures in order to mitigate the occurrence and impact of accidents and marine incidents (Argüello, 2022).

The increasing quantity of electric vehicles being carried via maritime routes (Göksu and Bayramoglu, 2023) has raised concerns regarding the occurrence of EV fires aboard ships (Funk et al., 2023). Although electric vehicles are generally considered safe, there is a potential risk of fire if the batteries become damaged or experience excessive heat (Brzezinska and Bryant, 2022). In recent years, there have been numerous notable incidents involving fires in electric vehicles that occurred on ships. In the year 2022, the cargo vessel named Felicity Ace experienced a fire incident while in transit with a cargo load exceeding 4000 electric vehicles (Allerth and Niklasson, 2022). The vessel submerged, resulting in the loss of all electric vehicles. In the year 2023, an incident occurred wherein a fire erupted aboard the cargo vessel named Fremantle Highway, which was transporting a cargo of approximately 3800 new cars and including 500 electric vehicles (Dnistran, 2023). The fire was ultimately suppressed; however, it resulted in the unfortunate fatality of a crew member and caused injuries to several others. Extinguishing electric vehicle fires aboard ships can pose challenges due to the persistent combustion potential of batteries, which may endure even after the flames have been suppressed (Dorsz and Lewandowski, 2022). The reason for this phenomenon is that batteries have the potential to emit combustible gases when subjected to combustion (Cui, Liu, et al., 2022).

The primary objective of ship fire safety regulations is to mitigate the occurrence and prevent the spread of flames on board ships while simultaneously safeguarding the safety of passengers and crew members in the event of a fire incident. The rules are made by the International Maritime Organization (IMO), and they are then enforced by maritime officials at the national level (Gulbrandsen, 2013). The IMO established the International Convention for the Safety of Life at Sea (SOLAS), which contains the main regulations governing fire safety on board ships. According to the SOLAS convention, it is mandatory for all vessels to possess a fire safety plan, which necessitates the approval of the appropriate maritime regulatory authority (Zisimopoulos, 2016). The fire safety plan encompasses several key components, including a comprehensive depiction of the ship's fire detection and extinguishing systems, procedures for identifying, reporting, and extinguishing fires, guidelines for evacuating the ship in the event of a fire, and provisions for training crew members on appropriate fire response procedures (Kang et al., 2017).

In addition, SOLAS establishes precise criteria for the installation and operation of fire detection and extinguishing systems aboard maritime vessels. As an illustration, it is a requirement for all cruise ships to be equipped with a stationary fire suppression system (Tarelko, 2012). It is imperative for cargo vessels to be equipped with a fire detection system that encompasses all cargo holds and other confined areas (Kang et al., 2017). In conjunction with the SOLAS rules, shipboard fire safety is subject to many additional national and international laws.

An illustration of this can be seen in the laws established by the International Labour Organization (ILO) pertaining to fire prevention and firefighting protocols implemented aboard ships (Shan, 2022). Adequate training for the crew members on fire response procedures is also essential. Moreover, ships must maintain a specific quantity of fire-fighting equipment, including fire extinguishers, hoses, and masks (Wu et al., 2014). Lastly, regular fire drills are to be conducted on ships to ensure that the crew is well-acquainted with the fire safety plan and associated procedures. The significance of ship safety regulations lies in their ability to safeguard the lives and assets of both passengers and crew members. By following these guidelines, ship operators can lessen the likelihood of fires occurring and respond more effectively to them if they do.

2. Literature Review

Fires that occur on ships tend to rapidly propagate and provide significant challenges in terms of containment and suppression. Both passengers and certain members of the ship's crew may lack familiarity with real-life fire incidents. Failure to effectively manage or promptly intervene in the initial stages could result in severe harm to the vessel, potentially resulting in loss of human life. Computational simulation methods are employed in the ship design process to forecast and mitigate the propagation of fire. The implementation of simulation might provide challenges due to the inherent limitations imposed by financial and time-based constraints on the design process. Nevertheless, it is advisable to employ dynamic fire models as a means of enhancing the assessment of heat and smoke patterns and dynamics in relation to their origins, spatial distribution, and prevailing environmental variables (Kang et al., 2017).

One of the studies that characterize the technical features of the fire that may occur caused from electric vehicles on ships encompassed the examination of the effects of electric vehicle fires on structures by Funk et al. (2023). The findings indicated that during the initial phases of a single-car fire in a well-ventilated enclose with an insulated ceiling, the gas temperatures at the uppermost part

of the enclosure above 1000°C for around 5 minutes. Furthermore, the rate at which the flame propagated from the initial car to the adjacent vehicles was seen to be most rapid under conditions of battery overcharging, resulting in a spread time of around three minutes.

The performance efficiency of water spray fire suppression systems (called "drencher systems") aboard ro-ro cargo and passenger ships has been examined due to the rise of electric cars. In 2023, Arvidson and Westlund tested two geometrically comparable both gasoline-fueled and battery-electric vehicles under as similar test conditions as feasible. The heat dissipation rate, gas temperature above the vehicle, and target steel sheet surface temperature on the vehicle sides were measured during the test. Both vehicle types had separate yet similar flames. The EV battery pack fire develops slower, is smaller, and burns longer, requiring more extinguishing liquid.

The incidence of EV fire accidents resulting from the thermal runaway of lithium-ion batteries is becoming more prevalent. However, there is still a lack of understanding regarding the fire dynamics of EVs parked in a linear arrangement. Cui et al. (2022) conducted a study to investigate the fire development process and features of two EVs positioned in parallel inside an open space. The analysis focused on examining the combustion behavior and thermal fields of the EVs. The findings indicated that the initial indication of a fire in the battery electric vehicle was the emission of white smoke from the chassis. The manifestation of flames was not observed until the amassed smoke discharged and enveloped both electric automobiles. In the case of a single-vehicle fire, it was noticed that flames engulfed the entire vehicle during a span of around 7 minutes. On the other hand, in an incident involving two adjacent vehicles, it was noted that the flames encircled both vehicles for approximately 17 minutes.

According to Brzezinska and Bryant (2022), it is advisable to consider an approximate heat release rate (HRR) of 7 MW as the commonly accepted value for fire engineering design in car parks while exploring the boundaries of engineering knowledge pertaining to EV fire hazards. Furthermore, it may be inferred once more that the rate of EV fire growth surpasses that of conventionally fueled vehicles. According to existing literature, the suppression of electric vehicle fires has challenges primarily attributed to limited accessibility to the battery pack housed within the vehicle structure, as well as the potential hazards associated with re-ignition. Successful extinguishment of such fires often necessitates the utilization of substantial quantities of water.

According to the findings of (Cui, Cong, et al., 2022) study on plug-in electric vehicles (PHEVs) of the SUV (Sport Utility Vehicle) category, it was

determined that the transition from chassis flames to a fire in the passenger compartment occurred within a duration of 9 minutes and 11 seconds. The rear portion of the vehicle became fully engulfed in flames after a duration of 9 minutes and 56 seconds, owing to the relatively sluggish advancement of the fire in the sedan-type PHEV. The PHEV fires exhibited a maximum temperature of 843.6°C, with a corresponding maximum fire height of around 3 meters. Additionally, the radiant heat emitted from the combustion of PHEVs was measured to be 1.151 kW/m2 at a distance of 1 meter.

The study used Bayesian Network (BN) analysis to clarify the significance of fires in the incidence of fires on Ro-Ro passenger ships, with the ultimate aim of enhancing the efficacy of operational countermeasures. Based on the findings of this investigation, BN has identified many fire-related incidents that are given priority as vehicle engine fire, vehicle electrical fire, used car electrical fire, refrigeration unit electrical fire, and spontaneous combustion of cargo (Bao et al., 2023).

The presence of fire hazards on ships is consistently evident throughout several studies conducted on the topic. Different researchers have employed various techniques to explore the parameters that contribute to the incidence of fire and the technical properties associated with these parameters. The primary objectives of these studies include the modeling of fire spread patterns, quantifying the energy released into the environment due to the fire, assessing surface temperatures, and identifying the underlying causes of the fire. Based on the aforementioned factors, a prioritization of risks is undertaken, precautionary measures are implemented to mitigate the occurrence of hazardous situations, and a set of rules and regulations are established to ensure compliance.

3. Main Characteristics of Car Carriers

Car carrier vessels are customized ships that are utilized for the transportation of many types of vehicles, including cars, trucks, buses, and construction machines (Fu et al., 2023). Additionally, there exist certain categories referred to as pure car carriers (PCCs) or pure car and truck carriers (PCTCs). Car carrier vessels include several distinctive characteristics that make them very suitable for the transportation of automobiles (Puisa, 2021):

- The aft ramp facilitates the expeditious and effective entry and exit of vehicles onto and off the vessel.
- Car carrier vessels are equipped with many decks to facilitate the accommodation of a maximum number of vehicles. Decks are commonly linked using internal ramps.

- The decks of a car carrier vessel include the capability to be modified to accommodate various sizes of vehicles. The ship possesses the capability to facilitate the transportation of a diverse range of vehicles, including both compact cars and huge lorries.
- The unit of measurement known as Lanes in Meters (LiM) is utilized to quantify the capacity of a vehicle carrier ship.

Table 1 presents a compilation of Ro-Ro passenger ships with diverse dimensions, varying quantities of cars, and passenger capacity, all including the aforementioned attributes.

Table 1. The particulars of the current Ro-Ro passenger ships

Name	Length overall [m]	Breadth [m]	Passenger capacity	Vehicle capacity	Charging on board
Vizzavona	188	28.70	800	130 cars & 155 trucks	Not available
Cruise Roma	253.80	30.40	3343	215 cars	Not available
W.B. Yeats	194.80	31.60	1800	1216 cars	Not available
Megastar	212	36	2800	150 cars & 250 trucks	Available
Amorella	169.40	28.20	2172	440 cars & 50 trucks	Not available
Sunflower Satsuma	192	27	709	134 cars & 121 trucks	Not available
Stena Scandinavica	240	30	1300	300 cars	Available
Spirit of France	212	31	2000	1059 cars & 180 trucks	Available
Galicia	215	28	1680	550 cars & 130 trucks	Available
Viking Glory	223	35	2800	600 cars & 90 trucks	Not available
Color Fantasy	224	35	2750	750 cars	Not available
Fjord FSTR	109	31	1200	404 cars	Available
Express 4	109	31	1006	425 cars	Available
Visborg	200	32	1650	500 cars	Available

Annually, a substantial number of vehicles are transported from manufacturing plants to dealerships and ultimately to consumers, resulting in a significant volume of movement. Car carrier ships own several supplementary

attributes. Firstly, they typically exhibit substantial dimensions, enabling them to accommodate numerous vehicles, often numbering in the thousands. Secondly, these vessels are equipped with a diverse array of security features, including fire detection and extinguishing systems, as well as cargo lashing systems, which serve to safeguard the transported vehicles (Spaniol and Rowland, 2022). Lastly, car carrier ships are meticulously designed to optimize fuel efficiency and minimize their environmental impact, thereby adhering to principles of sustainability (Wan et al., 2018). Also, these vessels hold a major role in the worldwide economy and persistently undergo advancements in order to respond to the demands of the automobile sector.

4. Current Situation on Electric Vehicles

The prevailing electric vehicle (EV) models currently being manufactured encompass various categories, namely BEV (battery electric vehicle), PHEV (plug-in hybrid electric vehicle), HEV (hybrid electric vehicle), and MHEV (mild hybrid electric vehicle) (Dorsz and Lewandowski, 2022). Battery electric vehicles (BEVs) are automobiles that exclusively include an electric motor or motors, deriving their power exclusively from the energy stored in the vehicle's batteries. Plug-in hybrid electric vehicles (PHEVs) are automobiles that incorporate both an electric motor and an internal combustion engine. These two power sources operate in combination, depending on the vehicle's power demands. Furthermore, PHEVs offer the capability to recharge their batteries directly from the electrical grid. Hybrid Electric Vehicles (HEVs) are a type of automotive technology that incorporates both a combustion engine as the primary power source and an electric motor as a secondary power source. On the other hand, Mild Hybrid Electric Vehicles (MHEVs) are a variant of HEVs that employ a similar design concept, but primarily utilize electric energy to operate electrical components within the vehicle, thereby reducing the workload on the combustion engine.

BEVs include several distinctive characteristics that differentiate them from conventional engines fueled by fossil fuels. The summarized characteristics encompass (Grunditz and Thiringer, 2016):

- BEVs are characterized by their lack of exhaust emissions, which renders them more environmentally friendly and beneficial to public health.
- BEVs exhibit reduced operational expenses due to the utilization of electricity as a more cost-effective energy source compared to fossil fuels.
- BEVs have the characteristic of immediate torque, enabling them to achieve rapid and seamless acceleration.

• BEVs exhibit much-reduced noise emissions compared to vehicles fueled by fossil fuels, resulting in a more pleasurable driving experience.

The International Energy Agency (IEA) estimates the total number of EVs on the road in 2021 at 16.5 million, with a further 10 million cars sold in 2022 (IEA, 2023). In the European Union (EU) in 2022, petrol-powered cars made up 36.4% of all newly registered vehicles, while diesel cars made up 16.4% of all registrations. A total of 21.6% of newly registered passenger cars in the EU are classified as electrically chargeable vehicles, consisting of 12.1% BEVs and 9.4% PHEVs. Additionally, HEVs make up 22.6% of overall automobile sales. Figure 1 illustrates the prevailing pattern in the fuel categories of newly manufactured automobiles for the period spanning from 2018 to 2022 (ACEA, 2023).

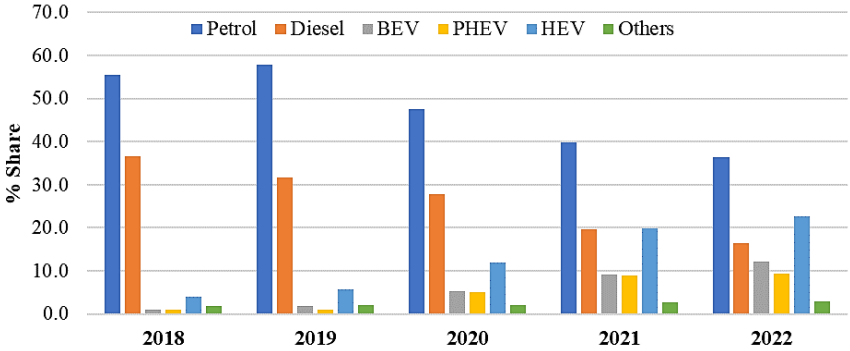

Figure 1. New EU car registrations 2018-2022

EVs often offer a wide range of advantages when compared to vehicles solely powered by fossil fuels. First and foremost, electric vehicles exhibit a considerably reduced environmental footprint, rendering them a more ecologically sustainable mode of transportation. Moreover, electric vehicles exhibit a higher degree of cost-effectiveness in terms of operational expenses, attributable to their reduced energy consumption. Additionally, electric vehicles demonstrate superior efficiency in terms of energy conversion, hence augmenting their attractiveness as a feasible substitute for traditional automobiles. Given the continuous progress and growing accessibility of technology, it is expected that electric vehicles will assume a major role in the realm of transportation in the foreseeable future.

5. Electric Vehicle Fires and Incidents on Ro-Ro Ships

The presence of a large number of automobiles during the transportation of new and second-hand vehicles on ships increases the risk of damage to both the ship and its cargo (Koromila et al., 2021). Any malfunction or mistake can

trigger various factors that contribute to the extent of the damage (Yin et al., 2023), potentially resulting in the loss of the ship, cargo, and even human life.

At the beginning of 2020, Norway emerged as the nation boasting the most substantial percentage of electric vehicles within its passenger automobile fleet, with EVs accounting for 17.3% of the total. When examining data pertaining to car fires, it is shown that electric vehicles account for 2.7% of reported incidents, despite constituting 17.3% of the overall passenger car fleet. This finding suggests that EVs have a significantly lower fire frequency compared to internal combustion engine vehicles (ICEVs), with a reduction of around eight-fold. The collection of data on car fires is conducted by the Swedish Civil Contingencies Agency (MSB). It has been observed that the occurrence of fires in ICEVs and EVs, including plug-in hybrid electric vehicles, is significantly lower in EVs compared to ICEVs, with a frequency of approximately one-tenth as common (Sun et al., 2020).

Based on the existing data, the primary inference drawn is that the occurrence of electric vehicle fires does not exhibit a higher likelihood compared to fires in internal combustion engine vehicles. However, it is noteworthy that the incidence of fires in ICEVs is around 8 to 10 times more than that in electric vehicles. Nevertheless, due to the novelty and limited quantity of electric vehicles, there is a mounting apprehension regarding the potential escalation of fires as the EV fleet expands and ages (Hynynen et al., 2023).

The incident known as the “Felicity Ace” accident, which transpired in recent years and garnered significant media attention, resulted in an estimated financial loss of roughly $500 million in 2022 (IUMI, 2022). The accident involving the fire of electric automobiles aboard the vessel named “Fremantle Highway” in the year 2023 resulted in an estimated financial loss of around $13 million for the Mercedes-Benz automobile company (Maritime Executive, 2023). This particular company had a relatively modest cargo of 350 vehicles aboard the vessel at the time of the incident. It is worth noting that the first recorded occurrence of an electric vehicle fire onboard a ship was reported in 2010 (Williamsson, 2022). The first accident reported in the literature, a fire in the battery of a compact SUV, occurred on 17 November 2010, during the Oslo-Copenhagen voyage of the “Pearl of Scandinavia” ship. Similar events have continued to occur ever since.

DNV (Det Norske Veritas) has recently published research pertaining to fire incidents occurring in Ro-Ro spaces. The purpose of this report is to address the increasing safety concerns within this particular sector and offer shipowners valuable information. The study titled “Fires on Ro-Ro decks” conducted by DNV has investigated incidents of fires occurring in Ro-Ro spaces on various

types of vessels including Ro-Pax (Ro-Ro passenger) vessels, vehicle carriers, and standard Ro-Ro cargo vessels. The study has documented a total of 35 such fires that occurred between the years 2005 and 2016; and also, the research indicates that a total of 18 incidents occurred on Ro-Pax vessels throughout the period spanning from 2005 to 2016. During the identical time period, a total of nine incidents of fires were documented on pure car carriers (PCC) and pure car and truck carriers (PCTC), whereas eight incidents were reported on cargo Ro-Ro vessels. A prior publication by DNV in 2005 documented a total of 25 incidents of fires occurring in Ro-Ro spaces during the period spanning from 1990 to 2003 (Späth, 2016).

In September 2019, a maritime incident occurred wherein a cargo vessel, laden with a total of 4200 automobiles, experienced a catastrophic event resulting in its capsizing. The incident involving the capsizing of the cargo ship "Golden Ray" with a deadweight tonnage (DWT) of 20995 off the coast of Georgia, led to extensive financial losses amounting to over $200 million (Mok et al., 2023). This unfortunate event was mostly attributed to erroneous stability calculations pertaining to the ship. A total of $142 million in damages was incurred specifically in relation to the transported cargo (Riess and Gray, 2021).

The fire incident on the vessel "Höegh Xiamen" was attributed to a combination of factors, namely a malfunctioning vehicle battery and an electrical fault arising from the improper disconnection of a battery in a used vehicle (Bao et al., 2023). This unfortunate event occurred on a vehicle carrier, resulting in significant cargo damages estimated at $40 million (Osler, 2021). On June 4, 2020, a significant incident occurred at the port of Jacksonville, Florida, resulting in the loss of 2420 used automobiles (Cui, Cong, et al., 2022). On 17 June 2020, a fire accident occurred at the Port of Zeebrugge, Belgium, involving the vessel named "Polaris Highway", which was registered under the Panama flag and had a deadweight tonnage of 20494 (Bush, 2020).

On June 18, 2020, the Ro-Pax vessel known as the "Cruise Bonaria" experienced an incident with a fire on its cargo deck. The incident transpired when the vessel arrived at Olbia, Sardegna from Livorno. The ignition occurred within a refrigerated vehicle and was attributed to a negligent action. There were no documented instances of injuries. Grimaldi has advocated for more stringent cargo regulations in response to a series of cargo fires occurring on its vessels (Voytenko, 2020). On April 19, 2021, a fire of undetermined origin occurred aboard the vessel named "Zhong Hua Fu Qiang", which was constructed in the year 2020 (Hu and Ma, 2022). During the occurrence that transpired while the vessel was departing from the harbor, there were a total of 230 automobiles and 2300 individuals on board, and fortunately, no fatalities were reported.

6. Characteristics of Battery Fires and the Risks of Transportation on Ro-Ro Passenger Ships

There exist notable distinctions between fires involving electric vehicles and those involving internal combustion engine vehicles (Cui, Liu, et al., 2022). Frequently, these entities exhibit distinctive patterns of conduct, characterized by the emission of voluminous formations of contrasting dark and light vaporous substances, accompanied by audible bursts, as well as the projection of flame-like streams in a manner like to that of a jet, reaching temperatures as high as 1000 degrees Celsius (Funk et al., 2023). The identification of these indicators can facilitate the prompt implementation of emergency measures. Thermal runaway refers to an autonomous chemical process occurring within a battery, which has the potential to initiate a fire (Yin et al., 2023). The phenomenon arises when a cell within the battery experiences excessive heat accumulation and is unable to dissipate it, so initiating a cascading effect that raises the temperature of adjacent cells (Wang et al., 2021). The level of charge, commonly referred to as state of charge (SoC), significantly influences the likelihood of thermal runaway in batteries. Specifically, batteries with SoC below 50% have reduced susceptibility to thermal runaway (Nguyen et al., 2019).

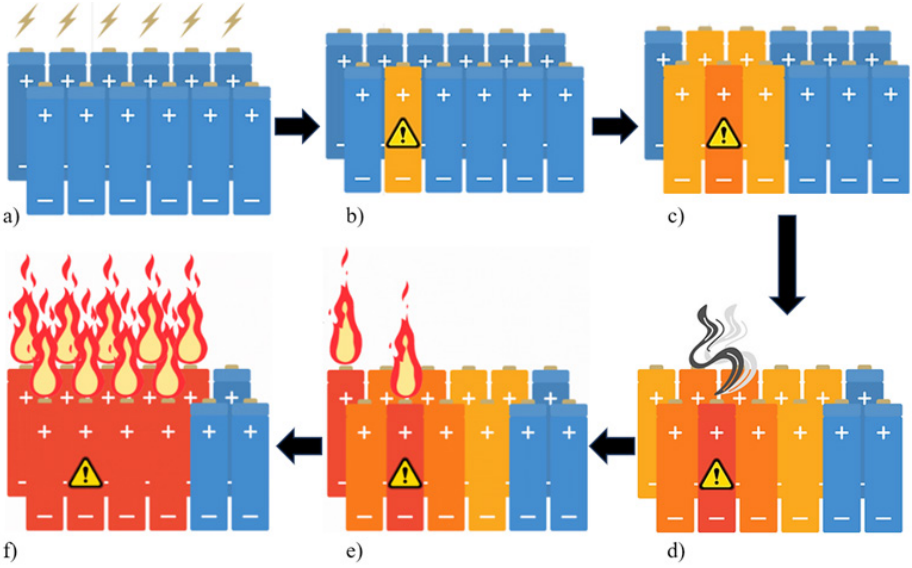

Figure 2. Thermal runaway and battery fire progression (a- battery module, b- the cell affected by short circuit, c- heating nearby battery cells, d- starting of the thermal runaway, e- cell ignition, f- car fire and explosion) (EVFireSafe, 2021)

Thermal runaway may also occur in an electric vehicle that has been exposed to flooding or seawater (Chen et al., 2022). In the occurrence of

water infiltration, the presence of saline water might establish a conduit for the generation of electrical sparks, so initiating thermal runaway (Schmidt, 2023). Therefore, Figure 2 has been compiled to represent the schematic view of the thermal runaway process and battery fire progression (EVFireSafe, 2021).

Table 2. Potential risks for car transportation on Ro-Ro passenger ships

Mechanical aspects	Systemic aspects	Procedural aspects
• Vibration	• Alarm system capability	• Instruction for fire teams
• Power grid system design	• Availability of manual and remote switch-off	• Passenger information system
• Electric cables	• Monitoring of the power system	• Signage and marking at the charging location
• Ventilation of car decks	• Voltage and frequency deviations	• The protocols pertaining to the storage, connection, and disconnection of cables.
• Protection classes of the electrical devices	• Compatibility with the power management system installed onboard	• Special handling of risky goods/battery condition
• Protection of the ship structure from explosion	• Alarm and monitoring system integration in the vessel	
• Compatibility from electromagnetic field	• Optimization of the power system parameters	
• Protection the components and cables from mechanical damages		

Numerous research is conducted in both academic and sectoral settings to provide insights into this matter. The occurrence of fire mishaps in automobile battery packs is mostly attributed to the phenomenon known as thermal runaway, as documented by (Wang et al., 2021). This implies that batteries undergo an uncontrolled exothermic reaction resulting in a rapid increase in temperature. Due to the volatile operational conditions inherent to electric vehicles, the battery packs are susceptible to experiencing thermal runaway in the event of exposure to thermal damage, electrical failure, or mechanical abuse. Moreover, it is worth noting that EVs include a higher quantity of high energy density combustibles compared to internal combustion engine vehicles. Consequently, fires involving EVs exhibit distinct features such as heightened flame intensity,

quick propagation, and the potential for explosions (Cui and Liu, 2021). The suppression of electric vehicle fires may only be achieved by the utilization of specifically engineered firefighting equipment, such as electric vehicle fire enclosures (EVFE) and water spray systems (Cui, Cong, et al., 2022).

The consequences of a disaster arising on a Ro-Ro vessel that entails passengers are considerably more extensive and severe, when evaluating the potential risks associated with the transportation of vehicles and passengers on Ro-Pax vessels, it is imperative to take into account many elements. Table 2 presents a comprehensive compilation of potential hazards; yet, it should be noted that it needs to conduct a fully exhaustive assessment (EMSA, 2022).

In addition to the mentioned risks, variables such as challenging weather and sea conditions, ship stability, external fire events, loading-unloading errors, theft, and intentional damage can also lead to the initiation of a fire incident and subsequent damage to vehicles transported on Ro-Ro ships.

7. Rules and Regulations about Carrying Electric Vehicles on Ro-Ro Passenger Ships

The regulation concerning the transportation of electric automobiles via maritime vessels is now undergoing continual development due to the evolving nature of technology and the dynamic growth of Ro-Ro usage. However, numerous international and national regulations exist regarding the ocean transportation of electric vehicles.

The point of view of this study is the evaluation of the IMDG (International Maritime Dangerous Goods) Code, specifically Chapter 2.9, which pertains to the transportation of battery-powered vehicles on ships. Chapter 2.9 specifically addresses the handling of “Miscellaneous dangerous substances and articles (class 9) and environmentally hazardous substances”. Furthermore, it should be noted that substances and objects falling under class 9 are further categorized within section 2.9.2.2 and listed below (IMDG, 2018).

- UN 3090 LITHIUM METAL BATTERIES (including lithium alloy batteries)
- UN 3091 LITHIUM METAL BATTERIES CONTAINED IN EQUIPMENT (including lithium alloy batteries)
- UN 3091 LITHIUM METAL BATTERIES PACKED WITH EQUIPMENT (including lithium alloy batteries)
- UN 3480 LITHIUM-ION BATTERIES (including lithium-ion polymer batteries)

- UN 3481 LITHIUM-ION BATTERIES CONTAINED IN EQUIPMENT (including lithium-ion polymer batteries) or
- UN 3481 LITHIUM-ION BATTERIES PACKED WITH EQUIPMENT (including lithium-ion polymer batteries)

Cells and batteries, regardless of whether they are integrated within equipment or manufactured beside equipment, and possess lithium in any state, ought to be classified under the relevant UN codes, specifically 3090, 3091, 3480, or 3481. If the conditions described in Section 2.9.4 are met, it is feasible to execute them in accordance with the mentioned entries, especially in the "Manual of Tests and Criteria" (IMDG, 2020).

In relation to the International Maritime Dangerous Goods (IMDG) Code, the following substances or products that pose a risk during transportation, but don't meet the criteria for classification under any other class, are listed below (IMDG, 2020).

- UN 3171 BATTERY-POWERED VEHICLE or
- UN 3171 BATTERY-POWERED EQUIPMENT

The products transported under this entry encompass many types of vehicles or equipment that are powered by wet batteries, sodium batteries, or lithium batteries. These batteries are installed within the articles themselves, which may include electrically powered cars, lawnmowers, wheelchairs, and other mobility aids.

The SOLAS Convention delineates the fundamental criteria governing the construction, outfitting, and operation of ships, with the aim of supporting their safety (Zisimopoulos, 2016). The aforementioned encompasses regulations pertaining to the arrangement, equipment, electrical components, fire prevention measures, life-saving devices, radio communication systems, navigational safety, and transportation of cargo. The regulatory standards specified below pertain to the regulations encompassed by the SOLAS convention, as relevant to the scope of this study (IMO, 2023b).

- SOLAS Chapter II-2, Regulation 15 – "Instructions, onboard training and drills": Implementing effective training protocols and conducting exercises for personnel on board who are tasked with executing ship procedures in emergency situations in order to mitigate the effects of fire.
- SOLAS Chapter II-2, Regulation 16 – "Operations": The objective of this regulation is to furnish guidance and instructions related to the appropriate

management of ships and cargo in terms of fire safety. In order to accomplish this, operational booklets on fire safety shall be supplied on board, and the venting of flammable vapors from cargo tanks shall be regulated.

- SOLAS Chapter II-2, Regulation 20 – "Protection of vehicle, special category and ro-ro spaces": In order to effectively satisfy the fire safety objectives outlined in this chapter, it is imperative to implement supplementary safety measures for ships equipped with vehicle, special category, and ro-ro areas. In order to fulfill this objective, it is imperative to install fire protection systems that are capable of effectively safeguarding the ship against fire hazards that may arise in vehicle, special category, and ro-ro spaces. Additionally, it is crucial to ensure the segregation of ignition sources from these aforementioned spaces. Furthermore, it is essential to provide sufficient ventilation in vehicle, special category, and ro-ro spaces.
- The SOLAS Chapter III, Part B, specifically focuses on the "Requirements for ships and life-saving appliances". Within this chapter, Section I addresses the regulations pertaining to both passenger ships and cargo ships. Regulation 19 specifically deals with "Emergency training and drills". Additionally, Section II of this chapter is dedicated to passenger ships, with Regulation 29 focusing on the "Decision support system for masters of passenger ships" and Regulation 30 addressing the conduct of "Drills".

During its 101st session held from 5 to 14 June 2019, the Maritime Safety Committee (MSC) granted approval to the "Interim Guidelines for Minimizing the Incidence and Consequences of Fires in Ro-Ro Spaces and Special Category Spaces of New and Existing Ro-Ro Passenger Ships". These guidelines were developed by the Sub-Committee on Ship Systems and Equipment. The following subjects are applicable to both newly constructed and currently operational vessels by interim guidelines (IMO, 2023a).

- Inspection of ship's power supply equipment and cables
- Maintenance plan for electrical cables and their sockets in Ro-Ro and special category spaces intended for power supply to vehicles or cargo units
- Electrical cables
- Shock/waterproof rating of electrical connections
- Circuit breakers
- Electrical connections and disconnections of cargo units and electrical vehicles
- Check points at patrols
- Strengthening of the requirement for elimination of sources of ignition

Ship owners and ship operators have a legal obligation to comply with all pertinent rules and regulations. By strictly adhering to the defined norms and regulations, it is possible to augment the safety of carrying electric vehicles through marine vessels. The ongoing development of regulations and standards for the transportation of electric vehicles via ships is a significant aspect to consider, given the recent developments in technology and the rapid growth of the sector.

8. Conclusion

The occurrence of electric car fires in both closed and open land areas reduces the severity of the hazardous scenario but to a relatively limited extent. In the context of maritime transportation, it is important to note that the absence of open spaces poses a unique challenge when it comes to fire incidents. In such scenarios, the ship's current tools are utilized to address and mitigate fires that occur in the open sea. The absence of external firefighting teams or equipment at sea necessitates a more meticulous examination of the difficulties involved in transporting such vehicles on ships. The emission of hazardous gasses and various chemical substances resulting from a fire incident involving an electric vehicle with a compromised or overheated battery has the potential to impede the prompt reaction of maritime personnel. Furthermore, the occurrence of an explosion poses a potential risk to navigation as it may result in detrimental effects on the ship's machinery and equipment. One of the most perilous scenarios involves a potential incident where a vehicle, while carrying a passenger, catches fire on the vehicle deck of a Ro-Ro cruise ship. Such an occurrence has the potential to inflict substantial harm to human life, property, and the environment.

In addition to the considerations, there are several issues pertaining to the transportation of electric vehicles via maritime vessels. The increased weight of electric vehicles in comparison to conventional vehicles will result in a reduction in their load-carrying capability. The rise in vehicle weight results in a reduction in the number of vehicles that can be accommodated within a given area on a Ro-Ro vessel that is exclusively occupied by electric vehicles. Furthermore, the requirement for regular charging of these vehicles poses a notable challenge. In this scenario, it is necessary to conduct an extensive analysis and make necessary modifications to both the ship's electrical generation system and the car deck arrangement. Furthermore, it is imperative to assess whether the ship's crew possesses adequate expertise in effectively addressing emergencies, as well as to evaluate the adequacy of the crew's number.

Despite the inherent risks and limitations, a significant increase in the maritime transportation of electric vehicles is expected in the foreseeable future. The increasing worldwide popularity and market demand for electric vehicles can be ascribed to this phenomenon. To mitigate the hazards inherent in the maritime transportation of electric vehicles, it is advisable to conduct comprehensive inspections of such vehicles prior to their boarding onto ships, and then transport them in an isolated location to ensure their safe conveyance. Furthermore, it is imperative to incorporate comprehensive fire detection and extinguishing systems, offer extensive training to crew members, and secure the adoption of measures pertaining to these aspects by global maritime agencies in accordance with distinct guidelines and regulations.

References

ACEA. (2023). *Fuel types of new passenger cars in the EU*. https://www.acea.auto/figure/fuel-types-of-new-passenger-cars-in-eu/#:~:text=36.4%25 of all new cars,accounts for 16.4%25 of registrations

Allerth, D., & Niklasson, A. (2022). *How is Electrification Affecting the Onboard Fire Safety?* Chalmers University of Technology.

Argüello, G. (2022). The International Maritime Organization's Contribution to Regime Interaction: Past, Present, and Future. *Max Planck Yearbook of United Nations Law Online*, 1–25. https://doi.org/10.1163/18757413

Arvidson, M., & Westlund, Ö. (2023). Water Spray Fire Suppression Tests Comparing Gasoline-Fuelled and Battery Electric Vehicles. *Fire Technology*, 1–24. https://doi.org/10.1007/s10694-023-01473-w

Bao, J., Bian, Z., Li, B., Li, Y., & Gong, Y. (2023). A Hybrid Approach for Quantitative Analysis of Fire Hazards in Enclosed Vehicle Spaces on Ro-ro Passenger Ships. *Sustainability (Switzerland)*, *15*(17). https://doi.org/10.3390/su151713059

Brcko, T., Pavić, I., Mišković, J., & Androjna, A. (2023). Investigating the Human Factor in Maritime Accidents: A Focus on Compass-Related Incidents. *Transactions on Maritime Science*, *12*(2). https://doi.org/10.7225/toms.v12.n02.w01

Brzezinska, D., & Bryant, P. (2022). Performance-Based Analysis in Evaluation of Safety in Car Parks under Electric Vehicle Fire Conditions. *Energies*, *15*(2). https://doi.org/10.3390/en15020649

Bush, D. (2020). *Höegh Xiamen highlights PCTC fire risks*. https://lloydslist.com/LL1132742/Hegh--Xiamen-highlights-PCTC-fire-risks

Chen, J., Li, K., & Yang, S. (2022). Electric Vehicle Fire Risk Assessment Based on WBS-RBS and Fuzzy BN Coupling. *Mathematics*, *10*(20), 3799. https://doi.org/10.3390/math10203799

Chen, X., Li, F., Jia, B., Wu, J., Gao, Z., & Liu, R. (2021). Optimizing storage location assignment in an automotive Ro-Ro terminal. *Transportation Research Part B: Methodological*, *143*, 249–281. https://doi.org/10.1016/j.trb.2020.10.009

Cui, Y., Cong, B., Liu, J., Qiu, M., & Han, X. (2022). Characteristics and Hazards of Plug-In Hybrid Electric Vehicle Fires Caused by Lithium-Ion Battery Packs With Thermal Runaway. *Frontiers in Energy Research*, *10*(April), 1–11. https://doi.org/10.3389/fenrg.2022.878035

Cui, Y., & Liu, J. (2021). Research progress of water mist fire extinguishing technology and its application in battery fires. *Process Safety and Environmental Protection*, *149*, 559–574. https://doi.org/10.1016/j.psep.2021.03.003

Cui, Y., Liu, J., Cong, B., Han, X., & Yin, S. (2022). Characterization and assessment of fire evolution process of electric vehicles placed in parallel. *Process Safety and Environmental Protection*, *166*(August), 524–534. https://doi.org/10.1016/j.psep.2022.08.055

Dias, J. C. Q., Calado, J. M. F., & Mendonça, M. C. (2010). The role of European «ro-ro» port terminals in the automotive supply chain management. *Journal of Transport Geography*, *18*(1), 116–124. https://doi.org/10.1016/j.jtrangeo.2008.10.009

Dnistran, I. (2023). *Report: EVs Onboard Cargo Ship That Caught Fire "In Good Condition"*. https://insideevs.com/news/683115/evs-on-fremantle-highway-cargo-ship-good-condition-report/

Dorsz, A., & Lewandowski, M. (2022). Analysis of fire hazards associated with the operation of electric vehicles in enclosed structures. *Energies*, *15*(1). https://doi.org/10.3390/en15010011

EMSA. (2022). *Guidance for AFVs carriage in ro-ro spaces*.

EVFireSafe. (2021). *What is thermal runaway?* https://www.evfiresafe.com/ev-fire-what-is-thermal-runaway%0A

Fu, Q., Yao, J., Ya, S., & Zhao, F. (2023). Study on Fire Risk of Pure Car Carrier Vessels Carrying New Energy Vehicle. *2023 7th International Conference on Transportation Information and Safety (ICTIS)*, 2498–2505. https://doi.org/10.1109/ictis60134.2023.10243699

Funk, E., Flecknoe-Brown, K. W., Wijesekere, T., Husted, B. P., & Andres, B. (2023). Fire extinguishment tests of electric vehicles in an open sided enclosure. *Fire Safety Journal*, *141*(August), 103920. https://doi.org/10.1016/j.firesaf.2023.103920

Göksu, B., & Bayramoglu, K. (2023). Effect of electric vehicle transportation and carbon capture system on concept Ro-Ro ship stability and

EEDI. *Marine Science and Technology Bulletin*, *12*(3), 267–281. https://doi.org/10.33714/masteb.1313638

Grunditz, E. A., & Thiringer, T. (2016). Performance analysis of current BEVs based on a comprehensive review of specifications. *IEEE Transactions on Transportation Electrification*, *2*(3), 270–289. https://doi.org/10.1109/TTE.2016.2571783

Gulbrandsen, C. (2013). Navigating from Conflict to Working Arrangement: EU Coordination in the International Maritime Organization. *Journal of European Integration*, *35*(7), 749–765. https://doi.org/10.1080/07036337.2012.732072

Hu, Y., & Ma, M. (2022). A Study on the Current Situation of Safety Management of Bohai Bay Ro-Ro Passenger-Ship Terminals in Shandong Province in China. *Proceedings of the 2022 3rd International Conference on Management Science and Engineering Management (ICMSEM 2022)*, 315–323. https://doi.org/10.2991/978-94-6463-038-1

Hynynen, J., Quant, M., Pramanik, R., Olofsson, A., Li, Y. Z., Arvidson, M., & Andersson, P. (2023). *Electric Vehicle Fire Safety in Enclosed Spaces* (Issue 2023:42).

Iannone, R., Miranda, S., Prisco, L., Riemma, S., & Sarno, D. (2016). Proposal for a flexible discrete event simulation model for assessing the daily operation decisions in a Ro-Ro terminal. *Simulation Modelling Practice and Theory*, *61*, 28–46. https://doi.org/10.1016/j.simpat.2015.11.005

IEA. (2023). *Electric Vehicles*. https://www.iea.org/energy-system/transport/electric-vehicles%0A

IMDG. (2018). *International Maritime Dangerous Goods (IMDG) Code, 2018 Edition* (Vol. 2018). International Maritime Organization.

IMDG. (2020). *International Maritime Dangerous Goods (IMDG) Code, 2020 Edition* (Vol. 2020).

IMO. (2023a). *Interim Guidelines for Minimizing the Incidence and Consequences of Fires in Ro-Ro Spaces and Special Category Spaces of New and Existing Ro-Ro Passenger Ships*. https://www.imorules.com/GUID-D7AD7608-7EF7-48BD-B738-27BB7D89531F.html%0A

IMO. (2023b). *SOLAS - International Convention for the Safety of Life at Sea*. https://www.imorules.com/SOLAS.html%0A

IUMI. (2022). *Quarterly news from the International Union of Marine Insurance* (Issue 39).

Kang, H. J., Choi, J., Lee, D., & Park, B. J. (2017). A framework for using computational fire simulations in the early phases of ship design. *Ocean Engineering*, *129*, 335–342. https://doi.org/10.1016/j.oceaneng.2016.11.018

Kaptan, M. (2022). Analysis of accidents during vehicle stowage on RO-RO vessels by using Fuzzy Bayesian networks. *Ocean Engineering*, *260*(July), 111997. https://doi.org/10.1016/j.oceaneng.2022.111997

Koromila, I., Pouangare, A. C., & Spyrou, K. J. (2021). Design Fires for Vehicle Decks of RO / RO Passenger Ships. *Proceedings of the 1st International Conference on the Stability and Safety of Ships and Ocean Vehicles*, *June*.

Kotowska, I. (2015). The role of ferry and Ro-Ro shipping in sustainable development of transport. *Review of Economic Perspectives*, *15*(1), 35–48. https://doi.org/10.1515/revecp-2015-0010

Maritime Executive. (2023). *Fremantle Highway Fire Lessens as Vessel Continues to Drift off Dutch Coast*. https://maritime-executive.com/article/fremantle-highway-fire-lessens-as-vessel-continues-to-drift-off-dutch-coast

Mok, I. S., D'Agostini, E., & Ryoo, D. K. (2023). A validation study of ISM Code's continual effectiveness through a multilateral comparative analysis of maritime accidents in Korean waters. *Journal of Navigation*, *76*(1), 77–90. https://doi.org/10.1017/S0373463322000571

Nguyen, T. T. D., Abada, S., Lecocq, A., Bernard, J., Petit, M., Marlair, G., Grugeon, S., & Laruelle, S. (2019). Understanding the thermal runaway of ni-rich lithium-ion batteries. *World Electric Vehicle Journal*, *10*(4), 79. https://doi.org/10.3390/wevj10040079

Osler, D. (2021). *Höegh Xiamen fire caused by vehicle battery*. https://lloydslist.com/LL1139363/Hegh-Xiamen-fire-caused-by-vehicle-battery%0A

Puisa, R. (2021). Optimal stowage on Ro-Ro decks for efficiency and safety. *Journal of Marine Engineering and Technology*, *20*(1), 17–33. https://doi.org/10.1080/20464177.2018.1516942

Riess, R., & Gray, M. (2021). *The Golden Ray cargo ship capsized because of inaccurate stability calculations, the NTSB finds*. https://edition.cnn.com/2021/09/14/us/golden-ray-cargo-ship-ntsb-report/index.html

Rodrigue, J. P., Comtois, C., & Slack, B. (2020). The geography of transport systems. In *The Geography of Transport Systems*. https://doi.org/10.4324/9781315618159

Schmidt, B. (2023). *Understanding electric vehicle fires: A comprehensive guide*. https://www.mynrma.com.au/electric-vehicles/basics/understanding-electric-vehicle-fires%0A

Shan, D. (2022). Enforcement of fishing Occupational Health and Safety (OHS) standards: Challenges in Atlantic Canada. *Marine Policy*, *145*(November 2021), 105282. https://doi.org/10.1016/j.marpol.2022.105282

Spaniol, M. J., & Rowland, N. J. (2022). Business ecosystems and the view from the future: The use of corporate foresight by stakeholders of the Ro-Ro

shipping ecosystem in the Baltic Sea Region. *Technological Forecasting and Social Change*, *184*, 121966. https://doi.org/10.1016/j.techfore.2022.121966

Späth, N. (2016). *Enhancing fire safety on Ro-Ro decks*. https://www.dnv.com/news/enhancing-fire-safety-on-ro-ro-decks-69059

Sun, P., Bisschop, R., Niu, H., & Huang, X. (2020). A Review of Battery Fires in Electric Vehicles. In *Fire Technology* (Vol. 56, Issue 4). Springer US. https://doi.org/10.1007/s10694-019-00944-3

Taiebat, M., Brown, A. L., Safford, H. R., Qu, S., & Xu, M. (2018). A review on energy, environmental, and sustainability implications of connected and automated vehicles. *Environmental Science and Technology*, *52*(20), 11449–11465. https://doi.org/10.1021/acs.est.8b00127

Tarelko, W. (2012). Origins of ship safety requirements formulated by International Maritime Organization. *Procedia Engineering*, *45*, 847–856. https://doi.org/10.1016/j.proeng.2012.08.249

Voytenko, M. (2020). *Grimaldi's ferry fire*. https://www.fleetmon.com/maritime-news/2020/29975/grimaldis-ferry-fire-sardinia-video/

Walker, T. R., Adebambo, O., Del Aguila Feijoo, M. C., Elhaimer, E., Hossain, T., Edwards, S. J., Morrison, C. E., Romo, J., Sharma, N., Taylor, S., & Zomorodi, S. (2018). Environmental effects of marine transportation. *World Seas: An Environmental Evaluation Volume III: Ecological Issues and Environmental Impacts*, *September*, 505–530. https://doi.org/10.1016/B978-0-12-805052-1.00030-9

Wan, Z., el Makhloufi, A., Chen, Y., & Tang, J. (2018). Decarbonizing the international shipping industry: Solutions and policy recommendations. *Marine Pollution Bulletin*, *126*, 428–435. https://doi.org/10.1016/j.marpolbul.2017.11.064

Wang, Z., He, T., Bian, H., Jiang, F., & Yang, Y. (2021). Characteristics of and factors influencing thermal runaway propagation in lithium-ion battery packs. *Journal of Energy Storage*, *41*, 102956. https://doi.org/10.1016/j.est.2021.102956

Weng, J., & Yang, D. (2015). Investigation of shipping accident injury severity and mortality. *Accident Analysis and Prevention*, *76*, 92–101. https://doi.org/10.1016/j.aap.2015.01.002

Williamsson, J. (2022). EV Charging on Ferries and in Terminals—A Business Model Perspective. *Energies*, *15*(18), 6723.

Wu, J., Jin, Y., & Fu, J. (2014). Effectiveness Evaluation on Fire Drills for Emergency and PSC Inspections on Board. *TransNav, the International Journal on Marine Navigation and Safety of Sea Transportation*, *8*(2), 229–236. https://doi.org/10.12716/1001.08.02.08

Yin, S., Liu, J., & Cong, B. (2023). Review of Thermal Runaway Monitoring, Warning and Protection Technologies for Lithium-Ion Batteries. *Processes*, *11*(8). https://doi.org/10.3390/pr11082345

Zisimopoulos, D. A. (2016). *Use of Fiber Reinforced Plastics in Ship Construction: A Study of SOLAS regulation II-2/17 on Alternative Design and Arrangements for Fire Safety*.

CHAPTER V

THE BEHAVIOUR OF A TUBULAR SPACE TRUSS UNDER BENDING IN ELASTIC AND ELASTIC-PLASTIC REGION*

Muhammet Zeki ÖZYURT[1] & H. Halit DEMİR[2]

[1](Asst. Prof. Dr.), Sakarya University, Sakarya, Turkey
E-mail: ozyurt@sakarya.edu.tr
ORCID: 0000-0002-1593-4581
[1](Prof. Dr.), Istanbul Technical University, Istanbul, Turkey
E-mail: demirh@itu.edu.tr

1. Introduction

Space trusses which are widely used in technology have found wide application in the fields of construction of buildings, industrial plants, highway and railway bridges, antenna towers, off-shore platforms and space constructions.

Avent and Issa have studied on the beam element stiffness matrix for x-braced trusses. They have also compared the results of the trusses considered, with the results of solid beams (Avent and Issa, 1982). Besides, Schmidt and Hanaor have investigated the behaviour of space trusses subject to limit forces and the failure of the system with several restraints (Schmidt and Hanaor, 1979). Sheu and Schmit have studied on the minimum weight design of elastic redundant trusses under multiple static loadings (Sheu and Schmit, 1972). Ökten and Kasap have studied on the behavior of the tubular square space trusses consisting of hollow bars under torsion with bending in elastic and elastic-plastic region as well (Ökten and Kasap, 1997).

The aim of this study is to investigate the elastic and elastic-plastic behavior of square tubular space trusses subject to bending.

*This chapter produced from the first author's doctoral thesis titled "Dikdörtgen Kesitli Tübüler Uzay Kafes Kirişlerin Elastik Ve Elastik-Plastik Analizi".

A typical example of a tubular space truss is given in Figure 1.

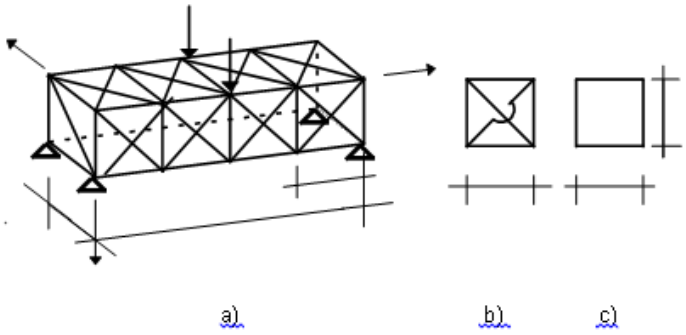

Figure 1. Typical tubular space truss

The dimensions of the space truss are assumed as follows;

span length	:	L = 4 m ; 6 m ; 8 m ; 12 m
cross-section	:	b / h = 1 m / 1 m
vertical bar spacing	:	a = 1 m ; 2 m

The tubular space trusses consist of rods with hollow cross-sections. The type of steel used in the rods is St 37. Cases of trusses with or without inner diagonals are considered.

As shown in Figure 2, tubular space trusses are considered under three different support conditions corresponding to the roller, hinged and fixed supports.

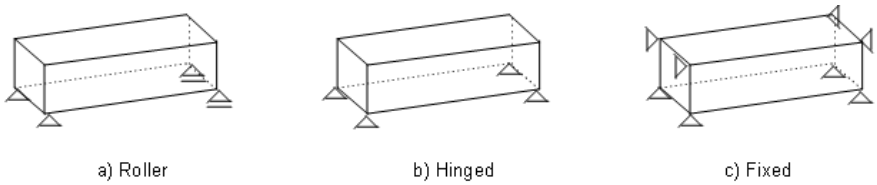

Figure 2. Support conditions

Loading conditions. Three different kinds of loading are applied to the tubular space trusses (Fig 3). Loads are applied to the joints and consist of one or two equal vertical forces or a force couple.

Basic assumptions of the analysis are given below:

- Joints are ideal hinges
- In horizontal and vertical planes of space truss and in the plane of the cross-section of the truss it is assumed that diagonals do not intersect each other.
- The behavior of steel is assumed to be ideal elastic- plastic.

- It is assumed that cross sectional areas of bars can be arbitrary.
- It is assumed that the system is not subject to any lateral buckling.

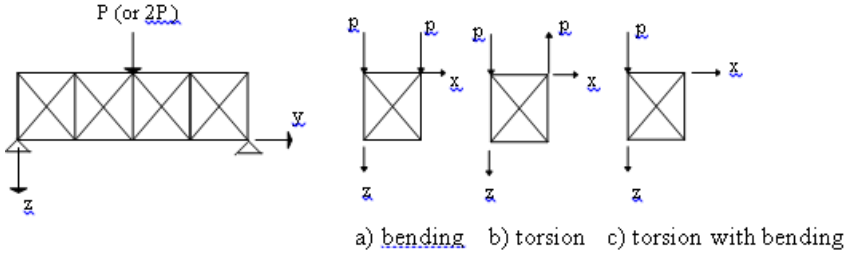

Figure 3. Loading conditions

2. Elastic Analysis

Tubular square space trusses described in the first section have been designed for three loading cases (bending, torsion with bending, torsion) under the service load of Ps =120 kN using the allowable stress method. Firstly, the system is solved as elastic by the computer program using the matrix deflection method, by assuming an arbitrary cross-sectional size (area, A,radius of inertia, i) for each bar group (bar groups: vertical bars, transversal bars, upper chords, lower chords, horizontal, vertical and inner diagonals). Cross-sections of the bars are designed according to the forces assumed as $\sigma max \cong \sigma all$, and the system is solved with these new dimensions. Here sall is taken as 140 N/mm2 and buckling calculations have been performed by ω numbers method. Space trusses, which are investigated, are designed as explained above and the cross sectional areas of the bar groups in each system is given in Table 1.

Designing process of the square space truss is performed by the allowable stress method at service loading. At the same time, vertical displacements of the joints have also been determined under combined loading of bending. E is taken as 21000 kN / cm^2

Vertical displacements of lower points of middle cross section of space trusses under bending are given in Table 2. According to these results, deflection-span (δ-L) diagrams are drawn for each system (Fig. 4).

Table 1. Cross-sectional areas of bars (cm^2) (b/ h = 1 m / 1 m)

Vertical Spacing		a = 1 m						a = 2 m					
Support Conditions		Roller		Hinged		Fixed		Roller		Hinged		Fixed	
Inner Diagonals	L	exist	absent	exist	absent	exist	Absent	exist	absent	Exist	absent	Exist	absent
Verticals	4m	5.13	4.95	4.92	4.68	5.01	5.01	5.46	5.55	4.65	3.93	5.34	5.31
	6m	4.95	4.77	4.86	4.65	4.95	4.92	-	-	-	-	-	-
	8m	4.89	4.68	4.86	4.62	4.95	4.86	5.61	5.37	5.43	4.62	5.55	5.46
	12m	4.86	4.62	4.80	4.59	4.92	4.83	5.55	5.37	5.43	4.95	5.52	5.66
Transversal bars	4m	2.58	2.37	1.80	2.07	1.98	2.16	2.91	2.91	0.63	0.63	0.63	0.63
	6m	2.90	2.43	2.13	2.28	2.13	2.28	-	-	-	-	-	-
	8m	2.97	2.76	2.37	2.40	2.40	2.43	5.34	4.44	3.12	3.03	2.52	2.91
	12m	3.15	2.58	2.79	2.58	2.82	2.70	6.03	4.77	4.11	4.05	3.69	4.02

Table 1. Cross-sectional areas of bars (cm^2) (b/ h = 1 m / 1 m) (Continue)

Vertical Spacing		a = 1 m						a = 2 m					
Support Conditions		Roller		Hinged		Fixed		Roller		Hinged		Fixed	
Inner Diagonals	L	exist	absent	exist	absent	exist	Absent	exist	absent	Exist	absent	Exist	absent
Upper chords	4m	7.44	7.68	6.99	7.47	3.18	3.72	6.54	7.56	5.31	5.61	0.63	0.63
	6m	11.28	11.46	11.10	11.52	5.16	5.82	-	-	-	-	-	-
	8m	15.24	15.24	15.18	15.48	7.23	7.98	14.01	16.20	12.51	15.48	6.18	8.08
	12m	22.71	23.19	22.63	23.31	11.22	12.09	21.63	24.69	20.31	24.30	9.72	12.39
Lower chords	4m	5.85	8.55	3.30	3.84	3.51	4.14	4.35	8.85	0.63	0.63	0.63	0.63
	6m	10.26	12.78	4.98	6.06	5.40	6.33	-	-	-	-	-	-
	8m	14.58	17.24	6.90	8.34	7.47	8.52	8.01	17.64	5.85	7.65	6.44	8.40
	12m	23.20	25.62	10.77	12.51	11.43	12.63	15.44	25.92	8.94	11.43	9.87	12.57
Vertical Diagonals	4m	5.85	6.30	6.66	6.66	6.18	6.21	9.48	9.87	11.46	11.73	9.75	9.81
	6m	6.12	6.48	6.96	6.93	6.24	6.36	-	-	-	-	-	-
	8m	6.18	6.66	7.05	6.99	6.24	6.45	9.12	9.87	11.52	12.12	9.60	9.66
	12m	6.27	6.54	7.17	7.05	6.24	6.39	9.27	9.87	12.12	12.39	9.60	9.57
Horizontal Diagonals	4m	4.02	2.70	3.81	2.61	3.93	2.67	6.33	5.10	5.37	3.81	5.46	0.63
	6m	4.14	2.88	4.17	2.85	4.08	3.00	-	-	-	-	-	-
	8m	4.08	3.30	4.08	3.03	4.08	3.24	8.10	7.38	7.65	6.90	6.63	5.85
	12m	4.14	3.15	4.11	3.51	4.08	3.60	8.85	7.95	8.67	7.80	7.80	7.35
Inner Diagonals	4m	4.71	-	4.56	-	4.62	-	5.13	-	4.29	-	4.35	-
	6m	4.56	-	4.56	-	4.59	-	-	-	-	-	-	-
	8m	4.53	-	4.50	-	4.56	-	5.19	-	5.04	-	5.07	-
	12m	4.44	-	4.41	-	4.53	-	5.07	-	5.01	-	5.04	-

Table 2. Deflection values at the middle of the space trusses and K values (δ values are cm)

L	a	inner	Roller				Hinged				Fixed			
(m)	(m)	diagonals	δ	δ′	K	K′	δ	δ′	K	K′	δ	δ′	K	K′
	1	exist	0.33	0.23	0.0296	0.0208	0.22	0.34	0.0135	0.0208	0.18	0.11	0.0082	0.0052
		absent	0.29	0.19	0.0321	0.0208	0.22	0.30	0.0153	0.0208	0.17	0.10	0.0091	0.0052
4	2	exist	0.29	0.26	0.0233	0.0208	0.17	1.35	0.0026	0.0208	0.14	0.60	0.0012	0.0052
		absent	0.25	0.19	0.0279	0.0208	0.17	1.34	0.0026	0.0208	0.14	0.60	0.0012	0.0052
6	1	exist	0.62	0.48	0.0270	0.0208	0.45	0.75	0.0125	0.0208	0.36	0.24	0.0077	0.0052
		absent	0.57	0.42	0.0279	0.0208	0.44	0.65	0.0142	0.0208	0.34	0.21	0.0085	0.0052
	1	exist	1.02	0.82	0.0260	0.0208	0.76	1.28	0.0123	0.0208	0.59	0.41	0.0074	0.0052
		absent	0.95	0.75	0.0263	0.0208	0.73	1.14	0.0135	0.0208	0.55	0.37	0.0077	0.0052
8	2	exist	1.09	1.19	0.0190	0.0208	0.66	1.53	0.0090	0.0208	0.53	0.48	0.0057	0.0052
		absent	0.85	0.72	0.0245	0.0208	0.60	1.19	0.0105	0.0208	0.50	0.37	0.0070	0.0052
	1	exist	2.10	1.79	0.0244	0.0208	159	2.82	0.0118	0.0208	1.19	0.91	0.0068	0.0052
		absent	2.00	1.69	0.0247	0.0208	1.19	2.52	0.0127	0.0208	1.12	0.83	0.0070	0.0052
12	2	exist	2.23	2.28	0.0203	0.0208	1.41	3.31	0.0089	0.0208	1.11	1.05	0.0055	0.0052
		absent	1.82	1.62	0.0233	0.0208	1.28	2.64	0.0101	0.0208	1.02	0.82	0.0064	0.0052

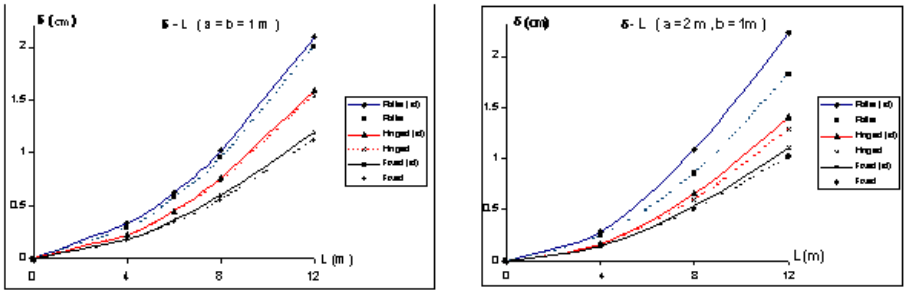

Note: Systems with inner diagonals are symbolized as (id).

Figure 4. Deflection-span (d-L) diagrams

As a second approach, the same space trusses are considered as consisting of only upper and lower chords like a solid beam and the deflections (δ′) at the middle of these beams are calculated with equation below (Fig. 5).

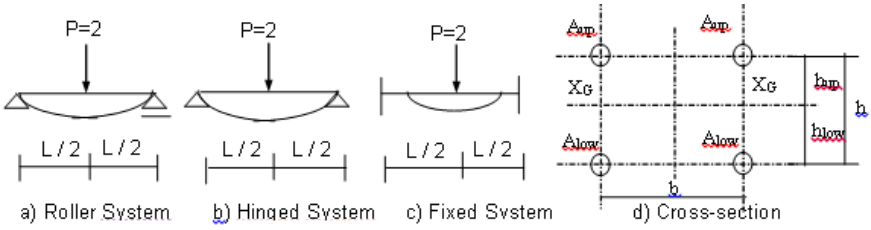

Figure 5. The space trusses are considered like a solid beam

$$\delta\ '= K\ ' \frac{P\ L^3}{E\ I} \tag{1}$$

In this equation, inertia I is taken as below.

$$I = 2\ A_{up}\ h_{up}^2\ +\ 2\ A_{low}\ h_{low}^2 \tag{2}$$

If deflection at the middle of space trusses is

$$\delta = K\ \ \frac{P\ L^3}{E\ I} \tag{3}$$

K will be

$$K = \delta\ \ \frac{E\ I}{P\ L^3} \tag{4}$$

And K-L curves depicting the relationship between K values and span are given in Fig 6.

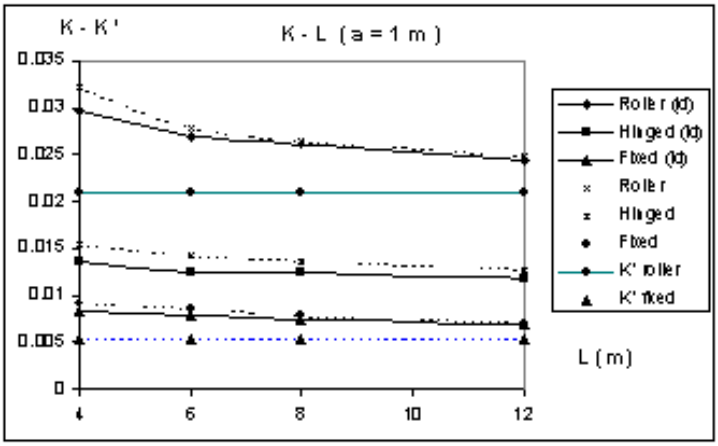

Figure 6. K-L curves

Deflections at the middle of the span of a tubular space truss loaded by service load (Ps = 120 kN) are given in Table 2. According to these values, span-deflection diagrams are shown in Figure 4. The equations of the curves obtained by the method of least squares have been found as follows.

$$\delta = c\ L^d \tag{5}$$

While the coefficients K′ in equation (1) are constant (for example K ' =1/48 for roller and hinged systems) for a solid beam, they are variable for trusses and given as

$$K = m\ L^n \tag{6}$$

Coefficients c, d, m and n appearing in the relations depend on vertical bar spacing, on whether there are inner diagonals or not and on the support conditions (Table 3). Values of L and δ are given in meters and centimeters respectively.

Table 3: *c*, *d* , *m* and *n* coefficients

Inner	a		Support Condition		
Diagonals	(m)		Roller	Hinged	Fixed
exist	1	*c* ; *d*	0.0310 ; 1.687	0.0180 ; 1.802	0.0166; 1.719
		m ; *n*	0.0373 ; 0.173	0.0158 ; 0.122	0.0104; 0.167
	2	*c* ; *d*	0.0221 ; 1.863	0.0118 ; 1.929	0.0103 ; 1.888
absent	1	*c* ; *d*	0.0249 ; 1.759	0.0187 ; 1.771	0.0158 ; 1.713
		m ; *n*	0.0436 ; 0.236	0.0192 ; 0.170	0.0129 ; 0.246
	2	*c* ; *d*	0.0204 ; 1.802	0.0133 ; 1.836	0.0114 ; 1.811

Deflection values are determined according to the existence or absence of inner diagonals, different support conditions and different vertical bar spacing. Then the effects of inner diagonals, support conditions and vertical bar spacing on deflection are investigated.

3. Elastic-Plastic Analysis

The elastic-plastic analysis has been performed for only fixed supported space trusses using the load increment technique. The service loads have been increased until the maximum stress reached $\sigma max \cong \sigma y$ in a bar (or a group of bars) and so the first yielding is obtained, the bar stresses obtained for this loading are denoted in the table by σ1. It has been assumed that bars approaching σy ($\sigma \cong 235$ N/mm^2) at the end of this loading yield. Then, they are taken out from the system and the new system with other bars is loaded again from zero with an increasing ΔP1 load and then Δσ stresses are obtained in the bars. At some bars, the value of ($\sigma 1 + \Delta\sigma 1 \cong \sigma y$) ΔP1 loading is calculated while the value of σ1 + Δσ1 does not exceed the value of σy and the stresses σ2 are obtained as a sum of σ1 and Δσ1 stresses. Bars in which the σ2 stress approaches σy are taken out from the system and ΔP loading is applied again. Similarly, Δσ stresses have been calculated and total stresses have been obtained. ΔP loading process is repeated while the failure load of the space truss has been computed as bars in which stress approaches to σy are taken out at each step. So, elastic-plastic analysis is performed. The values of deflection which occurs at each step are added to the previous deflection values and so deflection values at yielding are obtained.

The load capacity of space trusses at yielding (loads corresponding to yielding) and displacement (δ) in the cross-sections in the middle of the span of space truss are found; the deflections are given in the Table 4. Using these values, load-deflection (P- δ) curves in bending are given in the Fig.7 and Fig. 8.

Table 4. Deflections at the middle of space trusses at the yielding time

L m	A M	Inner Diagonals	Support Condition									
4	1	Exist	Roller	P_i	201.10	202.95	203.40	205.05	208.24	211.65		
				δ_i	0.54	0.5466	0.5529	0.5769	0.6359	0.7226		
			Hinged	P_i	199.40	201.15	202.15	202.55	202.65	214.10		
				δ_i	0.38	0.386	0.390	0.394	0.418	0.568		
			Fixed	P_i	195.00	201.00	204.00	205.50	210.00	226.35	229.40	
				δ_i	0.29	0.299	0.306	0.310	0.345	0.378	0.395	
		Absent	Fixed	P_i	197.50	198.10	199.60	201.80				
				δ_i	0.28	0.2809	0.2831	0.2881				
8	1	Exist	Roller	P_i	201.34	201.40	201.51	203.78	203.89	206.19		
				δ_i	1.71	1.7115	1.7196	1.9196	1.9292	2.2510		
			Hinged	P_i	194.48	200.12	201.77	202.61	207.60	207.77		
				δ_i	1.22	1.262	1.279	1.304	1.454	1.4593		
			Fixed	P_i	201.90	203.00	217.67	223.88	227.76	228.21	233.41	234.99
				δ_i	0.99	0.9984	1.1484	1.2134	1.2643	1.2805	1.4765	1.5935
		Absent	Fixed	P_i	199.01	202.72	203.29	204.67				
				δ_i	0.91	0.927	0.9293	0.9350				
	2	Exist	Roller	P_i	202.13	202.30	202.71	202.84	204.47	205.83		
				δ_i	1.84	1.8419	1.8468	1.8492	1.9102	2.0392		
			Hinged	P_i	201.81	202.07	203.16	203.23	204.62	205.73	209.51	
				δ_i	1.11	1.1115	1.1225	1.1232	1.1482	1.1792	1.2294	
			Fixed	P_i	199.72	201.65	202.18	202.45	221.02	221.50	221.62	245.14
				δ_i	0.88	0.8867	0.8921	0.8940	1.0340	1.0381	1.0392	1.2692
		Absent	Fixed	P_i	201.44	201.94						
				δ_i	0.83	0.8311						
12	1	Exist	Roller	P_i	201.34	203.38	204.73					
				δ_i	3.53	3.95	4.42					
			Hinged	P_i	201.43	204.70	207.05	207.58	208.11			
				δ_i	2.68	2.90	3.07	3.19	3.82			
			Fixed	P_i	202.21	211.26	215.78	218.32	218.67	220.28		
				δ_i	2.01	2.21	2.31	2.62	2.69	3.26		
		Absent	Fixed	P_i	201.72							
				δ_i	1.88							

P_i is kN, δ_i is cm

The real safety factors (Pu / Ps) are found using the ratio between the load carrying capacity at failure and service load. Ductility δu / δ1) of systems are found using the ratio between the values of deflection at failure and at the first yielding (Table 5).

Table 5. P, d ratios

Ratios	Inner Diagonals	Support Condition	L (m)			
			4	8		12
			a = 1 m	a = 1 m	a = 2 m	a = 1 m
P_u / P_s	exist	Roller	1.763	1.712	1.715	1.706
		Hinged	1.784	1.731	1.746	1.734
		Fixed	1.966	1.958	2.043	1.835
	absent	Fixed	1.682	1.705	1.683	1.681
δ_u / δ_1	exist	Roller	1.338	1.316	1.108	1.252
		Hinged	1.495	1.196	1.107	1.425
		Fixed	1.362	1.609	1.442	1.621
	absent	Fixed	1.028	1.027	1.001	1.000

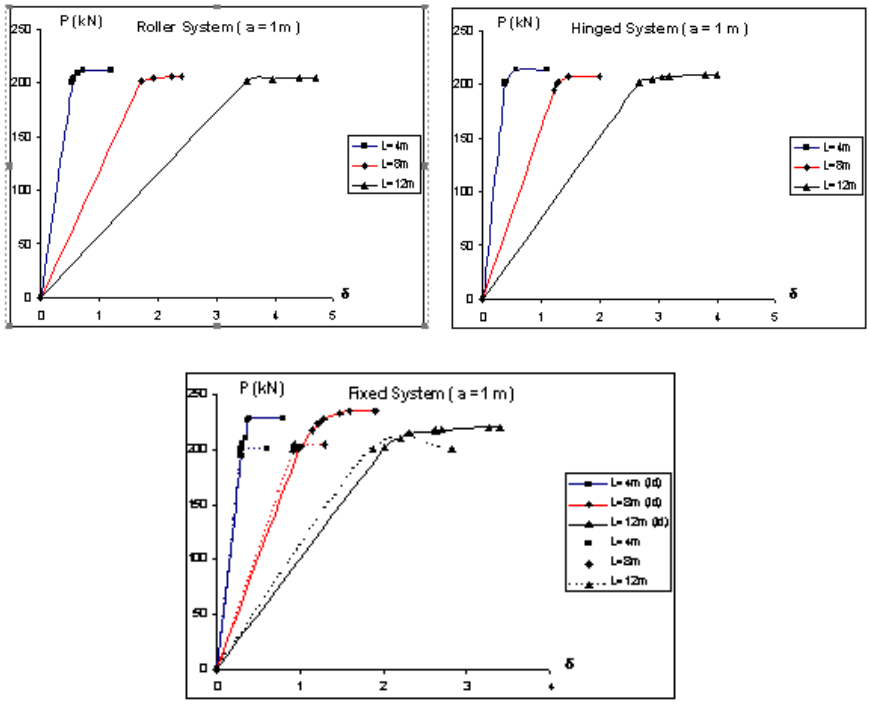

Figure 7. (P-δ) curves in bending for a=1.

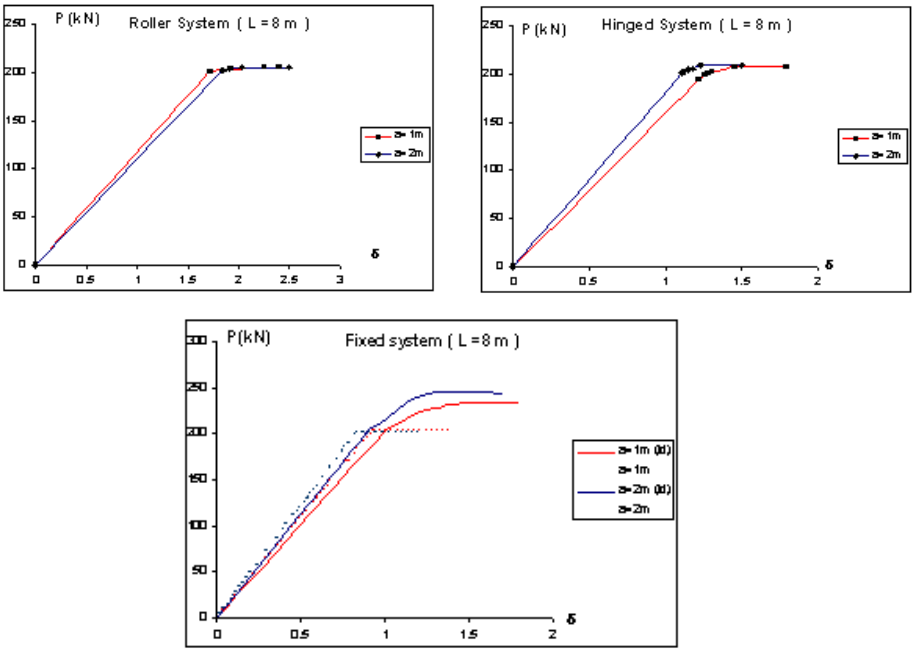

Figure 8. (P-δ) curves in bending for L=8 m

The changes (increase and decrease) in the real safety factors and ductility are found by using the ratio between real safety and ductility according to the existence or absence of inner diagonals with different vertical bar spacing.

4. Conclusion

The results of elastic and elastic-plastic analysis of tubular square space truss according to bending effect are found as follows.

The values of deflection at the middle of span of the truss under bending are given as function of the span. These relationships concerning deflections for the system without inner diagonals are exponential.

The crossectional area of the upper and lower members of the space trusses is reduced at the presence of inner diagonals (as compared to the case without inner diagonals). It is seen that there is a 28% increment in the deflection due to the effect of inner diagonals.

It is observed that there is 14%, 50% increment in the real safety and ductility, respectively, in the cross section of the space trusses with inner diagonals. It can be said that there is a positive effect of inner diagonals on the real safety and ductility capability. For the space trusses without inner diagonals, it is observed that failure occurs near the primary yielding loading case, there is no ductility.

Positive effect of the reactions on the supports of space trusses is observed at increasing the number of reactions. Deflection decreases by 31% in hinged systems as compared to roller systems; 47% and 24% in fixed systems as compared to roller and hinged systems, respectively.

Generally reduction value up to 23% in the deflections with the increase in the vertical bar spacing in space trusses is observed. This reduction increases in cases of short spans.

The real safety in the trusses does not change so much in roller and hinged systems and in fixed systems without inner diagonals but it increases 4% in fixed systems with inner diagonals when the vertical bar spacing is increased two times. However, 7-14 % reduction in the ductility for the systems with inner diagonals is found. It can be said that the increase in the vertical bar spacing has negative effect on the ductility.

References

Avent, R.R., Issa, R.R.A. (1982). Beam Element Stiffness Matrix For X-Braced Truss, Asce , Journal of The Structural Division, Vol. 108, No. 10, pp. 2192-2209.

McCallen, D.B., Romstad, K.M. (1988). A Continuum Model for the Non-linear Analysis of Beam-Like Lattice structures, Computers and Structures, Vol. 29, No.2, pp.177-197.

Ökten, S., Kasap, H. (1997). The Torsion With Bending Behaviour of A Tubular Truss, Engineering Transactions, Vol. 45, No. 1, pp. 119-131.

Renton, J.D. (1984). The Beam-like Behaviour of space Trusses, AIAA Journal, Vol. 22, No.2, pp. 273-279.

Schmidt, L.C., Hanaor, A. (1979). Force Limiting Devices In Space Trusses, ASCE, Journal of The Structural Division, Vol. 105, No. ST5, pp. 939-951.

Sheu, C.Y., Schmit, L.A. (1972). Minimum Weight Design of Elastic Redundant Trusses Under Multiple Static Loading Conditions, AIAA Journal, Vol. 10, No. 2, pp. 155-162.

Affan, A., Calladine, C.R. (2017). Initial bar tensions in pin-jointed assemblies, International Journal of Space Structures, 4(1).

Alçiçek, H.E, Vatansever. C. (2016). Uzay kafes çatı sistemlerinin artan düşey yükler altında doğrusal olmayan davranışı, Uluslararası Katılımlı 7. Çelik Yapılar Sempozyumu, 83–92.

Roudsari, M.T., Gordini, M. (2015). Random imperfection effect on reliability of space structures with different supports, Structural Engineering and Mechanics, 55(3), 461–472.

Alçiçek, H.E., Vatansever, C. (2017). Uzay kafes çatı sistemlerinin artan düşey yükler altında doğrusal olmayan davranışı, Uluslararası Katılımlı 7. Çelik Yapılar Sempozyumu, S. 83-92.

Lee, P.S., Noh, H.C. (2010). Inelastic buckling behavior of steel members under reversed cyclic loading, Engineering Structures, Vol. 32, No. 9, pp. 2579-2595.

Piroglu, F., Ozakgul, K. (2016). Partial collapses experienced for a steel space truss roof structure induced by ice ponds, Engineering Failure Analysis, Vol. 60, pp. 155.165.

Riley, G., Gebremedhin, K.G., White, R.N. (1993). Semi-rigid analysis of metal plate-connected wood trusses using fictitious members, Transactions of the ASAE, 36, 3, pp. 887-894.

Onoda, J. (1988). Two-dimensional deployable truss structures for space applications, J. Spacecraft, 25, 2, pp. 109-116.

Farshchin, M., Camp, C.V., Maniat, M. (2016). Optimal design of truss structures for size and shape with frequency constraints using a collaborative optimization strategy, Expert Syst. Appl., vol. 66, pp. 203–18.

Ho-Huu, V., T. Nguyen-Thoi, T. Truong-Khac, L. Le-Anh, T. Vo-Duy (2018). An improved differential evolution based on roulette wheel selection for shape and size optimization of truss structures with frequency constraints, Neural Comput. Appl., vol. 29, no. 1, pp.167–185.

Özyurt, M., Z. (2000). Dikdörtgen kesitli tübüler uzay kafes kirişlerin elastik ve elastik-plastik analizi, Doktora Tezi, İstanbul Teknik Üniversitesi Fen Bilimleri Enstitüsü, İstanbul.

Odabaşi, Y., Ahşap ve Çelik Yapı Elemanları (200). Beta Basım Yayım Dağıtım A.Ş., İstanbul, Türkiye.

CHAPTER VI

HYBRID MULTILAYER ARTIFICIAL NEURAL NETWORK-CULTURAL ALGORITHM BASED PHOTOVOLTAIC OUTPUT POWER ESTIMATION FOR ÇUKUROVA REGION

Kübra TÜMAY ATEŞ

Çukurova University, Department of Engineering,
E-mail: ktumay@cu.edu.tr,
ORCID: 0000-0002-3337-7969

1. Introduction

The rise in global temperatures and the rapid depletion of fossil fuels have prompted the widespread establishment and growth of renewable energy facilities. Solar energy, being a sustainable and clean alternative, is abundant in nature and is increasingly replacing traditional fossil fuels. However, the immediate variability in power output from photovoltaic (PV) energy plants, used for solar electricity generation, presents a challenge, leading to sudden imbalances in power generation. These abrupt shifts in PV energy-related power systems have raised concerns. Researchers are tackling this issue by employing artificial intelligence-based algorithms to predict power, aiming to forecast energy generated by PV plants and proactively address and mitigate potential imbalances.

Almonacid et al. (2014) introduce a novel approach based on a dynamic artificial neural network to forecast the output of an FV energy plant one hour in advance. The study results demonstrate the viability of the proposed method in predicting FV plant power output with acceptable accuracy one hour ahead. Cervone et al. (2017) present a methodology utilizing Artificial Neural Networks (ANN) and an Analog Ensemble for creating 72-hour deterministic and probabilistic predictions of power generated by FV energy plants. This

approach incorporates inputs from a numerical weather prediction model and calculated astronomical variables. The findings reveal that the hybrid model yields the best results and is well-suited for large-scale computations. Shuang et al. (2019) suggest a new medium-to-long-term forecasting method for wind and photovoltaic power production. Their approach is based on a copula function and a long short-term artificial intelligence network. Essential meteorological factors impacting wind and photovoltaic energy production are efficiently extracted using a copula function. Independent wind/photovoltaic prediction models based on a long short-term artificial intelligence network are established, compared with a persistence model, and optimized with the most effective input conditions. Li et al. (2016) assess the effectiveness of two commonly used methods, Artificial Neural Network (ANN) and Support Vector Regression (SVR), in forecasting energy production from a solar PV energy plant in Florida for 15 minutes, 1 hour, and 24 hours ahead. They suggest a hierarchical approach based on well-tested machine learning algorithms. Mohammed et al. (2018) devise an intelligent algorithm utilizing Genetic Algorithm (GA) to optimize the energy management and design of a hybrid system consisting of wind, PV, tidal, and storage batteries in an independent system located in Brittany, France. They propose solutions for load demand under diverse climate conditions, considering various scenarios and numerous constraints over a 25-year period. Theocharides et al. (2020) tackle this challenge by introducing a hybrid method with enhanced accuracy for day-ahead hourly average photovoltaic power predictions, employing data-driven machine learning techniques and statistical post-processing. The findings suggest that the application of linear regression coefficients to the predicted outcomes of the improved day-ahead photovoltaic power production neural network improves accuracy by addressing solar radiation prediction biases. Given the impact of unpredictable weather conditions on the output power of photovoltaic energy plants, the demand for a sophisticated prediction model is escalating rapidly. VanDeventer et al. (2019) propose a Genetic Algorithm-based Support Vector Machine (GA-SVM) model for short-term power prediction in a residential-scale PV energy plant. The GA-SVM model initially categorizes historical weather data using an SVM classifier and is subsequently fine-tuned using genetic algorithms through a collaborative approach. Abedinia et al. (2018) propose a novel prediction approach, combining a neural network with a metaheuristic algorithm as a hybrid prediction model. The metaheuristic algorithm optimizes the free parameters of the neural network, and the results demonstrate the superiority of this approach over other prediction methods. The obtained prediction results play a crucial role in optimizing the utilization

of solar energy plants and managing the electrical grid. Barrera et al. (2020) develop a solar energy prediction model using artificial neural networks based on open data. Accurate prediction of solar energy output can significantly improve the efficiency of sustainable energy investments. Comparing the results with existing literature in terms of Mean Squared Error (MSE), our developed prediction model is observed to enhance accuracy.

Upon reviewing the literature, it is evident that various artificial intelligence-based algorithms have been employed to optimize the operation of solar PV energy plants or address power imbalances caused by weather conditions. Due to the faster convergence of cultural algorithms compared to other evolutionary algorithms, this study believes that effective results can be achieved in PV power energy plants. Consequently, this study introduces, for the first time in the literature, a solar PV energy plant output power prediction using a CA based artificial intelligence method.

2. Material and Methods

2.1. Cultural Algorithm

Cultural Algorithms (CA) were initially introduced by R. G. Reynolds in 1994 as a form of evolutionary algorithm. These algorithms are based on computational models that utilize various agent-based techniques, drawing upon acquired experience and knowledge over time. This facilitates the practical implementation of the learning process, aligning with the principles of human social-cultural evolution. The cultural process enhances the effectiveness of finding optimal solutions within a search space and contributes to the identification of the overall optimal solution. Cultural changes in an optimization problem model represent the transmission of information within and between populations.

The core principle of CA is to preserve socially accepted beliefs while eliminating unacceptable ones. CA comprises two main components: the population space and the belief space. The fitness of each individual in the population is determined by a fitness function, and an acceptance function identifies which individuals influence the belief space. Information gathered during population searches, such as the best solution in the population, is preserved in the belief space in each generation (Talbi, 2009). Individuals identified by the acceptance function impact the belief space through the update function. The information in the belief space influences the selection of individuals in the next generation through the influence function. The interaction and collaboration

between these two spaces resemble the evolution of human culture (Reynolds and Peng, 2004). The essential components of CA are depicted in Figure 1.

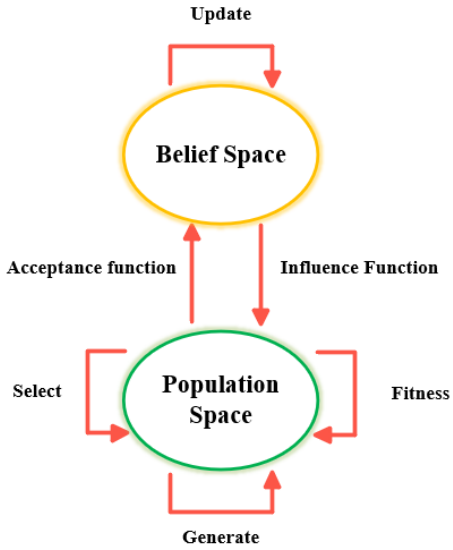

Figure 1. Overall framework of the Cultural Algorithm.

Utilizing a binary evolutionary approach, the Cultural Algorithm incorporates periodic entry of lower-level populations into top-level beliefs. Conversely, a high-level belief is cultivated to exert influence on these elite individuals, forming subgroups (Ma and Wang, 2009). This mechanism results in an increased diversity within the population and, as a result, enhances convergence characteristics.

2.2. Cultural Algorithm applied to Train the Neural Network Model

In this research, a multilayer feed-forward artificial neural network (ANN) model was selected, and for the training of its weight and bias variables, the Cultural Algorithm (CA) was employed. This combined structure is referred to as MLNN-CA. The application of the Cultural Algorithm to train the multilayer neural network (MLNN) involves addressing two primary considerations: defining the weights and biases as the search vector for the Cultural Algorithm and selecting an appropriate fitness function for the training process.

Given that all weights and biases within an MLNN can be organized into a vector, its representation is straightforward. This vector serves to represent each individual within the search space of the Cultural Algorithm. The overall steps of the proposed MLNN-CA approach are depicted in Figure 2.

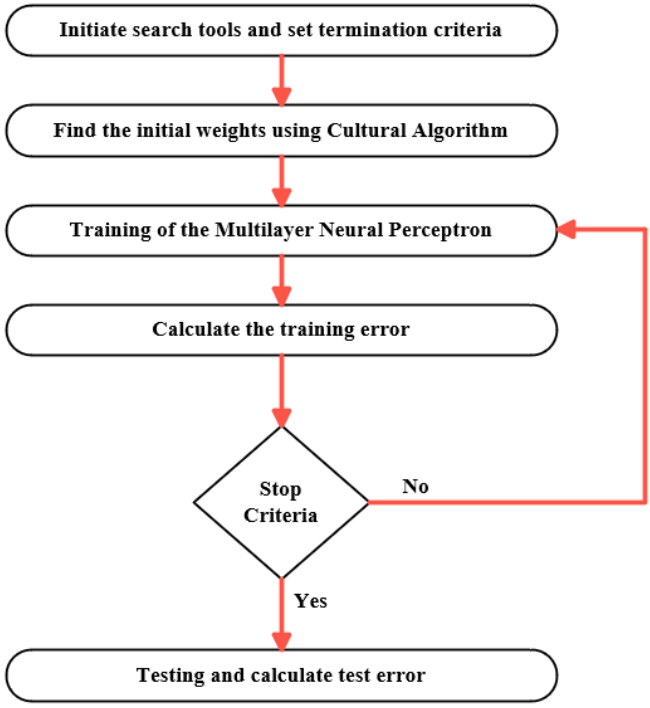

Figure 2. Diagram illustrating the operation of neural networks utilizing a cultural algorithm.

The procedural steps for implementing the Cultural Algorithm in training a neural network model are outlined as follows:

1. Initialization: For training purposes, search vectors and belief spaces within the population are randomly generated. Each search vector within a belief space denotes potential coefficients and bias values for a multi-layered neural network. The study's dataset is divided into training and testing sets for application in both phases.

2. Fitness Evaluation: The effectiveness of each solution within the population is assessed using a fitness function. Typically, the Mean Squared Error is selected as the fitness function, depending on the neural network training model and the specific problem under consideration.

3. The accepted population undergoes updates in the belief space.

4. Steps 2 to 3 are iteratively executed until a termination condition is satisfied.

5. The optimal solution obtained is utilized to construct a multi-layered neural network, marking the commencement of the testing phase.

The Mean Squared Error (MSE), depicted in Equation 1, calculates the average of squared errors across all training examples, serving as the fitness function. Each error corresponds to the disparity between the output values of the actual multi-layered neural network.

$$OKH = \frac{1}{n}\sum_{i=1}^{n}\left(EC_O - EC_P\right)^2 \quad (1)$$

Where EC_p is the short-term output power value generated from the multilayer neural network and EC_o is the actual short-term output power value. The basic code for the MLNN-CA structure employed in the research is illustrated in Figure 3.

Step 1: Create the artificial neural network
Define to network structure
Step 2: Determine the parameters of the neural network
Assign initial values for weights and biases
Step 3: Start optimization step
Create initial population
Assign initial values to the parameters of KA
Calculate fitness value for each individual
While (termination criterion)
Running the fitness function in population space
Exercise the acceptance function in belief space
Exercise the influence function in population space
Creating the new population
End while
Step 4: Creating the neural network with optimum weight and bias values
Step 5: Passing the test data through the artificial neural network
Step 6: Printing the prediction results to the screen

Figure 3. The basic code for the MLNN-CA structure.

3. Result and Discussions

In this study, it is utilized real-time data collected hourly from an inverter in a photovoltaic (PV) power plant. The study involved effective simulation using two distinct methods by processing the acquired data. The chosen approach in this investigation is the Multilayer Neural Network – Cultural Algorithm. The optimization method is employed to train the network. Initially, the Cultural Algorithm is operated with a randomly distributed population in the search space. The success of each particle in this space is evaluated using an objective function that determined its fitness value. The process involved updating particle information based on the algorithm's structure, creating a new

generation, and repeating these steps until a termination criterion is met. After training, the Artificial Neural Network (ANN) was constructed using optimal values from the best particle, and the testing phase ensued. The training phase employed 80% of the data, while 20% was reserved for testing to assess the network's success.

The data for training and testing the artificial neural network is collected in Turkey for the year 2016. Using the ANN, predictions were made for the first three months of 2017, and the results are compared with real data. The input layer of the network is fed with ambient temperature, solar radiation, and PV panel temperature. The output layer represented instantaneous PV plant power.

In this method, the network structure included 8 neurons in the hidden layer, 3 neurons in the input layer, and 1 neuron in the output layer. The decision on the number of neurons in the hidden layer is achieved through trial and error, experimenting with different numbers to find the most suitable configuration. The network training involved 24 weight parameters (between input and hidden layer), 9 bias parameters (belonging to hidden and output layer), and 8 weight parameters (between hidden and output layers).

The study's outcomes were assessed using the Mean Absolute Percentage Error (MAPE) criterion. This metric quantifies the average percentage difference between the predicted values and the actual values. The MAPE is computed by employing the following Equation.

$$MAPE = \frac{1}{N}\sum_{i=1}^{N}\left|\frac{\hat{y}_i - y_i}{y_i}\right| \tag{2}$$

y_i and $\hat{y}_i$ is the actual result and the predicted result. N is the number of data in the data set.

The programs created for each method underwent 20 iterations, and the optimal outcomes from these runs were selected. The prediction results, derived from the optimization studies, were then compared based on the Mean Absolute Percentage Error (MAPE) criterion. Table 1 presents the MAPE values and regression results obtained from three distinct methods.

Table 1. Test phase results

Method	MAPE	Regression value
MLNN-CA	17,1937	0,98533

Also, the real-time results and test results obtained with MLNN-CA are shown graphically in Figure 4.

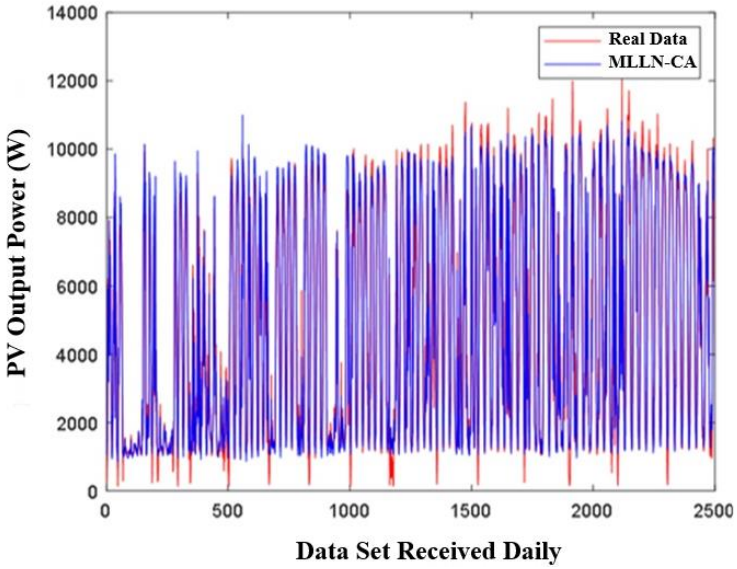

Figure 4. Comparison of the data obtained as a result of the MLNN-CA prediction method and the real data.

Figure 5 displays the regression graphs generated at the conclusion of the testing phase. These graphs illustrate the connection between the intended outcome and the results achieved through the MLNN-CA method. Upon reviewing these graphs and regression values, it becomes evident that there is a correlation between the outcomes obtained using the MLNN-CA method and the desired results.

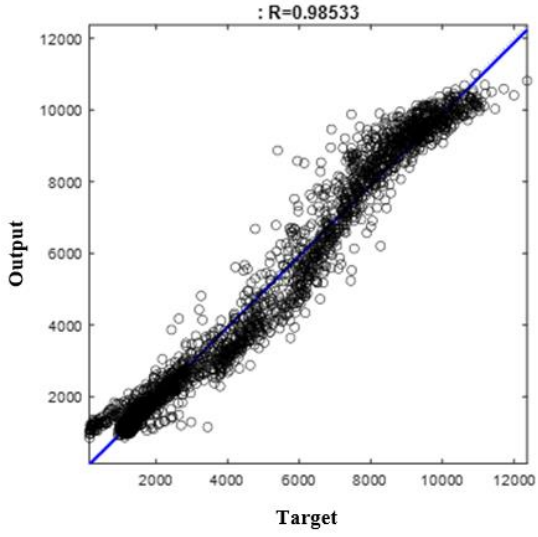

Figure 5. Regression graph obtained as a result of the prediction process.

Figure 6 shows the error graph of the prediction result obtained using the optimization method.

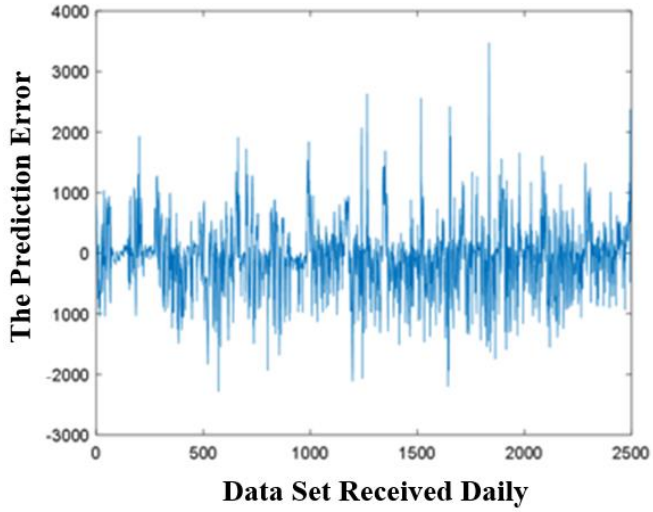

Figure 6. Error graph obtained as a result of the prediction process.

Figures 4-6 present the visual outcomes obtained after the testing phase. A detailed examination of the results, including data distributions, reveals the effectiveness of the results obtained from MLNN-CA. Additionally, a scrutiny of the numerical outcomes in Table 1 highlights the favorable performance of the MLNN-CA method in estimating PV power.

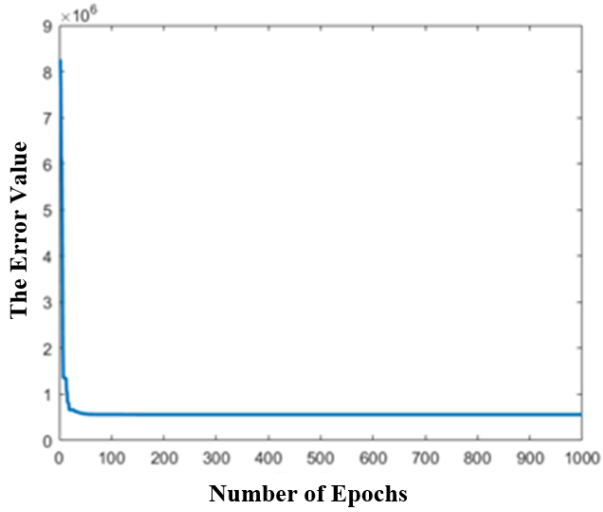

Figure 7. Error change graph obtained during the training phase.

The error change graphs obtained during the training of the multilayer neural network with different heuristic methods are shown in Figure 7. The findings of this study highlight the effectiveness of the MLNN-CA method in predicting short-term output power for a solar PV power plant based on real-time data from Turkey. As the installation of solar PV power plants continues to grow globally, the instability of their output power remains a significant challenge. This study addressed the importance of accurate short-term power predictions, especially considering the impact of unbalanced power flow on system controls when these plants are connected to the grid. The results obtained through mathematical and graphical analyses demonstrate that the MLNN-CA method performs exceptionally well in forecasting three-month forward power output. The method's high performance is crucial for anticipating and mitigating sudden power fluctuations, thereby enhancing the overall stability and reliability of the PV power plant within the larger energy system. The study's focus on utilizing real-time data from a specific solar PV power plant in Turkey adds practical relevance to the findings, showcasing the method's applicability in a real-world context. The successful application of the MLNN-CA method in short-term power prediction contributes valuable insights to the broader field of solar energy and grid integration. It is worth noting that as solar energy continues to play a key role in the global transition to sustainable energy sources, the development and refinement of accurate prediction methods, such as the MLNN-CA approach, will be crucial for maximizing the efficiency and reliability of solar PV power plants. Further research and application of advanced forecastingtechniques can contribute to addressing the challenges associated with the intermittency of solar power and enhance the overall performance of solar energy systems.

4. Conclusion

With the increasing global potential for solar energy, the installation of solar PV power plants is on the rise. Despite their widespread deployment, these plants face a significant challenge-their output power is inherently unstable. Given their connection to the grid, fluctuations in power output can disrupt system controls. Therefore, accurately predicting short-term power output and implementing measures to mitigate sudden fluctuations are crucial. This study focused on predicting short-term output power from a solar PV power plant in Turkey, utilizing real-time data. The MLNN-CA method was employed for forecasting future power outputs. Analysis of the obtained mathematical and graphical results underscores the MLNN-CA method's strong performance in predicting three-month forward power output.

References

Abedinia O., Amjady N., Ghadimi N. Solar energy forecasting based on hybrid neural network and improved metaheuristic algorithm. Computational Intelligence 2018;34:241–60.

Almonacid F., Pérez-Higueras PJ., Fernández EF., Hontoria L. A methodology based on dynamic artificial neural network for short-term forecasting of the power output of a PV generator. Energy Conversion and Management 2014;85:389–98.

Barrera JM., Reina A., Maté A., Trujillo JC. Solar Energy Prediction Model Based on Artificial Neural Networks and Open Data. Sustainability 2020;12:6915.

Cervone G., Clemente-Harding L., Alessandrini S., Delle Monache L. Short-term photovoltaic power forecasting using Artificial Neural Networks and an Analog Ensemble. Renewable Energy 2017;108:274–86.

Eberhart R., Kennedy J. A new optimizer using particle swarm theory. MHS'95. Proceedings of the Sixth International Symposium on Micro Machine and Human Science, IEEE; 1995, p. 39–43.

Hazem Mohammed O., Amirat Y., Benbouzid M. Economical Evaluation and Optimal Energy Management of a Stand-Alone Hybrid Energy System Handling in Genetic Algorithm Strategies. Electronics 2018;7:233.

Kennedy J., Eberhart R. Particle swarm optimization. Proceedings of ICNN'95-international conference on neural networks, IEEE; 1995;4:1942–1948.

Li Z., Rahman SM., Vega R., Dong B. A Hierarchical Approach Using Machine Learning Methods in Solar Photovoltaic Energy Production Forecasting. Energies 2016;9:55.

Ma H., Wang Y. Cultural Algorithm Based on Particle Swarm Optimization for Function Optimization, Fifth International Conference on Natural Computation, 14-16 Ağustos 2009, sayfa no:224-228, Tianjian, Çin.

Reynolds R.G. An introduction to cultural algorithms. In Proceedings of the third annual conference on evolutionary programming, River Edge, NJ: World Scientific 1994;24:131-139.

Reynolds RG., Peng B. Cultural algorithms: modeling of how cultures learn to solve problems. 16th IEEE International Conference on Tools with Artificial Intelligence, 15-17 Kasım 2004, sayfa no:166–172, Boca Raton, FL, USA.

Shuang H.,Qiao YH., Yan J., Liu Y., Li L., Wangb Z. Mid-to-long term wind and photovoltaic power generation prediction based on copula function and long short term memory network. 2019; 239: 181-191.

Talbi E. Population-based metaheuristics, Metaheuristics from Des. to implementation. John Wiley Sons, Inc., Hoboken, New Jersey 2009; 190–200.

Theocharides S., Makrides G., Livera A., Theristis M., Kaimakis P., Georghiou GE. Day-ahead photovoltaic power production forecasting methodology based on machine learning and statistical post-processing. Applied Energy 2020;268:115023.

VanDeventer W., Jamei E., Thirunavukkarasu GS., Seyedmahmoudian M., Soon TK., Horan B, et al. Short-term PV power forecasting using hybrid GASVM technique. Renewable Energy 2019;140:367–79.

CHAPTER VII

ANALYTICAL HIERARCHY PROCESS METHOD FOR ALTERNATIVE CROPS FROM A SUSTAINABLE WEED MANAGEMENT PERSPECTIVE

Melek IŞIK[1]

[1]*Çukurova University, Faculty of Engineering, Department of Industrial Engineering, Adana*
E-mail: demirtasm@cu.edu.tr
ORCID: 0000-0001-6078-7026

1. Introduction

The natural balance and diversity of ecological ecosystems are altered by weed invasions, and many plant and animal species are put in danger of extinction (Pyšek et al., 2012). In light of this, weed control is crucial for agricultural productivity. The socioeconomic standing of farmers and organizations that are important in disseminating information about weeds, as well as the impact of weed management methods on weed intensity in rice and wheat crops, were the main points of emphasis for Singh and Garde (Singh & Gharde, 2020). AHP identified the key organizations that are crucial in helping farmers learn about weed management methods. According to Bessette et al. (Bessette, Wilson, Beaudrie, & Schroeder, 2019), an intuitive online decision support tool was composed and put into use to help organic farmers define their goals for the farm, assess the effectiveness of their practices, and assess solutions that had been recommended by a panel of experts. In their paper, Lohr et al. (Lohr, Passeretto, Lohr, & Keighery, 2015) presented a model that made use of the pairwise comparison equations in the AHP, four metrics that characterize the logistical challenges associated with conducting operations in Western Australia's Pilbara islands, and two well-known indicators of an island's conservation value.

Many chemical pesticides contain harmful compounds that have been linked to soil and water degradation, as well as adverse effects on human health, biodiversity, and farm viability. Due to an over reliance on herbicides and the massive rise of weeds resistant to herbicides, agricultural systems in the Europe have become less sustainable and more susceptible (Tataridas, Kanatas, Chatzigeorgiou, Zannopoulos, & Travlos, 2022). In order to minimize the use of herbicides and guarantee crop protection, the study sought to offer a comprehensive framework for sustainable crop and weed management. Managing weeds is a difficult task in the production of crops. An emerging weed control technique for sustainable agriculture is integrated weed management, which includes the use of bioherbicides. The influence of bioherbicides on weed physiology, already marketed products, and potential factors influencing bioherbicide efficacy were all covered by Hasan et al. (Hasan, Ahmad-Hamdani, Rosli, & Hamdan, 2021). Site-Specific Weed Management was obtained possible by Integrated Weed Management and Unmanned Aerial Vehicles (drones). This approach was extremely effective and good for the environment. An overview of precision weed management was determined by Esposito et al. (Esposito, Crimaldi, Cirillo, Sarghini, & Maggio, 2021), with an emphasis on the potential and real-world applications of the most cutting-edge sensors on the market.

This study was composed the AHP approach to investigate a main criteria and sub-criteria for sustainable weed management in the Çukurova Region of Turkey. The primary requirements included were non-chemical tools, cultivation techniques and new technologies; however, the most crucial requirement was the use of non-chemical tools to ensure the sustainability of citrus, legume, and cereal crops.

2. Materials and Methods

First of all, the main criteria and sub-criteria for the region are determined. And then, sub-criteria appropriate to the region are selected. In figure 1, non-chemical tools, new technologies and cultivation techniques are as main criteria. Under the main criteria of non-chemical tools, there are natural and bio-herbicides, mechanical weeding, crop residues, mulches, and solarization, beneficial microorganisms and seed coating. Under the main criterion of cultivation techniques, it consists of crop rotation and diversification, tillage, seeding rates and intercropping. Remote sensing and weed detection, site specific weed management and bio and nano-technology sub-criteria are related to the new technologies main criterion (Tataridas, et al., 2022).

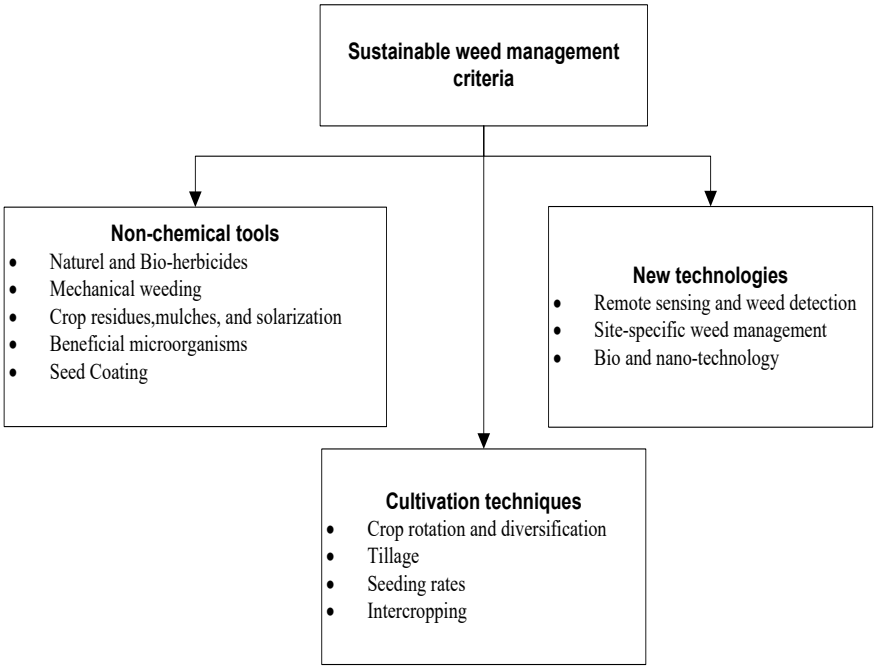

Figure 1. Sustainable weed management criteria for Çukurova region (Tataridas, et al., 2022)

AHP was developed as a model by Saaty (Saaty, 1977) for solving decision-making problems. AHP is a decision-making technique that provides the percentage distribution of choice points based on the decision-making scenario. It is utilized to define decision success. The steps are taken to solve a decision-making problem with AHP are described below (Saaty, 1977).

Step 1: The Decision Making Problem is defined.

There are two steps involved in defining the problem of decision-making. Decision points are identified in the first phase. The factors influencing the decision points are identified in the second step.

Step 2: Comparison Matrix Between Factors is composed.

A square matrix serves as the comparison matrix between the factors. The matrix components on the diagonal of this matrix take the value 1 i.e. when i=j. A one-to-one and reciprocal comparison of the elements is made based on how important they are in relation to one another. The importance scale in Table 1 is used for one-to-one comparison of factors.

Table 1. Importance scale (Saaty, 1977)

Importance	Value Definitions
1	Case where both factors are of equal importance
3	1. case 2. case of being more important than case
5	1. case 2. a case of being more important than a case
7	1. case 2. it has a very strong importance compared to the case
9	1. case 2. a situation in which it has absolute superior importance compared to the case
2,4,6,8	Intermediate value

Comparisons are demonstrated for values that lie above the diagonal of the comparison matrix, where all values are 1. Naturally, for the components below the diagonal, using Equation (1) will be sufficient for A Matrix.

$$a_{ji} = \frac{1}{a_{ij}}, \tag{1}$$

Step 3: Percentage Importance Distributions of Factors are determined

The factors' relative relevance within a given logic is displayed in the comparison matrix. However, the column vectors that make up the comparison matrix are utilized to ascertain the weights of these elements overall, or, to put it another way, their percentage importance distributions. Equation (2) is used to calculate B Column vectors.

$$b_{ij} = \frac{a_{ij}}{\sum_{i=1}^{n} a_{ij}}, \tag{2}$$

Percentage importance distributions that display the factors' relative importance can be obtained by utilizing the C matrix. For this, the arithmetic mean of the row components forming the C matrix is taken as shown in Equation (3) and the W column vector, called the Priority Vector, is obtained.

$$w_i = \frac{\sum_{j=1}^{n} c_{ij}}{n}, \tag{3}$$

Step 4: Consistency in Factor Comparisons is measured

One can assess the consistency of the priority vector discovered and, consequently, the one-to-one comparisons made between the factors, using the

Consistency Ratio that is produced. The decision maker's consistent comparisons are indicated by the estimated ratio value being less than 0,10. A value larger than 0,10 denotes a discrepancy in the decision maker's comparisons or an error in the AHP computation.

Step 5: For Each Factor, Percentage Importance Distributions at the Decision Point are found

This step is the same as the previous one, but this time, for each factor, the decision points' percentage importance distributions are found.

Step 6: Finding the Result Distribution at Decision Points

As a result, the percentage distribution of decision points is displayed in the column vector. The choice points' relative relevance is also displayed by this distribution.

3. Results

The main criteria selected for the Çukurova Region for sustainable weed management were determined as non-chemical tools, cultivation techniques and new technologies (Table 2). The criterion with the highest weight value of 0,58 was non-chemical tools. According to the opinions of the experts, the consistency index of the results was 0, and since this value was less than 0,1, it was concluded that they were consistent.

Table 2. Main criteria for sustainable weed management

Main Criteria	Non-chemical tools	Cultivation techniques	New technologies	Weight
Non-chemical tools	1	2	5	**0,58**
Cultivation techniques	0,5	1	3	0,31
New technologies	1/5	1/3	1	0,11

The most weighted sub-criterion was natural and bio-herbicides with a value of 0,43 for non-chemical tools and 0,44 of crop rotation and diversification for cultivation techniques (Table 3). It was resulted in remote sensing and detection sub-criteria with a value of 0,76 for new technologies.

Table 3. Sub-criteria for sustainable weed management

Non-chemical Tools Sub-Criteria	**W**	**Cultivation Techniques Sub-Criteria**	**W**	**New Technologies Sub-Criteria**	**W**
Naturel and Bio-herbicides	**0,43**	Crop rotation and diversification	**0,44**	Remote sensing and weed detection	**0,76**
Mechanical weeding	0,23	Tillage	0,38	Site specific weed management	0,14
Crop residues, mulches, and solarization	0,17	Seeding rates	0,10	Bio and nano-technology	0,10
Beneficial microorganisms	0,12	Intercropping	0,08		
Seed Coating	0,05				

Considering the Çukurova Region, evaluations were investigated for citrus, cereal and legume alternative crops, with which evaluated sustainable weed management. Citrus emerged as important alternatives for natural bio-herbicides with a value of 0,73, cereal for mechanical weeding and crop residues, mulches, and solarization with values of 0,74 and 0,76, respectively, and legume for beneficial microorganisms and seed coating with values of 0,67 and 0,56 (Table 4).

Table 4. Non-chemical tools sub-criteria for alternatives

Sub Criteria	**Naturel and Bio-herbicides**	**Mechanical weeding**	**Crop residues, mulches, and solarization**	**Beneficial microorganisms**	**Seed Coating**
Citrus	**0,73**	0,06	0,10	0,24	0,06
Cereal	0,19	**0,74**	**0,76**	0,09	0,38
Legume	0,08	0,20	0,14	**0,67**	**0,56**

The values of 0,67 and 0,65 for cereal crop rotation and diversification and seeding rates, respectively, and 0,73 and 0,74 for legume crop, were predominant for the tillage and intercropping sub criteria (Table 5).

Table 5. Cultivation techniques sub-criteria for alternatives

Sub Criteria	Crop rotation and diversification	Tillage	Seeding rates	Intercropping
Citrus	0,06	0,08	0,12	0,17
Cereal	**0,67**	0,19	**0,65**	0,09
Legume	0,27	**0,73**	0,23	**0,74**

Legume was choice for remote sensing and weed detection with a value of 0,67 and for site-specific weed management and bio and nano-technology with values of 0,65 and 0,73 for citrus, respectively (Table 6).

Table 6. New technologies sub-criteria for alternatives

Sub Criteria	Remote sensing and weed detection	Site spesific weed management	Bio and nano-technology
Citrus	0,10	**0,65**	**0,73**
Cereal	0,23	0,12	0,19
Legume	**0,67**	0,23	0,08

4. Discussion

When non-chemical tools sub-criteria were considered in general, mechanical weeding and crop residues, mulches, and solarization obtained similar results for cereal (Figure 2). Consistency indexes were respectively given the values of 0,06, 0,09, 0,01, 0,09, 0,07 to give a consistent result.

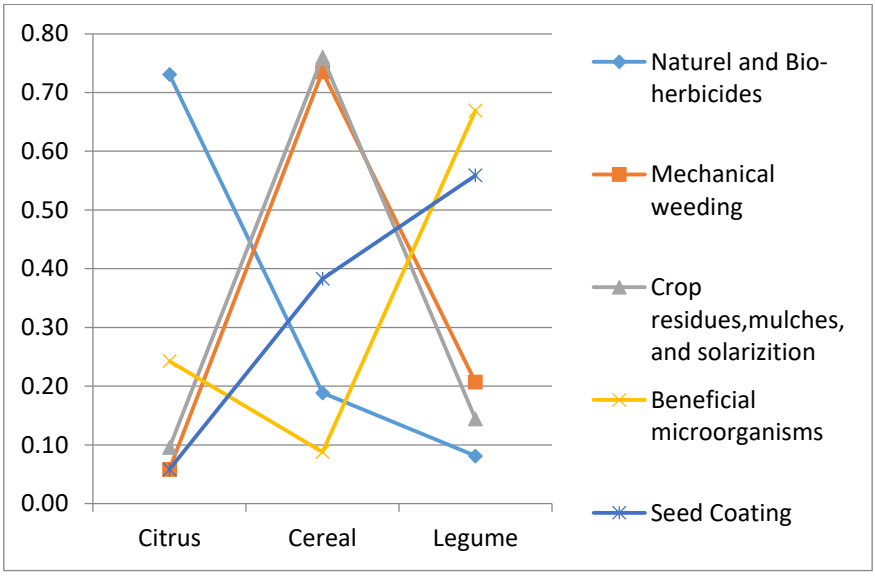

Figure 2. Non-chemical tools sub-criteria benchmarking

While there are similar values for the cultivation techniques sub-criteria in citrus, there was a closeness between crop rotation and diversification and seeding rates for cereal and legume, and a closeness between tillage and intercropping (Figure 3). The consistency index turned out to be consistent with values of 0,01, 0,03, 0, 0,06.

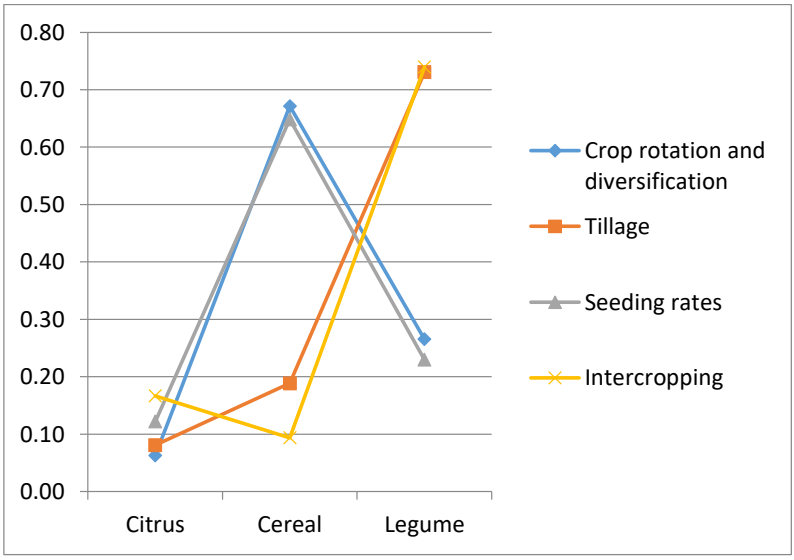

Figure 3. Cultivation techniques sub-criteria benchmarking

For new technologies sub-criteria, cereal values were close to each other, and for citrus, site specific weed management bio and nano-technology values were close to each other (Figure 4). Consistency index values were 0,07, 0, 0,06.

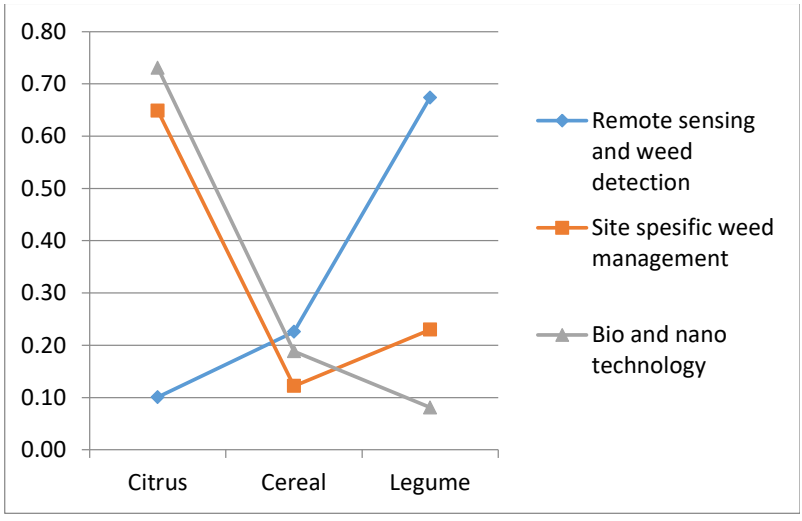

Figure 4. New technologies sub- criteria benchmarking

5. Conclusions

The topic of sustainable weed management has been preferred theme in recent years, particularly for the agriculture discipline that serves the entire world. This study was composed sustainable weed management in the Çukurova Region in Turkey. AHP method was used by using expert opinion. The main criteria were non-chemical tools, cultivation techniques and new technologies, and the most important main criterion was non-chemical tools for sustainability. Among the citrus, legume and cereal crops grown in the region, the final AHP score was listed as citrus with a value of 0,26, cereal with a value of 0,40, legume with a value of 0,34. It has been determined that these criteria are most applicable to cereal, then legume and finally citrus. In future studies, different methods for different crops can be used for sustainable weed management.

References

Bessette, D., Wilson, R., Beaudrie, C., & Schroeder, C. (2019). An online decision support tool to evaluate ecological weed management strategies. *Weed Science, 67*(4), 463-473.

Esposito, M., Crimaldi, M., Cirillo, V., Sarghini, F., & Maggio, A. (2021). Drone and sensor technology for sustainable weed management: A review. *Chemical and Biological Technologies in Agriculture, 8*(1), 1-11.

Hasan, M., Ahmad-Hamdani, M. S., Rosli, A. M., & Hamdan, H. (2021). Bioherbicides: An eco-friendly tool for sustainable weed management. *Plants, 10*(6), 1212.

Lohr, C., Passeretto, K., Lohr, M., & Keighery, G. (2015). Prioritising weed management activities in a data deficient environment: the Pilbara islands, Western Australia. *Heliyon, 1*(4).

Pyšek, P., Jarošík, V., Hulme, P. E., Pergl, J., Hejda, M., Schaffner, U., & Vilà, M. (2012). A global assessment of invasive plant impacts on resident species, communities and ecosystems: the interaction of impact measures, invading species' traits and environment. *Global Change Biology, 18*(5), 1725-1737.

Saaty, T. L. (1977). A scaling method for priorities in hierarchical structures. *Journal of mathematical psychology, 15*(3), 234-281.

Singh, P., & Gharde, Y. (2020). Adoption level and impact of weed management technologies in rice and wheat: Evidence from farmers of India. *Indian Journal of Weed Science, 52*(1), 64-68.

Tataridas, A., Kanatas, P., Chatzigeorgiou, A., Zannopoulos, S., & Travlos, I. (2022). Sustainable crop and weed management in the era of the EU Green Deal: A survival guide. *Agronomy, 12*(3), 589.

CHAPTER VIII

RISK ANALYSIS OF DC FAST CHARGING STATIONS FROM USER PERSPECTIVE

[1*]Kübra TÜMAY ATEŞ & [2]Murat Mustafa SAVRUN & [3]Cansu DAĞSUYU & [4]Mehmet Uğraş CUMA

[1]Çukurova University, Department of Industrial Engineering, 01330, Adana, Turkey, E-mail: ktumay@cu.edu.tr, ORCID: 0000-0002-3337-7969

[2]Adana Alparslan Türkeş Science and Technology University, Department of Electrical & Electronics Engineering, 01250, Adana, Turkey, E-mail: msavrun@atu.edu.tr, ORCID: 0000-0001-5847-5082

[3]Adana Alparslan Türkeş Science and Technology University, Department of Industrial Engineering, 01250, Adana, Turkey, E-mail: cdagsuyu@atu.edu.tr, ORCID: 0000-0001-7280-7733

[4]Çukurova University, Department of Electrical & Electronics Engineering, 01330, Adana, Turkey, E-mail: mcuma@cu.edu.tr, ORCID: 0000-0001-6040-0362

1. Introduction

Nowadays, there is a significant inclination towards electrification in transportation as environmentally friendly alternatives due to reasons such as air pollution, fossil fuel usage, and greenhouse gas emissions.

The increase in sustainability-related issues in recent years has become an important element in the search for a green environment (Ma et al., 2020, Duan et al., 2020, Duan, et al., 2021).

Turkey's greenhouse gas emissions in 2021 amounted to 564.4 Mt CO_2 equivalent, as stated in the 2023 Greenhouse Gas Emission Inventory Report. Consequently, the aggregate amount of greenhouse gas emissions, amounting to 523.9 Mt CO_2 equivalent in the year 2020, exhibited a growth of 7.7 percent in comparison to the preceding year. In 2021, energy-related emissions accounted for the highest proportion of total greenhouse gas emissions in terms of CO_2 equivalent, with a share of 71.3 percent. This was followed by industrial processes and product consumption, which contributed 13.3 percent, agricultural, which contributed 12.8 percent, and the waste sector, which contributed 2.6 percent. (https://data.tuik.gov.tr/Bulten/Index?p=Sera-Gazi-Emsyon-Istatistikleri-1990-2021-49672&dil=1).

Greenhouse gas emissions created by energy sources also include transportation. Hence, transportation is an indispensable source of movement for a society. It affects the economy, and no activity in the social economy can be done without transportation. Moreover, more than 90% of the fuel consumed in the transportation sector is provided by fossil fuels. Therefore, the most important problem of the transportation sector is to reduce dependence on fossil fuels while maintaining good performance (Netz et al., 2007), which makes transportation more important than ever to change the current energy consumption situation and reduce environmental pollution. In recent years, along with electric vehicle production technologies, electricity generation infrastructures have also developed and attracted increasing attention. While many companies have announced their plans to produce electric vehicles (Querini and Benetto, 2014), several other countries have begun to replace internal combustion engine vehicles (ICMAs) (Cai et al., 2014), making EVs a suitable alternative vehicle (Yazdekhasti et al., 2021).

Based on this, it may be possible to carry out studies to increase sustainability by using renewable energy sources. The literature widely documents the integration of renewable energy sources into charging electric vehicles (İnci et al., 2022).

In principle, EVs can be charged in a centralized or decentralized manner (Amjad et al., 2018). For decentralized charging, where AC is the only available option, long charging time is often needed overnight (Amjad et al., 2018, Makeen et al., 2018). As a result, researchers tend to apply fast-charging central stations supplied from the electric grid and renewable energy sources to fast

charge electric vehicles in DC (Domínguez-Navarro et al. 2019). The increasing use of fast charging stations brings with it many risks for users.

FMEA is one of the risk assessment methods commonly used in the literature. In this context, some studies addressing charging processes can be found in the literature. Haghbin (2016) detected the 3.3 kW onboard battery charging failure mode for the electric part of an electric vehicle charger by FMEA analysis. FMEA results suggest that it can be used to prioritize, investigate, and analyze major fault conditions in semiconductors, DC link capacitors, and sensors. Kivela et al., (2021) determined the risk assessment and derived functional safety requirements for the charging process using their own methods. Rastayesh et al., (2019) obtained critical components by classifying risk analysis with FMEA parts used in backup power applications in the telecommunications sector.

To address complex problems and avoid sequencing errors, many scientists have proposed fuzzy FMEA methods based on fuzzy information and multi-feature decision making method (Liu et al., 2013; Peng et al., 2021). Zhang et al., (2022) conducted service life cycle analysis and risk assessment using new integrated fuzzy FMEA methods for risk control and service optimization of self-service electric vehicles. Nuchpho et al., (2019) discussed the failure analysis of Indian railway signaling systems through fuzzy risk priority number (RPN) and FMEA. Chin et al. (2008) presented two approaches, fuzzy expected value method (FEVM) and fuzzy FMEA, for a complex infrastructure project.

The literature indicates that while the frequency of the use of fast charging stations is increasing, the risks associated with it are also increasing. It is important to determine these risks correctly, to prevent the identified risks, and to prevent the risk formation from its source. In this study, the structural elements of the charging station are divided into three main groups, namely system, user, and ergonomics, allowing the identification of potential risks throughout the charging process. In this context, risk analysis from the user perspective has been conducted and compared using classical FMEA and fuzzy FMEA approaches for DC fast charging stations.

2. Classical and Fuzzy FMEA

Classical Failure Mode and Effects Analysis (FMEA) is a proactive approach that anticipates and prevents system failures. FMEA utilizes three risk factors: occurrence (O), detectability (D), and severity (S). O represents the frequency of hazards, D denotes the predictability of risks, and S signifies the severity of the risk to the system. The risk priority number (RPN) is calculated by

multiplying the rankings of the failure modes, which are input parameters. Three input parameters are evaluated on a scale of 1 to 10 (Chin et al.,2008). Priority is given to the input parameters with the highest RPNs following multiplication. These results enable experts to determine failures and their causes. Experts set a threshold value to categorize failures, and corrective measures are needed for failures with a value over 100 RPN. These results enable experts to determine failures and their causes. Experts set a threshold value to categorize failures, and corrective measures are needed for failures with a value over 100 RPN.

FMEA is frequently used in studies, although it has specific constraints. The primary drawbacks of FMEA are as follows(Khasha et al. ,2013):

- Different combinations of O, S, and D can lead to identical RPN values, although failure modes sharing the same RPN may have different associated risk factors.
- In FMEA, O, S, and D are viewed as equally important. However, the importance of these characteristics may vary.
- RPN is calculated by multiplying the three input components independently, without accounting for potential indirect connections among them.
- The three parameters in FMEA calculations do not encompass all the causal factors that may result in a failure mode, including errors, inconsistencies, uncertainties, and ambiguities.

Fuzzy logic overcomes these constraints by employing linguistic variables. Using language variables to describe failure modes is simpler than using numerical assignments. The input parameters endure fuzzification by membership functions. The fuzzy parameters are evaluated by decision rules.

3. FMEA Risk Analysis for DC Station

Electric vehicle usage rates are increasing due to the reduction of green gas emissions to the environment and the increasing price of fossil fuel resources. This increase brings with it the need for electricel vehicle charging stations. Since vehicle charging takes an average of 20-60 minutes, charging is usually done by the vehicle driver without the help of a support operator. The work steps performed at the electric vehicle charging station can be summarized as follows.

- Vehicle arriving at the station
- Removing the plug from the station
- Placing the plug in the vehicle

- Starting the charging process
- Completing charging
- Payment processing

The vehicle driver's responsibility for each phase exposes the user to risks of varying degrees in the event of encountered hazards during the process. The risks at the charging station have been assessed in three categories: system-related hazards, user-related hazards, and ergonomic risks.

The hazards that may occur under each main heading and the risks that may occur due to these hazards are given in Table 1. According to the FMEA analysis of the identified risks, O, S and D values were determined by the expert team. The expert team consists of 4 expert and has 10 years of experience in the electric vehicle ecosystem and components. The RPN results from the FMEA analyze were categorized into three classes: 0-40, 41-100 and 100+ were classified as low, medium and high, respectively (Ford Motor Company, 1998). Table 1 provides the risk class determined by the RPN value of each risk. The most significant risk identified for users at DC fast charging stations is 'C5- Finishing the charge with the emergency stop button - New customers cannot start charging' with an RPN value of 432. The least critical risk is 'E5- Station place / size and shape - Inability to benefit from service / limb use' with an RPN value of 4, as shown in Table 1. Classical FMEA analysis identifies 4 system-related risks in the low-risk category, 6 in the medium-risk category, and 5 in the high-risk category. Additionally, there are 6 user-related risks in the low-risk category and 2 in the high-risk category, as well as 5 ergonomic hazards in the low-risk category and 1 in the high-risk category.

Table 1. FMEA from User Perspective of DC Fast Charging Stations

Hazard class	No	Potential hazards modes	Subhazards no	Hazards	O	S	D	RPN	RPN Class
System Based Risks	**S1**	Error in the interface (touch screen not working)	**S1**	Disconnection of system access and charging service	2	9	2	36	L
	S2	System heating	**S2**	User safety hazard and exposure to excessive energy	2	9	9	162	H
	S3	Power outage	**S3**	Disconnection of system access and charging service	3	10	1	30	L
	S4	Payment issues	**S4-1**	Failure to make payment	1	3	6	18	L
			S4-2	Lack of charging service	1	9	6	54	M
	S5	Insulation measuring device not working	**S5-1**	Electrical and thermal safety hazard for the user	1	10	9	90	M
			S5-2	Extreme energy exposure	1	10	7	70	M
	S6	The energy meter does not measure properly	**S6-1**	Incorrect calculation of payment	2	5	7	70	M
			S6-2	Decreased battery life	2	8	9	144	H
	S7	Communication protocol errors	**S7**	Failure to connect to the vehicle and provide charging service	2	9	8	144	H
	S8	Filling the station with water	**S8-1**	Electrical and thermal safety hazard for the user	1	10	10	100	H
			S8-2	Extreme energy exposure	1	8	9	72	M
	S9	Corrosion	**S9-1**	Electrical and thermal safety hazard for the user	1	10	10	100	H
			S9-2	Extreme energy exposure	1	8	9	72	M
	S10	Short circuit	**S10**	Fire	1	10	1	10	L

User-Based Risks	**C1**	Cable drop	**C1**	Mechanical deformation in the cable	4	5	2	40	L
	C2	Crashing into the station	**C2-1**	Simple injury	2	4	1	8	L
			C2-2	Station is out of operation	3	9	1	27	L
	C3	User unable to insert gun	**C3**	Inability to benefit from charging service	5	3	1	15	L
	C4	Theft (cable, pc, power source)	**C4**	Station is out of operation	5	9	4	180	H
	C5	Finish charging with emergency stop button	**C5**	New customers can't start charging	6	9	8	432	H
	C6	Drop the cable on the ground and drive over it with a car	**C6**	Mechanical deformation in the cable	3	5	2	30	L
	C7	Breaking the screen	**C7**	Inability to start/end charging and payment transactions	2	9	1	18	L
Ergonomic Risks	**E1**	Excessive over time while charging	**E1**	Psycho-social effects	4	4	2	32	L
	E2	Lighting (color and light intensity) problems at the charging station	**E2**	Inability to benefit from charging service/ Security problem	2	7	1	14	L
	E3	Environmental Temperature	**E3**	Health Risk / Being affected by very hot or very cold weather	1	4	1	4	L
	E4	Tools & equipment (charging cable length, weight etc.)	**E4**	Inability to benefit from the service/injured wrist	4	4	1	16	L
	E5	Station place /size and shape	**E5**	Inability to benefit from the service /limb injury	2	2	1	4	L
	E6	Cyber attack	**E6**	Security risk	3	8	9	216	H

4. Application of Fuzzy FMEA

Risk analyses are carried out to determine the importance levels of risks and take action according to their ranking. If the company's workforce and budget resources are limited, the effective use of company resources, in other words, determining the risk for which precautions need to be taken, becomes a significant problem. In the classical FMEA approach, O, S, and D values are multiplied when determining the RPN value. This situation has a very low probability value (1), a risk that is easy to detect (1) but has a very high severity (10); It causes a risk with a probability level of (2), a detectability level of average (5), and a risk with almost no severity (1) to have the same RPN value. This situation may prevent the risks from being considered a priority, which will have critical consequences if they occur. In this context, in this study, fuzzy logic decision rules for fast charging stations were determined, and the hazards in Table 1 were evaluated using Fuzzy-FMEA (F-FMEA).

The F-FMEA scale utilized in our research was developed by developing the classic FMEA scale for DC fast charging stations units and implementing the code using the Fuzzy Logic Designer Tool in Matlab 22b. In the F-FMEA analysis, each input (O, S and D) and output (RPN) were taken into account at 3 levels and 27 decision rules were created together with the expert team. Figure 1 illustrates the utilization of the 'Mamdani min max' approach. Figures 2 and 3 in this study display the fuzzy design, illustrating both the inputs and output.

The F-FMEA includes three levels with three inputs and one output. The Z-shaped, triangular, and S-shaped membership functions were utilized to represent low, medium, and high levels of definition, respectively. Figure 2 shows the membership function for the input, while Figure 3 shows the membership function for the output. Both Figures 2 and 3 display membership functions with low, medium, and high values. Table 2 contains the membership function values generated by the F-FMEA scale.

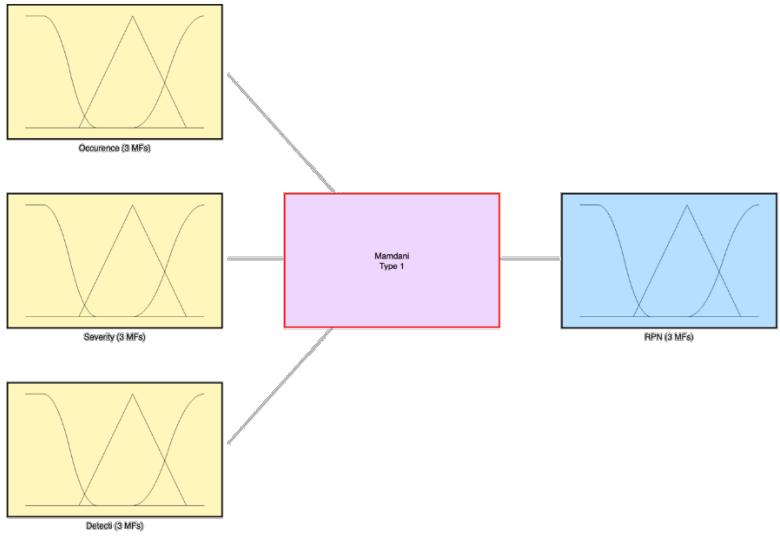

Figure 1. Design of F-FMEA

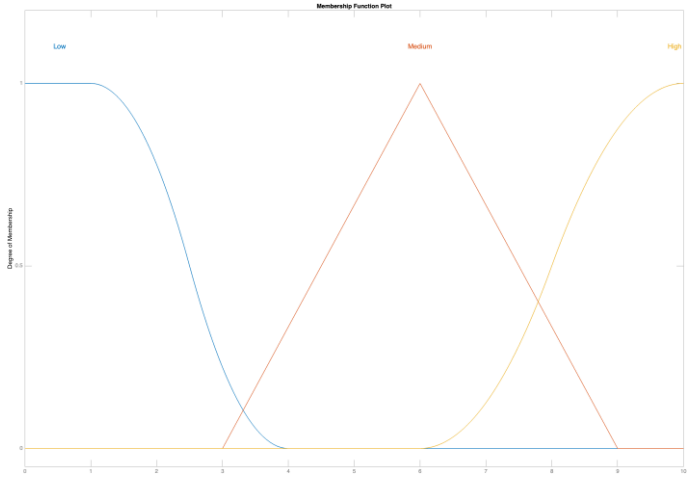

Input variable 'O, S, and D'

Figure 2. Membership function plots of input variables

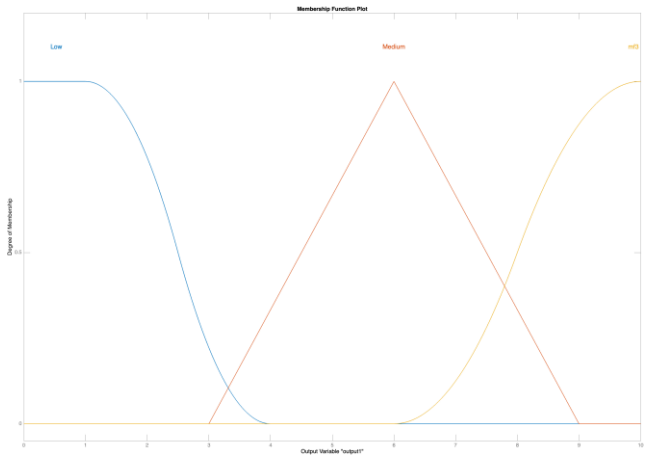

Figure 3. Membership function plots of output variable (RPN)

Table 2. Fuzzy Scale for Inputs

Defining	Fuzzy number
Low	Z-shaped [1,4]
Medium	Tria [3,6,9]
High	S-shaped [6,10]

The hazards of the DC fast charging stations were calculated using classical FMEA methodology based on decision rules and the risk assessment team assessed the risks using F-FMEA. The classical FMEA, F-FMEA, and risk classification system generated in this study are displayed in Table 3.

The prioritizing of risks differs between classical FMEA and F-FMEA, as demonstrated in Table 3. The hazards were classified according to their scores and RPN values, with corresponding categories given in Table 3.

Table 3. Classical and F-FMEA Risk Scores and Priorities for the DC Fast Charging Stations

Hazard class	No	Subhazard No	O	S	D	RPN	RPN Class	RPN Priority	Fuzzy RPN	Fuzzy RPN Class	Fuzzy RPN Priority
System Based Risks	**S1**	**S1**	2	9	2	36	L	12	6	M	8
	S2	**S2**	2	9	9	162	H	4	8,79	H	3
	S3	**S3**	3	10	1	30	L	14	6	M	8
	S4	**S4-1**	1	3	6	18	L	16	1,65	L	14
		S4-2	1	9	6	54	M	10	8,83	H	2
	S5	**S5-1**	1	10	9	90	M	7	8,83	H	2
		S5-2	1	10	7	70	M	9	8,74	H	4
	S6	**S6-1**	2	5	7	70	M	9	5,42	M	10
		S6-2	2	8	9	144	H	5	4,58	H	12
	S7	**S7**	2	9	8	144	H	5	6,61	H	7
	S8	**S8-1**	1	10	10	100	H	6	8,86	H	1
		S8-2	1	8	9	72	M	8	5,52	H	9
	S9	**S9-1**	1	10	10	100	H	6	8,86	H	1
		S9-2	1	8	9	72	M	8	5,52	H	9
	S10	**S10**	1	10	1	10	L	20	6	M	8

User-Based Risks	**C1**	**C1**	4	5	2	40	L	11	1,58	L	15
	C2	**C2-1**	2	4	1	8	L	21	1,58	L	15
		C2-2	3	9	1	27	L	15	6	M	8
	C3	**C3**	5	3	1	15	L	18	6	M	8
	C4	**C4**	5	9	4	180	H	3	8,54	H	6
	C5	**C5**	6	9	8	432	H	1	8,65	H	5
	C6	**C6**	3	5	2	30	L	14	1,65	L	14
	C7	**C7**	2	9	1	18	L	16	6	M	8
Ergonomic Risks	**E1**	**E1**	4	4	2	32	L	13	1,58	L	15
	E2	**E2**	2	7	1	14	L	19	2,64	L-M	13
	E3	**E3**	1	4	1	4	L	22	1,58	L	15
	E4	**E4**	4	4	1	16	L	17	1,58	L	15
	E5	**E5**	2	2	1	4	L	22	1,38	L	16
	E6	**E6**	3	8	9	216	H	2	4,94	H	11

Upon assessment based on Table 3, it is obvious that the risk categories of hazards have shifted along with the risk ratings. According to the classical FMEA approach, the most important hazards are C5, which is in the user-related risks group, E6, which is in the ergonomics-related risks group, and C4, which is in the user-related risks group. The F-FMEA evaluation ranks S9-1 as the most critical hazard in the system-related risks group, followed by S5-1 and S2 in the same group. F-FMEA analysis, created by taking into account process-specific evaluations, shows that system-related hazards are important for the process.

The confusion matrix in Table 4 displays the alterations in risk class due to Classical FMEA and F-FMEA. Table 4 indicates that 12 out of 29 hazards have been reclassified to a higher class. This situation shows that in the classical approach, the importance levels of hazards in lower risk classes are evaluated below the required criticality.

Table 4. Confusion Matrix

Low		F-FMEA			
		Low-Medium	Medium	High	
Classical FMEA	Low	8	**1**	**6**	
	Medium			1	**5**
	High				8

5. Conclusion

With increasing individual sensitivity about greenhouse gases and the aim of controlling them by law, electric vehicle usage rates are increasing day by day. This increase has caused more vehicle users to charge their vehicles at DC fast charging stations. In our country, assistance is received from operators in meeting the fuel needs of internal combustion engine vehicles, which causes individual users to have no experience in vehicle charging. In our country, the fact that operators receive help in meeting the fuel needs of vehicles causes individual users to have no experience in vehicle charging. This study identified potential hazards during the charging process based on the structural components of the charging station, categorized into three primary groups: system, user and ergonomics. Risk priority scores were then assigned accordingly. While determining the RPN values, the FMEA method was taken into account and 15 of the 29 hazards determined were in the Low group, 9 in the Medium group and the remaining 7 hazards in the High group. F-FMEA was developed for DC fast charging stations to address the limitation of obtaining RPN values by multiplying hazards from the O, S, and D scales in FMEA evaluation. While

system-related hazards were not among the top 3 priority hazards in the FMEA evaluation, according to the F-FMEA results, 2 of the first 3 hazards were in the system-related hazards group. This outcome will provide manufacturers with insights on enhancements or actions to be implemented during the design stage of DC fast charging stations.

In addition, according to the F-FMEA evaluation, it is seen that the class of 12 hazards has moved to the upper class. The goal is to reduce potential hazards at DC fast charging stations by emphasizing their relevance and facilitating quicker response and resolution.In this study, for the first time in the literature, classical FMEA and F-FMEA risk analysis for DC fast charging stations was performed and the results were compared.

In future studies, different risk analysis methods can be taken into account or optimization studies can be carried out in creating action selection plans.

Reference

Amjad, Muhammad, Ayaz Ahmad, Mubashir Husain Rehmani, and Tariq Umer. 2018. “A review of EVs charging: From the perspective of energy optimization, optimization approaches, and charging techniques.” Review of Transportation Research Part D: Transport and Environment 62:386-417.

Cai, H., Jia, X., Chiu, A. S., Hu, X., & Xu, M. (2014). Siting public electric vehicle charging stations in Beijing using big-data informed travel patterns of the taxi fleet. Transportation Research Part D: Transport and Environment, 33, 39-46.

Chin, K. S., Chan, A., & Yang, J. B. (2008). Development of a fuzzy FMEA based product design system. The International Journal of Advanced Manufacturing Technology, 36, 633-649.

Domínguez-Navarro, JA, R Dufo-López, JM Yusta-Loyo, JS Artal-Sevil, and JL Bernal-Agustín. 2019. “Design of an electric vehicle fast-charging station with integration of renewable energy and storage systems.” Review of International Journal of Electrical Power & Energy Systems 105:46-58.

Duan, G., Fan, T., Chen, X., Chen, L., & Ma, J. (2021). A hybrid algorithm on the vessel routing optimization for marine debris collection. Expert Systems with Applications, 182, 115198.

Duan, G., Nur, F., Alizadeh, M., Chen, L., Marufuzzaman, M., & Ma, J. (2020). Vessel routing and optimization for marine debris collection with consideration of carbon cap. Journal of Cleaner Production, 263, 121399.

Ford Motor Company (1998). FMEA training handbook version-2 (pp. 14–85).

Haghbin, S. (2016, September). Electrical failure mode and effect analysis of a 3.3 kW onboard vehicle battery charger. In 2016 18th European Conference on Power Electronics and Applications (EPE'16 ECCE Europe) (pp. 1-10). IEEE.

İnci M., Savrun, M.M., Çelik, Ö., (2022). Integrating electric vehicles as virtual power plants: A comprehensive review on vehicle-to-grid (V2G) concepts, interface topologies, marketing and future prospects. Journal of Energy Storage, Volume 55, Part B, pp. 1-20.

Khasha, R., Sepehri, M. M., & Khatibi, T. (2013). A fuzzy FMEA approach to prioritizing surgical cancellation factors. International Journal of Hospital Research, 2(1), 17–24.

Kivelä, T., Abdelawwad, M., Sperling, M., Drabesch, M., Schwarz, M., Börcsök, J., & Furmans, K. (2021). Functional Safety and Electric Vehicle Charging: Requirements Analysis and Design for a Safe Charging Infrastructure System. In VEHITS (pp. 317-324).

Liu, H.-C.; Liu, L.; Liu, N. (2013) Risk evaluation approaches in failure mode and effects analysis: A literature review. Expert Syst. Appl. , 40, 828–838.

Ma, J., Harstvedt, J. D., Jaradat, R., & Smith, B. (2020). Sustainability driven multi-criteria project portfolio selection under uncertain decision-making environment. Computers & Industrial Engineering, 140, 106236.

Makeen, P., Memon, S., Elkasrawy, M.A., Abdullatif, S.O., Ghali, H.A., (2018). Smart Green Charging Scheme of Centralized Electric Vehicle Stations. International Journal of Green Energy. Volume 19, 2022 - Issue 5.

Netz, B., Davidson, O. R., Bosch, P. R., Dave, R., & Meyer, L. A. (2007). Climate change 2007: Mitigation. Contribution of Working Group III to the Fourth Assessment Report of the Intergovernmental Panel on Climate Change. Summary for Policymakers. Climate change 2007: Mitigation. Contribution of Working Group III to the Fourth Assessment Report of the Intergovernmental Panel on Climate Change. Summary for Policymakers.

Nuchpho, P., Nansaarng, S., & Pongpullponsak, A. (2019). Modified fuzzy FMEA application in the reduction of defective poultry products. Engineering Journal, 23(1), 171-190.

Peng, H.-M.; Wang, X.-K.; Wang, T.-L.; Liu, Y.-H.; Wang, J.-Q. Extended failure mode and effect analysis approach based on hesitant fuzzy linguistic Z-numbers for risk prioritisation of nuclear power equipment failures. J. Intell. Fuzzy Syst. 2021, 40, 10489–10505.

Querini, F., & Benetto, E. (2014). Agent-based modelling for assessing hybrid and electric cars deployment policies in Luxembourg and Lorraine. Transportation Research Part A: Policy and Practice, 70, 149-161.

Rastayesh, S., Bahrebar, S., Blaabjerg, F., Zhou, D., Wang, H., & Dalsgaard Sørensen, J. (2019). A system engineering approach using FMEA and Bayesian network for risk analysis—a case study. Sustainability, 12(1), 77.

Yazdekhasti, A., Jazi, M. A., & Ma, J. (2021). Electric vehicle charging station location determination with consideration of routing selection policies and driver's risk preference. Computers & Industrial Engineering, 162, 107674.

Yu, H., & Stuart, A. L. (2017). Impacts of compact growth and electric vehicles on future air quality and urban exposures may be mixed. Science of The Total Environment, 576, 148-158.

Zhang, H., Tang, L., Yang, C., & Lan, S. (2019). Locating electric vehicle charging stations with service capacity using the improved whale optimization algorithm. Advanced Engineering Informatics, 41, 100901.

ISBN 978-2-38236-663-9

livredelyon.com
livredelyon
livredelyon
livredelyon